A NOVEL NON-CONTACT PROFILOMETER FOR CHARACTERISING GREY SURFACES BEFORE POLISHING

PENG ZHANG

A thesis submitted to the University of Huddersfield in partial fulfilment of the requirements for the degree of Doctor of Philosophy

The School of Computing and Engineering

The University of Huddersfield

Submission date as September 2018

PENG ZHANG

September 2018

Table of Contents

Table of Contents

Abstract

This thesis presents a novel design of a surface metrology instrument named Swinging Part Profilometer (SPP). Software design, components manufacture, instalment and whole system manipulation are included in this thesis. The motivation of designing a SPP is a critical jigsaw of the autonomous manufacturing for optical components. The SPP is designed to fill up the gap of surface metrology between grinding and polishing.

A detailed survey of current surface metrology methods which contained advantages and disadvantages was included in Chapter 2 of the thesis. The proposal of SPP was based on the short-comings of the current surface measurement techniques. The SPP technique also referenced and modified the principles of Swing Arm profilometer (SAP). It utilised the existing mechanical air-bearing rotary table and industrial robot can significantly reduce the total time of conducting a surface measurement process.

Initially, a basic surface measurement model was designed and all the SPP system components were drawn by Solidworks software based on this measurement model. Based on the Solidworks drawings all the SPP components were fabricated and installed. A Solartron pneumatic contact probe and two Armstrong@ Precitec probes with different vertical resolutions (300nm/20nm) were adopted in the SPP system. The SPP prototype was capable of measuring flat and concave spherical surfaces. The SPP prototype was tested by measuring a 300mm corner-to-corner hexagonal flat mirror and 400mm corner-to-corner hexagonal concave spherical mirror. The data stitching algorithm was also validated by Matlab programme.

The SPP was then utilised to test the mid-spatial frequency (MSF) errors on an off-axis parabolic aluminium mirror with the help of a high vertical resolution (20nm) chromatic probe. Finally, the performance of non-contact probe on a grey surface was tested in order to figure out the boundary of the probe's data collection.

Acknowledgements

Firstly, a special thanks to my parents for their continuous support and patience throughout my PhD.

I would like to express my deep and sincere appreciation to my main supervisor, Dr Guoyu Yu who provided me this opportunity of conducting this PhD in the field of optic fabrication and metrology. Dr Yu continuously gave me professional guidance on academic research during the last four years. This thesis cannot be completed without Dr Yu's help.

A special thanks to my supervisor Professor David Walker for his valuable support in many aspects.

A special thanks to an academic visitor Dr Yi Tian, who assisted me to use Matlab software to connect hardware. I would like to express my thanks to an academic visitor Dr Jie Li, who help me get started with Matlab programming. I also express my gratitude to Tony Li who is in my research group to correct the English language grammar of my thesis.

Special thanks to Dr Hongyu Li, who illustrated me the operation procedures of Zeeko IRP CNC polishing machine. Gary Davies for his guidance to use a 4D interferometer. Xiao Zheng in my research group for his guidance to use ADE white-light interferometer.

Finally, I would like express my appreciation to the University of Huddersfield which gave me financial support which enables me to undertake this PhD study.

List of Abbreviations

CGH	Computer-Generated Holography
CMM	Coordinate Measuring Machine
CNC	Computer Numerical Control
E-ELT	European Extremely Large Telescope
ESO	European Southern Observatory
GMT	Giant Magellan Telescope
GUI	Graphical User Interface
LBT	Large Binocular Telescope
MSF	Mid-Spatial Frequency
NPL	Large Binocular Telescope
ROC	Radius of Curvature
PSI	Phase Shifting Interferometer
PV	Peak to Valley
RMS	Root Mean Square
SA	Surface Average
SAP	Swing Arm Profilometer
SPP	Swinging Part Profilometer
SSI	Sub-aperture Stitching Interferometry
TMT	Thirty Meter Telescope
VLT	Very Large Telescope

List of Figures

List of Tables

Chapter 1 INTRODUCTION

1.1 Overview of Autonomous Manufacturing

The future of global economy is mainly dependent on high value products manufacturing. Autonomous manufacturing systems will play a critical role in future manufacturing. The autonomous system has the capabilities to gain information, analyse information and then make its own decisions. The autonomous system is considered as a necessary section of smart manufacturing. The applications of autonomous manufacturing can significantly promote productivity, flexibility and reliability. Autonomous systems can reduce human force in manufacturing process and can cooperate with humans or machines.

1.1.1 Autonomous Manufacturing History

First industrial revolution-introduction of mechanical facilities powered by water or steam. Edmund Cartwright designed the first power loom in 1784 and fabricated in 1785 [1].

- Second industrial revolution-massive use of electricity and adoption of industrial assembly line. The world first moving assembly line was built by Henry Ford in 1913 in order to achieve mass production of an entire automobile [1]. The application of assembly line successively saved the total fabrication time from 12 hours to 2.5 hours to build a car.
- Third industrial revolution-inventions and applications of atomic power, personal computers, space technology and biological engineering. The third industrial revolution started in 1980s and still on going. The first PLC (Programmable logic controller) was invented by Dick Morley in 1968 [1].
- The fourth industrial revolution-AI (artificial intelligence), industrial robotics, nanotechnology, quantum computing, 3-D printing, driverless vehicles and smart manufacturing. The nomination was firstly used by World Economy Forum in 2016 [1].

1.1.2 Automation Applications in Optical Fabrication and Surface Metrology

The E-ELT (European Extremely Large Telescope) was designed with an aperture of 39 metre and 798 segmented mirrors by ESO (European Southern Observatory) [2, 3]. The first three 1.4 metre hexagonal corner-to-corner prototype segmented mirrors were successfully fabricated in OpTIC Centre in North Wales and recognised by ESO. The raw segment mirror was firstly grinded by BOX™ CNC (Computer Numerical Control) grinding machine at Cranfield University [4]. Then, the grinded segment was transported onto the platform of Zeeko IRP1600 CNC polishing machine to conduct pre-polishing and form-correction process. Pre-polishing conducted by Zeeko CNC polishing machine was a time-consuming process in order remove grinding defects [5, 6]. If more aggressive polishing abrasives are used the contamination concern to Zeeko CNC polishing process could be considered. Based on the above two reasons a novel fabrication method which can overcome the above mentioned short-comings was introduced.

A grolishing process conducted by an industrial robot was adopted as a complementary method to Zeeko CNC machines [7]. The industrial used to conduct the grolishing process which is between grinding and polishing process. In the main zone of the Robot Lab there is a 1.2 metre air-bearing rotary table which was powered by a motor. A Fanuc 3.05m reach robot and an ABB robot were sitting around the air-bearing rotary table. Both industrial robot can conduct specific assignments on top of the air-bearing rotary table [8].

1.2 Surface Texture Measurement History

The surface texture is highly connected with the manufacture development of firearms and cannons. In 1429 the war of Siege of Orléans between England and France the firearms were firstly commonly considered used in Europe. In the early years of 15th century the method of guns manufacturing was blacksmithing [9]. This technology used a bunch of strips of steel spiralling around a straight rod. However,

it has been realized that smith forged guns were not solid enough to project a higher speed and longer projectile distance bullet [10].

In order to enhance the muzzle velocity and projectile distance a new manufacturing technology called gun grilling was invented based on a pragmatic need. The machining of gun barrels requires high barrel inner surface to be smooth and straightness. For early gun makers they usually heat and hammered a long rectangular flat iron for hundreds of times to make the iron flat thickness was a little more than finished barrel's thickness. After that this flat iron was reheated and hammered so that it can wrap a straight metal mandrel to become a tube [9].

The great need for surface texture measurement can be traced back to sixteenth century in England. During that time the need for high-precision cannons for the Royal Navy results in engineers pay interests in controlling the quality of surface [10-12]. Researchers and engineers began to study the features of the surface and develop instruments to quantify these surface features. In the early days the main method of evaluating surface quality was by using a thumbnail and human eyes conducted by experienced workman. The testing workpiece was compared manually with the calibrated surfaces with known roughness fabricated by the same process. In 1919 Tomlinson in National Physics Laboratory (NPL) developed the world first stylus type machine to magnify the small scale of surface texture by thirty times [13]. This is the first time that people can quantify the surface texture. In 1929 Schmalz was the first one who invented the stylus profiler to magnify and quantify the surface texture. He used optical technique to record the vertical motion of the probe with a magnification of a thousand times. Richard Reason from Taylor Hobson invented the first commercial instrument which can measure the surface texture [11, 12]. The widely usage of computers in the 1960s made the surface measurement instruments control automatically and the surface texture can be seen on screen directly.

Areal characterization in surface measurement was intensely needed in order to acquire the full surface topography map. Interferometry method is widely used for conducting areal characterization in surface metrology. In the year of 1887 American Physicist Albert A. Michelson invented the world first Michelson interferometer and successfully measured the speed of light [13]. The interference fringes change

sensitively when the surface local height varies. This can make the interferometers get high vertical resolution (10 nanometres) of surface texture.

1.3 Current Challenges

The need for fast and accurate surface metrology is highly required in the field of astronomy, semi-conductor manufacturing, tool making and medical artificial products. Surface metrology is a compulsory section through the fabrication of telescopes. The surface metrology result can guide the manufacturing process and control surface quality in order to satisfy the quality requirements for telescope.

During the last two decades the aperture (the diameter of a telescope's main light gathering mirrors or lens) for ground-based telescopes have been becoming larger and larger. This trend can be summarized into two reasons. One reason is larger size telescopes have a larger collecting area, so more incident light can be received. The light gathering power is the ability of a telescope to collect light. Most of telescopes' main mirror are circular shape and its area = $\pi \times$ (aperture of a telescope)$^2/4$. Therefore, doubling the size of a telescope's aperture will obtain four times light gathering power [41].

The other reason is larger aperture telescope has higher angular resolution if the diffraction limit can be achieved. The diffraction limit is defined as the minimum angle separation of two objects which can be observed by a telescope. This angle is determined by the wavelength of the incident light and the aperture of the telescope.

$$\boldsymbol{\theta = \frac{1.22 \times \lambda}{D}} \qquad (1\text{-}1)$$

Where 'λ' is the wavelength of light and 'D' is the aperture of a telescope. The coefficient 1.22 is obtained by calculation of the position of the first dark circular ring surrounding the central ring Airy Disk [41]. Based on the equation above increasing the size of a telescope's aperture the value of the minimum angle separation Θ is getting smaller. Therefore, higher angular resolution can be achieved.

Two types of telescopes are used in the world, ground-based and space-based telescopes. Ground-based telescopes have many advantages. Firstly, for the same budget ground-based telescopes can be built with large size. Secondly, they are easier to maintain and repair. Finally, they have lower risk of being damaged

by 500,000 space trash moving around the earth compared with the space-based telescopes. However, engineers have been designing and fabricating space-based telescopes which can get sharper images due to less atmospheric distortion. When ground-based telescope gather light from the universe the coming light will pass through the earth atmosphere before hitting telescope's main mirror. The incident light can be blurred if the earth air is turbulent. An adaptive optics system integrated with ground-based telescope can correct atmospheric distortion. The adaptive optics system has array of deformable mirrors and computers which can sharpen the images by measuring the distortions in a wavefront and compensating for them.

In the early days of 20th century the aperture of the primary mirror of a telescope rarely larger than 1 meter. As the improvement of computer technology in 1990s to achieve designing light-weight mirrors, a series of ground-based telescopes with an aperture of 8 meters were designed and built around the world (LBT, VLT). However, limited by current fabrication technology the maximum diameter of a single mirror was 8.4 meter. Therefore, increasing the aperture of telescopes can be achieved by using the technology of segmented mirrors. This technology is pragmatic in mirror manufacturing and transportation. Segmented mirror technology was firstly used in building Keck 1&2 ground-based telescope in 1993 and will be adopted in fabricating the European Extremely Large Telescope (E-ELT). The aperture of the E-ELT is 39.3 metre [3]. The Thirty Metre Telescope (TMT) has a 30 metres primary mirror and Giant Magellan Telescope (GMT) is equipped with a 24 metres primary mirror (E-ELT Construction Proposal) [14, 15].

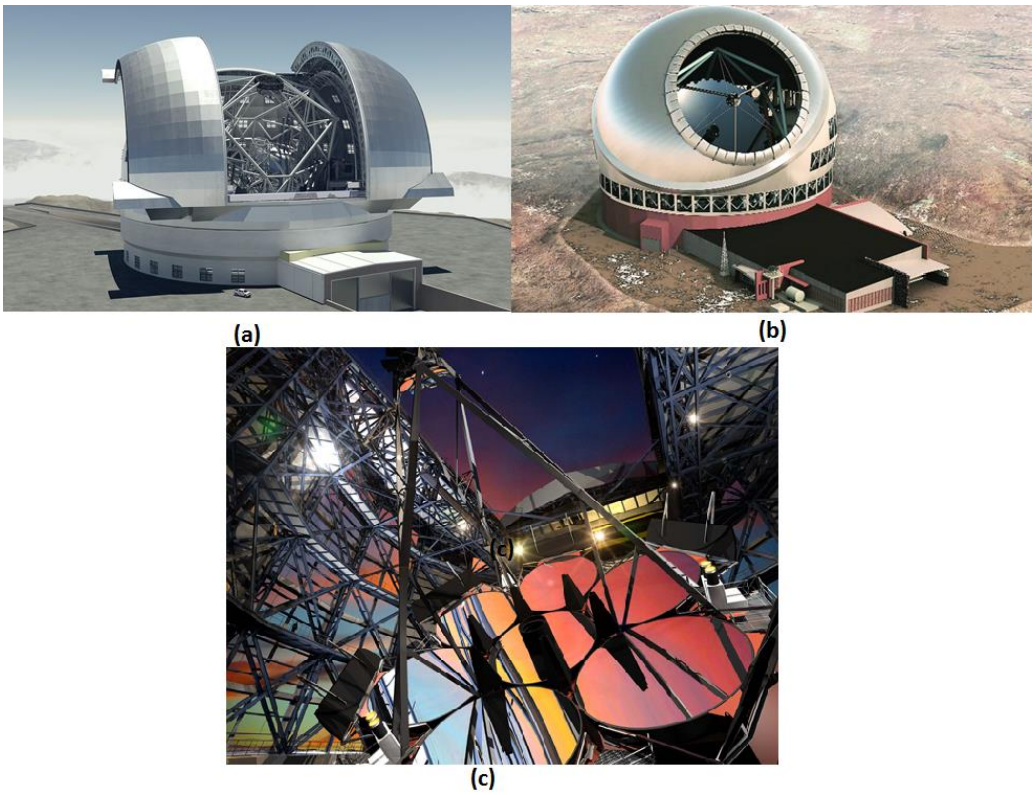

Figure 1-1 Large Telescopes: (a) E-ELT (b) TMT (c) GMT

Considering the limitations from both transportation and surface metrology the segment size of the E-ELT primary mirror was set as the 1.4 metres corner-to-corner [16]. The dimension of a segment is determined as above so that mirror segments can fit into a standard shipping container. Hexagonal segments with 1.4 metres corner-to-corner can be transported with road network, railways and shipping.

The E-ELT segment prototype fabrication chain starts with grinding, polishing, testing and second time polishing and testing [17, 18]. The accuracy and efficiency of the surface metrology will directly determine the cost and efficiency in the fabrication process.

The first three 1.4 metre hexagonal corner-to-corner prototype segmented mirrors were successfully fabricated in OpTIC Centre in North Wales and recognised by ESO. The raw segment mirror was firstly grinded by BOX^{TM} machine at Cranfield University [5]. Then, the grinded segment was transported onto the platform of Zeeko IRP1600 CNC polishing machine to conduct pre-polishing and form-correction process. Pre-polishing conducted by Zeeko CNC polishing machine was a time-consuming process in order remove grinding defects [18-20]. If more aggressive polishing abrasives are used the contamination concern

to the Zeeko CNC polishing process could be considered. Based on the above two reasons a novel fabrication method which can overcome the above mentioned short-comings was introduced.

A grolishing process conducted by an industrial robot was adopted as a complementary method to Zeeko CNC machines [7, 21]. The industrial robot was used to conduct the grolishing process which is between grinding and polishing process. In the main zone of the Robot Lab there is a 1.2 metre air-bearing rotary table which was powered by a motor. A Fanuc 3.05m reach robot and an ABB robot were sitting around the air-bearing rotary table. Both industrial robot can conduct specific assignments on top of the air-bearing rotary table [8].

1.4 The Need for New Metrology Method for Large Optics

The surface metrology for large scale mirrors has always been a challenge for engineers and researchers. Lens with large aperture (the diameter of the main lens or mirror) are beyond the measurement range of the metrology instruments. Furthermore, it is time-consuming and complicated to transport the large optics from the fabrication platform to the metrology station. In addition to this, the vibration and deformation of the testing workpiece caused by gravity can affect the accuracy of measurement.

The concept of in-situ measurement has been introduced in order to improve the overall efficiency of optic fabrication and surface metrology. Literally, in-situ means ‘on site’ or ‘in the original place’ to describe an event where it takes place. In-situ measurement describes the measurement is taken on the same place where the fabrication process is occurring.

The in-situ measurement can reduce the fabrication time by cutting off the transportation time of the mirror. It can also improve the accuracy of surface metrology by minimizing the chances of mirror’s damage. Currently, large amount of surface measurement instruments are tender since their high requirements on testing mirror surface quality. The interferometry can be used when the testing surface is polished. The current profilometer instruments are either short measurement range or 2D scale measurement. Moreover, the current surface measurement instruments are carried out off-line.

The in-situ measurement requires the metrology instruments embedded in the optic fabrication platform can enhance the overall efficiency of optics machining and surface metrology, leading to improve the competitiveness of the products. A new surface metrology instrument Swinging Part Profilometer (SPP) was developed for in-situ measurement of optics undergoing industrial robot processing in the ground (non-specular) state. The SPP can provide the surface measurement when the testing mirror is on the intermediate process between grinding and computer numerical control (CNC) polishing. The SPP comprises precision rotary table which was motored and precisely controlled by encoder, light-weight support and sliding system for the testing workpiece. A non-contact probe was embedded on the terminal of ABB industrial robot to conduct the lateral scan. A specific surface reconstruction method was also developed. The developed SPP surface metrology instrument has a compact configuration and is capable of conducting stable and fast in-situ measurement on both small and large scale (1 meter) mirrors with high accuracy (100nm).

1.5 Aim

Based on the current challenges mentioned in section 1.3, autonomous manufacturing cells for ultra-precision surfaces fabrication are being built. These autonomous manufacturing cells will finally contain CNC grinding (FANUC/ABB industrial robot), CNC polishing (Zeeko IRP), and in-situ metrology (Swinging Part Profilometer) (Figure 1-2). In order to fill the gap of surface metrology between CNC grinding and CNC polishing, a novel metrology instrument, the Swinging Part Profilometer (SPP) was developed.

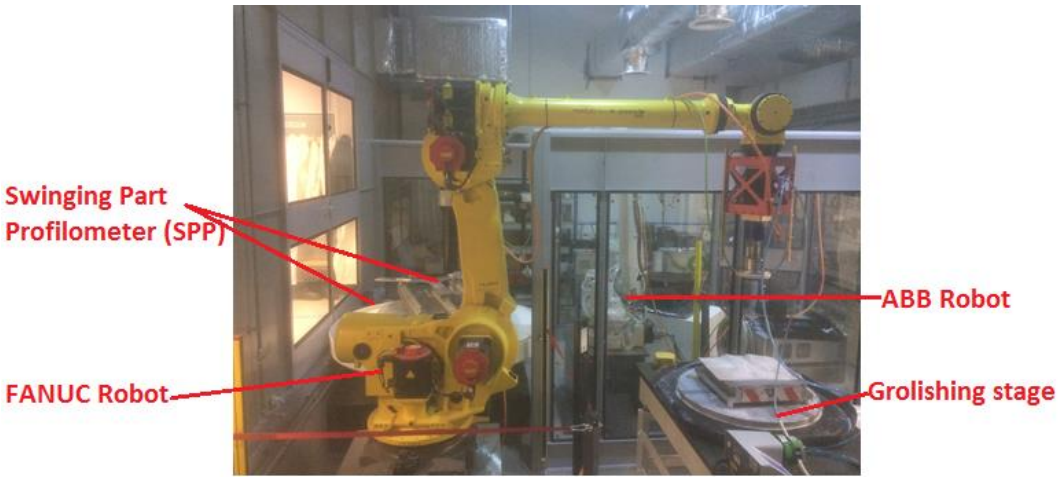

Figure 1-2 Autonomous manufacturing cell

The research aims to design and develop an in-situ surface measurement instrument for large optics before their surface quality is sufficiently refined to enable an optical interferometry to be conducted. This is to allow characterisation and some surface form-correction in grolishing (intermediate process between grinding and polishing) [7], which is a fast process compared with polishing. The whole SPP was embedded in the grolishing platform with the high resolution (300nm/20nm) and long measurement range (10mm/2mm) non-contact Armstrong Precitec chromatic probe. First, the glass work-piece was grolished by an industrial robot which can significantly reduce the overall fabrication time. Then, the surface of the work-piece would be tested by this SPP without being moved elsewhere. Finally, the surface error map gathered by SPP can be used by Zeeko IRP polishing machine to conduct the final surface polishing.

The research includes the design and installation of all the components of the SPP, air-bearing rotary table, a motor which can power the turntable rotation, an incremental encoder can indicate precisely the real-time position of the rotary table, control box can read the real-time value of both the motor and positional encoder, a supporting system that includes triple aluminium extrusions and stainless steel rails can support the testing work-piece. Furthermore, the research work will involve software manipulation of both the rotary table motion and non-contact probe data collection. The target is that the table movement and probe data logging can be triggered simultaneously. In this way the probe data can collect the work-piece's surface specified local height information. Moreover, a novel measurement mode which can deliver the surface

metrology as the grolishing process is finished by FANUC industrial robot should be developed. The relevant surface reconstruction algorithm will be developed and its validation should be verified.

1.6 Objectives

1. To design and install all the components of Swinging Part Profilometer.
2. To complete the synchronization between the rotary table rotation and probe data collection. It is necessary that the probe data can reflect the specified testing work-piece surface height information.
3. To develop the appropriate surface measurement mode which will guide the turntable rotation and testing work-piece de-centred position.
4. To develop the relevant surface reconstruction algorithms so that the SPP can generate a 3D surface error map. The surface reconstruction algorithms comprised the different methods for flat and concave spherical surfaces. All the algorithms were verified by Matlab simulation.
5. To complete the uncertainty budget of the SPP so that most error sources can be listed and quantified. The overall performance of the SPP can be optimized based on this uncertainty budget.
6. To investigate the measurement performance by testing flat and spherical surfaces with SPP. Compare the stitched error map gathered by SPP with the interferometer results.

1.7 Thesis Organization

This research work includes the hardware design, installation and development of profilometry data reconstruction method of the SPP. This SPP instrument is aim at measuring the large scale (aperture above 400mm) optics with the accuracy of 0.1 micron. The thesis comprises seven chapters to present the overall research aim.

- Chapter 2 gives a brief introduction regarding surface metrology. It includes the definition of surface, the property of surface and the importance of doing surface metrology. Furthermore, this chapter will introduce the current technology and methods of conducting the surface metrology.

- Chapter 3 introduces the measurement principle of the Swinging Part Profilometer. It also explains the profilometry data stitching algorithm in order to reconstruct the 3D surface error map. This chapter makes a comparison and contrast about the principles between the Swing Arm profilometer and SPP. At the end of this chapter the validation test is conducted by Matlab to confirm the data reconstruction algorithm is correct.
- Chapter 4 introduces the surface measurement experiment regarding the hexagonal flat mirror by using the SPP. This experiment involves four major steps. Firstly, a Matlab control interface is developed in order to synchronize both the rotary table motion and optical probe data collection. After that the testing workpiece should be placed properly on the rotary table. Then scan the testing workpiece by rotating the turn-table as the probe remains static. A measurement pattern includes series of con-centric profiles and one arc scan was designed. Finally, all the circular profile data and arc scan data are processed by Matlab in order to stitch the final 3D surface error map.
- Chapter 5 introduces the surface measurement experiment regarding the concave spherical mirror by using the SPP. Design a measurement pattern to collect the surface profile data. Collect all the scanned raw data and process the data by Matlab to stitch the final surface error map. Make an error analysis and list all the error sources.
- Chapter 6 introduces the experiments regarding using the SPP to test the Mid-spatial frequency (MSF) errors on the surface of an off-axis parabolic aspherical aluminium mirror.
- Chapter 7 introduces the uncertainty budget of the Swing Part Profilometer (SPP). Several experiments were conducted in order to figure out the error sources of the SPP.
- Chapter 8 introduces the experiment regarding the maximum measurement angle to surface of the chromatic probe which was used in the SPP. The relations between the probe's maximum measurement angle to surface and different surface texture have been found.

1.8 Author's Contributions

The thesis's author made many contributions to this SPP in-situ surface measurement project. Firstly, the author developed the basic measurement model of a SPP. Based on the theoretical model the author used Solidworks software to design all the components of the SPP. All the necessary components were manufactured by a factory. The author assembled all the components together and making use of an existing air-bearing rotary table with a diameter of 1.2 meter. The author ordered two different kinds of metrology probes, pneumatic and chromatic non-contact probes and tested their performance. He then developed Matlab GUI to control all the components such as rotary table's rotation with any specified angle and metrology probe's data logging. With the help of Matlab software both the metrology probe and rotary table's rotation can be conducted simultaneously. The author then developed an algorithm to stitch all the recorded probe data in order to gather a surface error map. A Matlab GUI was also developed to carry out the data stitching algorithm. The author used the SPP to test a flat hexagonal glass mirror, a concave spherical mirror. The author also used the SPP to test the existence of the mid-spatial frequency errors on the surface of an off-axis aspherical aluminium mirror.

Chapter 2 SURFACE METROLOGY

This chapter firstly gave the definition of 'surface' and 'surface metrology'. It then introduced surface metrology's importance in both industrial manufacture and academic research. Current techniques of measuring a surface were also stated in details in this chapter. Finally, a comparison and contrast regarding these metrology methods has been made.

Surface was defined as the outer or the topmost boundary of an object [13]. The surface of a solid can be considered as an interface at which the surface is in contacting the surrounding world.

Surface metrology is the measurement of the deviations of a workpiece from its intended shape, which is from the shape specified on the drawing [13]. Surface metrology includes the features such as roughness, waviness and error of form [13].

2.1 The Importance of Surface Metrology

The surface metrology can be important in two aspects, one is to control the whole manufacture process and the other is to concern in which way that the surface can influence how well the workpiece will function [13]. As the surface finish requirement was raised to nanometre level the surface measurement capability is becoming very important. Firstly, the surface metrology result can provide the information that can be used to guide the following manufacturing procedures with techniques and tools. Also, for some functional structural surfaces with specified functions such as sealing, lubrication and bearing, the geometrical figure was required at the first place.

2.2 Surface Texture Characterization

Surface texture is defined as the periodical or random deviation from the nominal surface that forms the surface [22]. The international standard organization (ISO) defines the parameters which are used to quantify the surface geometrical features (ISO 4287 (2000) Geometrical product specifications (GPS)) [23]. Surface texture consists of roughness, waviness and form [22, 24]. Geometrical product specifications (GPS)) [23]. In order to define and quantify the surface texture terms with a uniform pattern ISO also

defines the coordinate system in which all the parameters share the same coordinate system. In this Cartesian coordinate system the X axis is the direction in which the trace is carried out (Figure 2-1). The Z axis provides the amplitude information. The surface primary profile is defined as the continuous intersection line between the real surface and the specified flat plane. The selected plane is normally parallel to the testing surface [22].

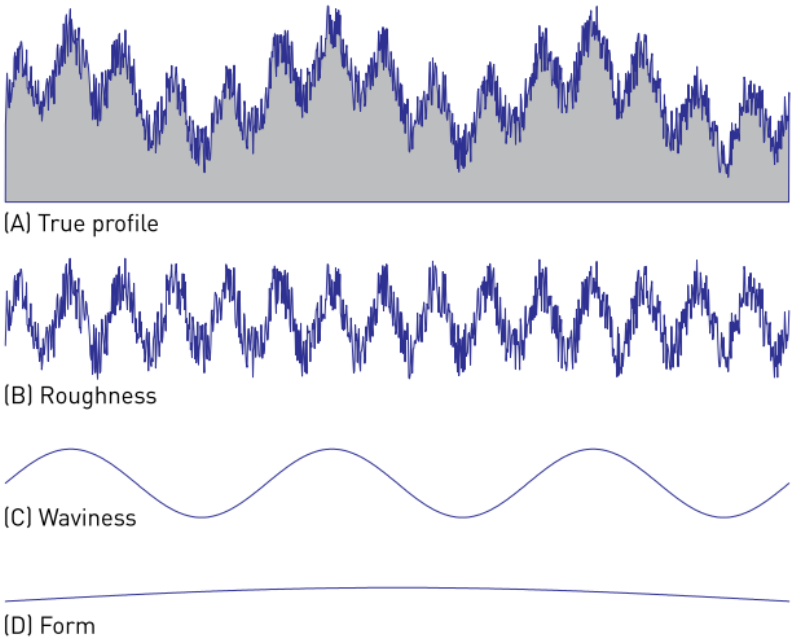

Figure 2-1 Surface roughness, waviness and form [25]

Roughness

Roughness is the deviations which consists of peaks and valleys [22, 24]. The roughness is evaluated by short lateral spacing compared with those of waviness and lay. The peak profile in the roughness profile is the local maximum and the valley is the local minimum of the roughness profile (Figure 2-1).

Waviness

Waviness is defined as the irregularities whose spacing value is larger than the roughness sampling length (Figure 2-1). Normally the waviness irregularities are caused by the imperfect machining process on the workpiece [13].

Form

Form consists of long-period or noncyclic deviations in the surface profile and these deviations were normally generated by abrasion of machines [13].

2.3 Surface Measurement Techniques

Currently, the optical components can be measured in two main methods, mechanical and optical. Mechanical method is the technique which uses a stylus tip to scan the testing surface and gather the surface profile information as a function of its own position. The mechanical method can be conducted by either moving a testing surface while the stylus tip remains static or moving the stylus tip when the testing surface remains fixed.

Optical methods normally use light to gather a testing surface's topography information. Optical methods consist of optical profilometers, confocal microscopes and interferometers.

This chapter summarized the current main surface metrology methods which were used to measure the optical surfaces (flat, sphere) and compared and contrasted these methods.

2.3.1 Mechanical Profilometry Technique

2.3.1.1 Contact Stylus Profilometer

The contact stylus type profilometers were firstly used to measure the surface texture. In 1941, Taylor-Hobson invented the first commercial profilometer named 'Talysurf 1' in the film industry [26]. From then on contact type profilometers have been widely used to measure the surface texture.

The contact type profilometer uses stylus which will physically touch the testing surface when it moves along the surface [27-29]. When using the stylus type profilometer the probe will firstly move vertically in contact with the testing surface [30]. Then the sample stage sitting on the air-bearing table will move laterally with a constant speed while the probe remains static. The profilometer can amplify the amplitude of the surface roughness by the amplifier inside the profilometer. The Taylor-Hobson profilometer Talysurf can have the vertical resolution of 10 nanometres (Figure 2-2). The other operation mode of profilometers

is that a testing surface remains still during the measurement. A probe is moving along the testing surface to collect the surface's local height reference.

Figure 2-2 Talysurf Profilometer

The contact stylus profilometers are widely used both in industry and academic research with the following advantages[26] [31]. Firstly, the current standard surface specifications are defined for profilometers. Secondly, the contact stylus profilometers are not sensitive to surface reflectance, both rough and specular surface can be measured.

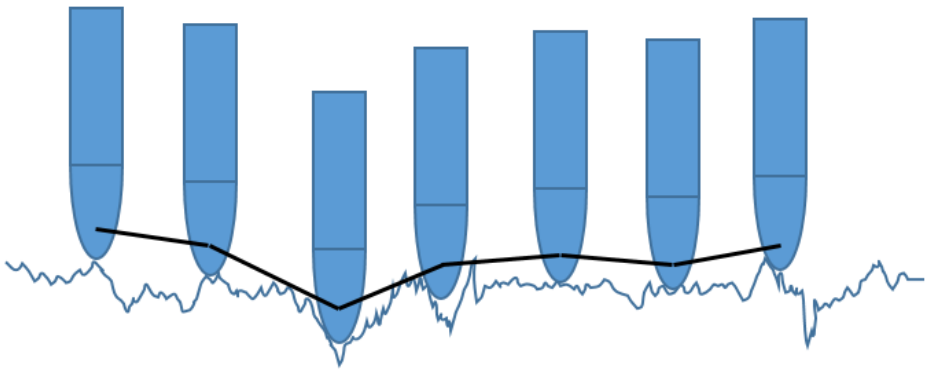

Figure 2-3 Roughness measurement by using contact stylus

However, the disadvantages of profilometers cannot be ignored. Firstly, since the stylus tip physically touches a testing surface when either moving the stylus or testing surface the testing surface will be damaged by the stylus tip. Secondly, the relation motion between contact stylus and the testing workpiece can cause the stylus wear [32].

2.3.1.2 Coordinate Measurement Machine (CMM)

An example of a contact stylus profilometer is Coordinate Measurement Machine (CMM). CMM is an instrument which can measure the surface topography of an object [27, 33, 34]. A common CMM consists of three main components, three perpendicular moving axes (X, Y, Z) based on the Cartesian coordinates system, measurement probe and data processing system (Figure 2-4). When conducting the measurement the probe will physically touch the testing surface and the space position of the probe on each tested point can be recorded based on the coordinates of three axes. Both contact and contactless probe can be used by CMM. When using the contactless optical probe the light from probe will be reflected from the testing surface and the wavelength of the reflected light can be analysed and calculated. The recorded wavelength will determine the distance between the probe and testing surface.

Figure 2-4 Coordinate measurement machine (CMM)

2.3.1.3 Swing Arm Profilometer (SAP)

The Swing Arm Profilometer (SAP) concept was first developed by J.P.R Angel and R.E Parks from University of Arizona in 1982 [35, 36]. James.Burge and Peng Su conducted further researched on SAP and successfully utilized it measured convex aspheric surface with 1.4 diameter [37, 38].The final surface metrology accuracy was achieved 10 nm when a high resolution contactless probe was adopted.

The metrology probe was mounted on the terminal of an arm which will swing across the testing surface (Figure 2-5) [39]. Each probe tip's trajectory will pass through the centre of the surface under test [39-41]. The probe readings of each trajectory shows the difference between the reference sphere and the surface under test. When the arm swing across once, the testing surface will rotate with a specified angle and then the arm with probe will swing again. Since the arcs cross each other while the sensor scans the mirror edge to edge, we know the surface heights must be the same at these scan crossings. This crossing height information is used to stitch the scans into a surface [42].

Figure 2-5 Swing arm profilometer in National Physical Laboratory (NPL) UK

2.3.1.3.1 SAP and SPP Principles Comparison

In SAP, a metrology probe is mounted on the terminal of an arm which swings across the surface under testing (Figure 2-6). The arm's rotation axis is designed to goes through the centre of curvature of the testing surface. When the arm is rotated the metrology probe will scan an arc path which is determined by this centre of curvature (Figure 2-6). The metrology probe is aligned perpendicular to the surface under testing on its vertex. The testing optic is rotated around its optic axis with an angle after an arc scan is conducted. Repeat the above steps until a number of arc scans can cover the whole surface under testing. When the SAP is used to conduct a surface measurement both the testing optic and metrology probe are moving. High precision measurement result requires high precision rotation arm.

In SPP, when conducting circular scan on testing surface the metrology is mounted on the terminal of an ABB industrial robot arm and remains static. The testing optic on top of an air-bearing rotary table will rotate continuously. The chromatic probe used in the SPP has a range of measurement angle to surface. The

probe can be tilted to the testing surface. Therefore, when measuring a concave spherical surface the probe and ABB industrial robot arm can remain static.

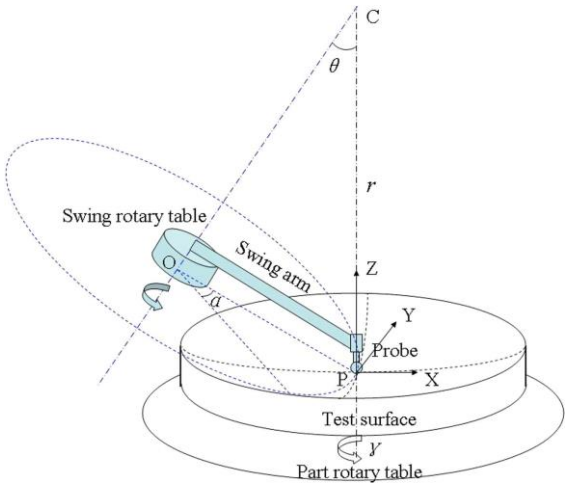

Figure 2-6 Principles of the SAP[43]

2.3.2 Optical Profilometry Technique

Compared with the stylus profilometers, non-contact profilometers use light to scan a testing surface rather than a stylus probe [22, 44, 45]. The fast and direct surface data acquisition and undamaged nature on testing surface determine the widely usage of the non-contact methods [29, 45, 46].

Optical systems are normally adopted in non-contact probing methods. In a non-contact profilometer the mechanical stylus was replace by the focus of the incident light beam [47, 48].

The chromatic aberration principle was used in the non-contact stylus method (Figure 2-7) [49]. Different wavelength of light has different refraction index when the light pass through the uncorrected lens. Within the visible spectrum region, the blue light has the minimum focal length due to its shortest wavelength. Similarly, the red light has the maximum focal length. The distance between the maximum and minimum focal length is the vertical measurement range. The testing surface's height variation within this range can be measured (Figure 2-7). Within the measurement range light of a tiny wavelength region is focused on the testing surface due to the confocal configuration of the probe design. Each point on the testing surface has its corresponding light which was focused and reflected on the surface. This unique focused and

reflected light will be received by the focusing lens. The wavelength of the received light and the corresponding vertical distance of the testing surface will be calculated [49-51].

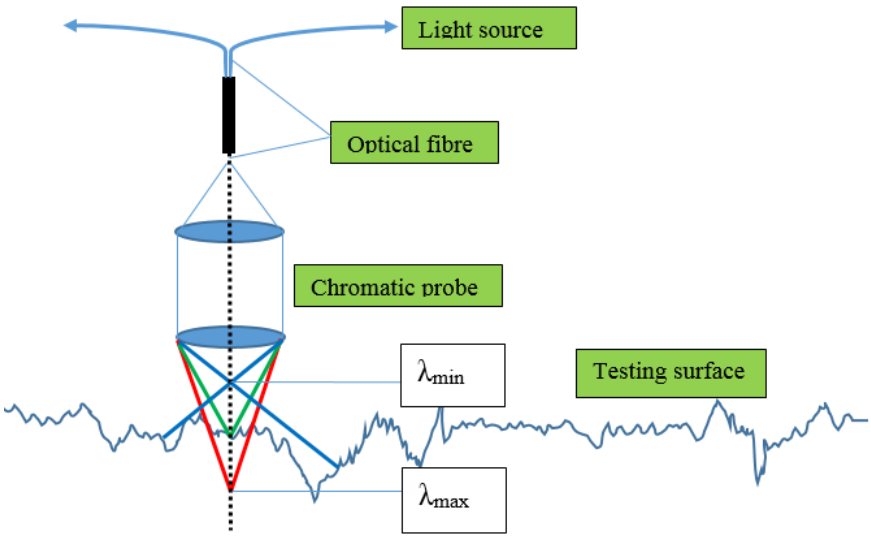

Figure 2-7 Working principle of chromatic probe

The advantages and disadvantages are listed below:

Advantages:

- No damage on a testing surface.
- Great application range: glass, metal, plastic component.

Disadvantages:

- Unable to measure a surface with high slope. The emitted light beam will be reflected away from its incoming path so the spectrometer cannot get the testing surface's height data.

2.3.3 Interferometry Methods

The interferometry method utilizes the principles of superposition of coherent light beams from the same light source to analyse the interference pattern [13, 52].

During interferometry testing the beam splitter separates the light source into two light beams (Figure 2-8). One of them reaches the testing surface and the other one is reflected by the reference mirror. The two

reflected light beams will be recombined and intervened and then captured by a detector (Figure 2-8). The light beams path difference can be analysed and calculated based on the interferogram.

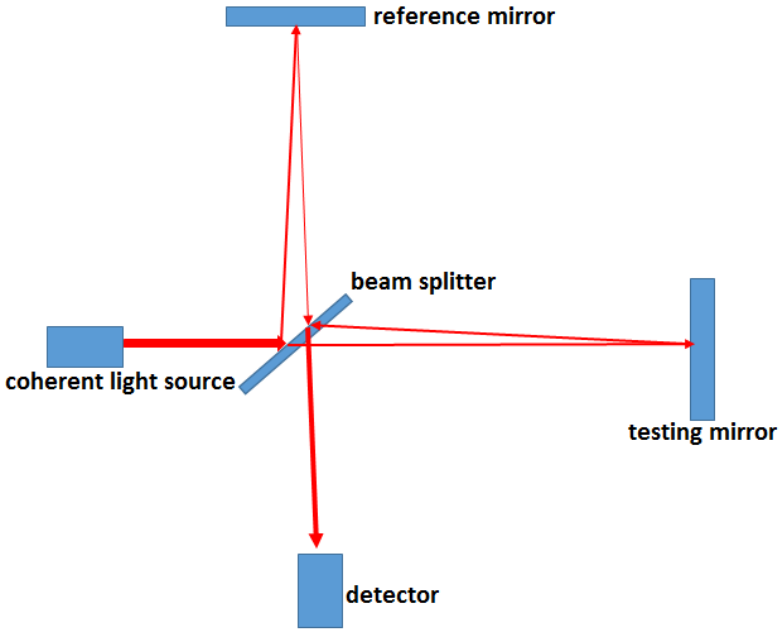

Figure 2-8 Interferometer principles

The interferometry technique is capable of testing surface with large scale (8.4 meter). It can provide the surface topography information with nanometre scale accuracy. The FISBA interferometer can measure flat surface with accuracy of λ/20. Since it uses light as the test medium the testing instrument is contactless with the workpiece, no surface damage will be introduced. As the involvement of modern computing techniques the final result can be obtained fast and accurately.

2.3.3.1 Computer Generated Holograms (CGH)

The computer generated holograms (CGH) method is commonly used to test aspherical surfaces [53-55]. Interferometers are capable of measuring flat and spherical surfaces with the accuracy of nanometres [55, 56]. When measuring a concave surface a reference concave mirror must be used to determine the deviations of the testing concave surface [39]. However, if an aspherical mirror is to be tested, a corresponding aspherical reference mirror must be fabricated. The fabrication of aspherical mirrors is expensive, difficult and time-consuming [56]. The CGH can change a spherical wavefront to the aspherical

one so that the interferometers can test the aspherical surfaces (Figure 2-9) [57, 58]. With this advantage no aspherical reference mirror is necessary when the mathematical description of the optic is available.

First step is to calculate the CGH pattern. The next step is record the calculated pattern on top of a transparent medium based on the calculated pattern. Then place the plotted substrate inside the interferometer (Figure 2-9).

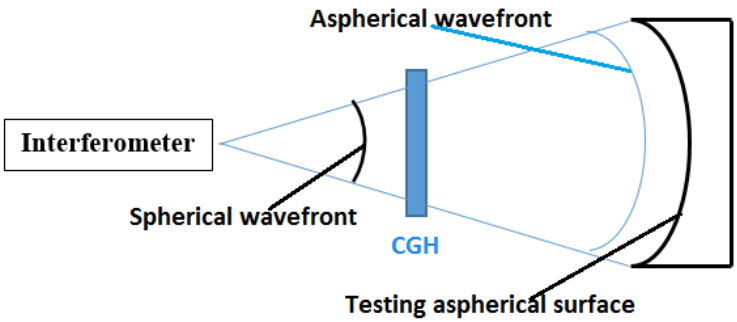

Figure 2-9 Measure aspherical surface with CGH

2.3.3.2 Phase Shifting Interferometry (PSI)

The phase shift interferometry (PSI) is used for surface topography measurement (Figure 2-10) [13]. PSI utilizes the computer controlled phase shift to generate the interference fringe pattern and calculate the pattern [59]. Normally, the phase shift is achieved by mechanically moving the interferometer objective continuously or in discrete steps. This motion is carried out by using piezoelectric transducer (PZT) [59]. After each phase shift is carried out the calculation of fringe pattern will be conducted based on the data stored.

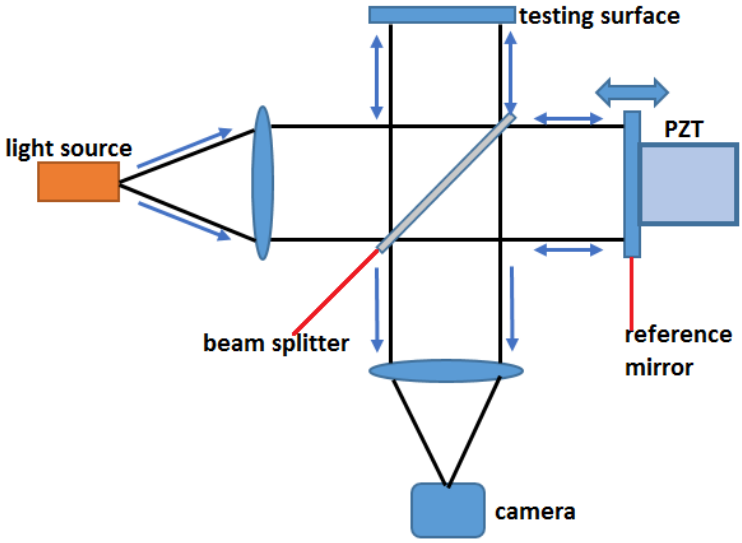

Figure 2-10 Phase Shift Interferometry (PSI) configuration

The advantages and disadvantages of PSI are listed below:

Advantages:

- PSI can provide a swift surface measurement
- PSI can provide high accuracy of 1/100λ
- PSI can measure surface in low contrast fringes

Disadvantages of PSI

- PSI is sensitive to the environment vibration
- PSI is unable to measure steep surface when the height difference between two points next to each other is larger than half of the wavelength of the light source

2.3.3.3 Sub-aperture Stitching Interferometer (SSI) Method

The sub-aperture technique was first developed by C.Kim and J.Wyant from the University of Arizona [60]. On the year of 1997 M.Bray designed the interferometer which used sub-aperture stitching principles and tested the large flat optic workpiece [60]. This proves the feasibility of the sub-aperture stitching method. In 2003, the American QED Corporation's product Sub-aperture Stitching Interferometer (SSI) was developed and it can measure the surface with the aperture of 200 millimetre [61].

The basic principle: divide the testing surface into a couple of sub-zones. Each sub-zone will overlap its adjacent one (Figure 2-11). Then use the interferometer to measure the surface topography of each zone with the pre-defined route. Stitch all the sub-aperture data to a full-aperture phase map based on the data from overlapped regions [62].

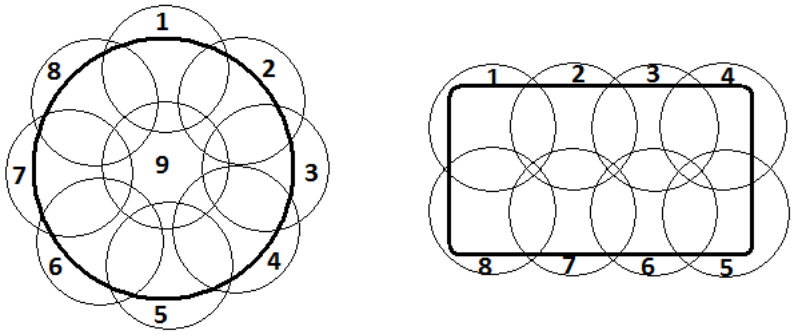

Figure 2-11 Principles of Sub-aperture Stitching Interferometer (SSI)

The advantages and disadvantages of SSI are stated below:

Advantages:

- Extend the measurement spatial range with current interferometers so that large optics can be tested.
- Inexpensive compared with large aperture interferometers.

Disadvantages

- Errors can be transferred during the sub-aperture stitching process.

2.3.4 Wavefront Sensing Methods

2.3.4.1 Shack-Hartmann Wavefront Sensing Method

A wavefront sensor is a device for measuring aberrations of an optical wavefront [63]. The wavefront sensing technique was used in Adaptive Optics (AO) systems and lens testing. The Shack-Hartmann wavefront sensing method was widely used to measure the shape of the wavefront in adaptive [64]. This method was invented by Roland Shack and Ben Platt in 1971 for the target of improving the quality images taken by satellites [64-66].

A microlens array is placed between the light source and detector [65]. The micro lenses array is a plate on which a uniform pattern of small holes are punched (Figure 2-12). With the help of the microlens array the incoming light can be focused on the detector. The focused spot pattern will be uniform if the incoming wavefront is a perfect plane wave. When the incoming wave is distorted, the captured spots will be deviated from its uniform pattern. The captured spots deviation can be divided into x, y directions and each of them is perpendicular[64] [67]. The x and y component of deviation are both proportional to the average slope of the incoming wavefront in x, y direction.

Therefore, the Shack-Hartmann wavefront sensing method is capable of measuring the wavefront slope. Based on the local slope of each sub-image the whole incoming wavefront can be reconstructed.

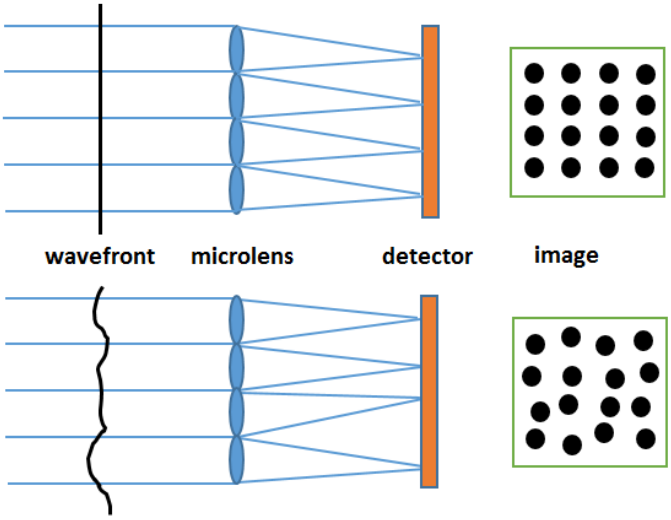

Figure 2-12 Shack-Hartmann wavefront sensing principle

The advantages and disadvantages of the Shack-Hartmann wavefront sensing method are listed below.

Advantages

- The configuration is easy to make
- High dynamic measurement range
- High measurement accuracy

Disadvantages

- System alignment can limit the final measurement accuracy

- Expensive cost due to the need of high resolution CCD camera

2.3.4.2 Phase Diversity and Wavefront Curvature Sensor Method

The Phase Diversity (PD) was first developed by Gonsalves in 1982 [68-70]. Gonsalves used Phase Diversity to solve the unique solution of the phase intensity calculation. Normally, it is not possible to get the unique solution based on a single phase intensity image. At least two intensity images are needed in order to get the unique solution. The testing wavefront phase can be determined based on the phase diversity information which can be obtained on the two images [69, 70]. However, the phase reconstruction methods developed by Gerchberg and Saxton are difficult to calculate and time-consuming. The disadvantage of time-consuming limits the usage of Phase Diversity Sensor in Adaptive Optics. The variation of PD named curvature sensor was introduced due to its much faster than PD sensor.

The wavefront curvature sensor was first developed by F. Roddier in 1988 [70]. Its working principle is based on the measurement of the intensity profile of two planes. The 'pre-pupil plane' is placed in front of the focal point and the 'post pupil plane' is placed behind the focal point (Figure 2-13). The two planes are imaged by the curvature sensor. If there is a bump on the incoming wavefront the illumination on 'pre-' and 'post' pupil planes will not be uniform. In details, if the local wavefront is concave it will converge and generate an illuminate spot on the 'post pupil plane'. On the contrary, the illuminate patch can be imaged on the 'pre-pupil plane'. The larger curvature of the sample will have greater aberrated wavefront and the refracted light will focus more strongly.

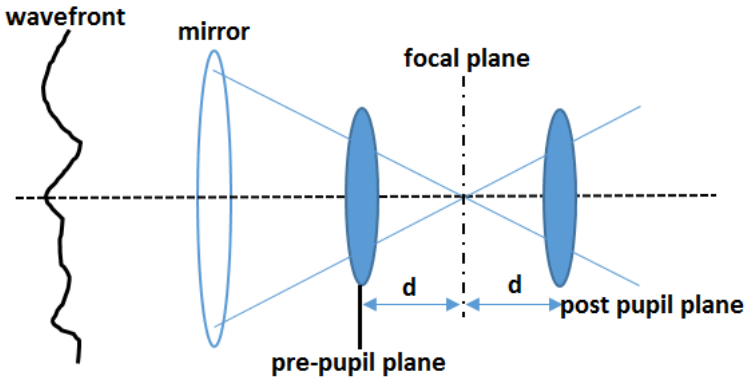

Figure 2-13 Curvature sensor principle

The contrast of the two images can give the curvature information of the incoming wavefront.

Unlike the Hartmann sensor which measures the slope of wavefront, the curvature sensing method measures the local wavefront curvature.

The advantages and disadvantages of the Phase Diversity and Wavefront Curvature Sensor Method are listed below.

Advantages

- Lower number of total detector pixels compared with Shack-Hartmann sensing method.
- Curvature sensing system is less expensive than Shark-Hartmann.

Disadvantages

- Algorithms are complex thus P-D requires long computation time.
- Smaller dynamic range compared with the Shack-Hartmann method.

2.3.4.3 Shearing Interferometers Methods

The shearing interferometer method is the technique that measures the phase differences of the wavefronts. It can be used to determine the slope of the wavefront. The testing wavefront will be divided into two sub-wavefronts and then interfere again. The testing wavefront will also be sheared and displaced by using the shear plate. Based on the intensity of interference patterns and the shearing distance the wavefront slope can be calculated.

The wavefront can be sheared with the following methods, lateral, radial and common path. In the lateral shearing interferometer, the interference pattern is determined by the phase difference between two wavefronts which are divided by the shear distance. The phase difference created by the shearing can be used to calculate the slope of the incoming wavefront. The slope direction is consistent with the shearing direction. In radial shearing interferometer the interference pattern is generated by magnifying one of the two wavefronts and then combine both of which.

Advantages

- No reference wavefront is needed.

- Shearing interferometers are easy to make and low cost.
- Shearing interferometers can be used for measuring large aperture optics.
- High tolerance for lab environment such as noise, vibration and turbulence.

2.3.5 Other Surface Metrology Methods

2.3.5.1 Deflectometry Method

The Deflectometry method is used to measure slopes on surfaces by recording the lateral displacement of light reflected from the testing surface [71, 72]. Height information can be reconstructed by integrating the slope data. Normally, a digital camera is used to capture the light which is reflected from the specular surface (Figure 2-14) [73, 74]. A projector is used as the source to generate this light [75, 76]. The light captured by the camera will be calculated so that the slope variation of the testing sample can be measured [73, 77]. The slope variation can be processed in order to provide the surface topography of the testing sample [78]. In 2004, Knauer invented the Phase Measuring Deflectometry (PMD) which uses LCD screen as the light source since LCD screen can precisely control the intensity of light [77].

The advantages and disadvantages of the deflectometry technology are listed below.

Advantages:

- The deflectometry method can provide larger tolerance of testing surface dynamic range compared to the interferometer technique.
- It has better tolerance to the testing environment.
- Deflectometry can measure surface slope changes with the accuracy of micron (μ) radians.

Disadvantages:

- Rough surface cannot be measured by deflectometry. An additional surface painting or coating is necessary to conduct the deflectometry testing.

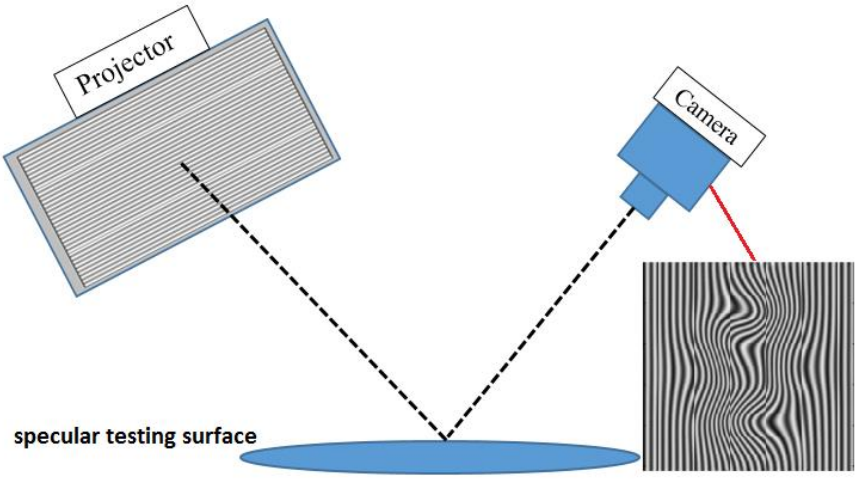

Figure 2-14 Deflectometry principle

2.3.5.2 Foucault Test

Foucault test is a simple and powerful method to observe small irregularities and smoothness of a testing spherical surface. The Foucault test was invented by French scientist Leon Foucault in 1858 [13]. The Foucault test can be conducted with simple component and get direct result. The reflected light from the testing surface can show the surface form information. The reflected light will be focused to a single point if the testing part is a perfect spherical surface. If the testing surface deviates from the perfect shape the focused point position will be changed. During the Foucault test a thin and opaque plate which has a straight and sharp edge is used. This plate is placed next to the focus point and moved perpendicular to the reflected light from the testing surface (Figure 2-15). During the plate motion a shadow movement will also be generated. The shape of the shadow can reflect the surface form directly. If the testing surface is spherical the shadow shape will be straight edge when the test thin plate is cutting the converging or diverging reflected light.

The Foucault test is very useful to give zonal height information of the testing surface. This zonal focus is useful for optical fabrication in which the local height information is needed.

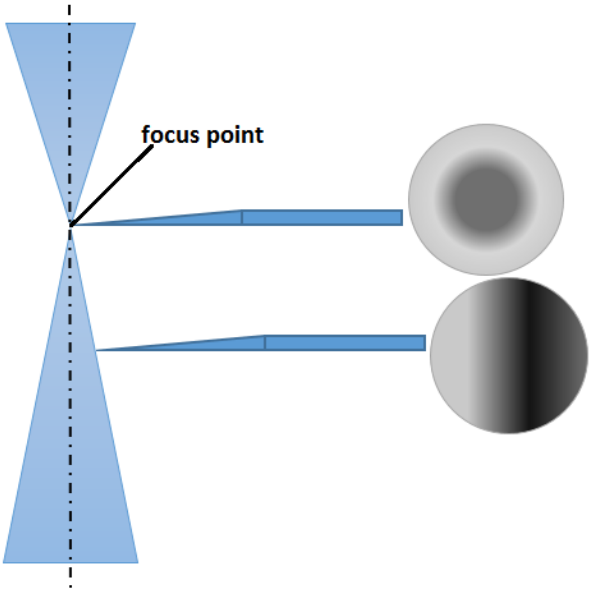

Figure 2-15 Foucault test

The advantages and disadvantages of the Foucault test method are listed below.

Advantages

- Foucault test is simple to conduct. The testing surface can be measured in a quick way and no additional optical instruments are needed.

Disadvantages

- Not quantitative when measuring the surface.

2.3.5.3 Ronchi Test

The Ronchi test was invented by Italian physicist Vasco Ronchi in 1923 [79]. It is actually a variation of Foucault test. The significant difference between Foucault and Ronchi test is replacing the thin and opaque testing plate by Ronchi grating. During test a Ronchi grating which consist of evenly spaced dark bars and stripes will be placed between the light source and testing surface (Figure 2-16). The incoming light passes through the Ronchi grating and reflected by the testing surface and then passes through the grating for the second time. There is one rule of explaining the observed patterns in the Ronchi test. The total amount of fringes observed is determined by the distance between the Ronchi grating and the focus of the testing surface. Specifically, the further the grating is moved from the centre of the curvature the patterns will

move closer. On the contrary, the fringe patterns will move more separately if the grating is moved towards the centre of the curvature.

If the testing surface has no aberrations the fringe pattern being watched should be clear straight dark and light bars. If the surface has any local surface form error the stripes will be dent due to the defocusing of reflected light.

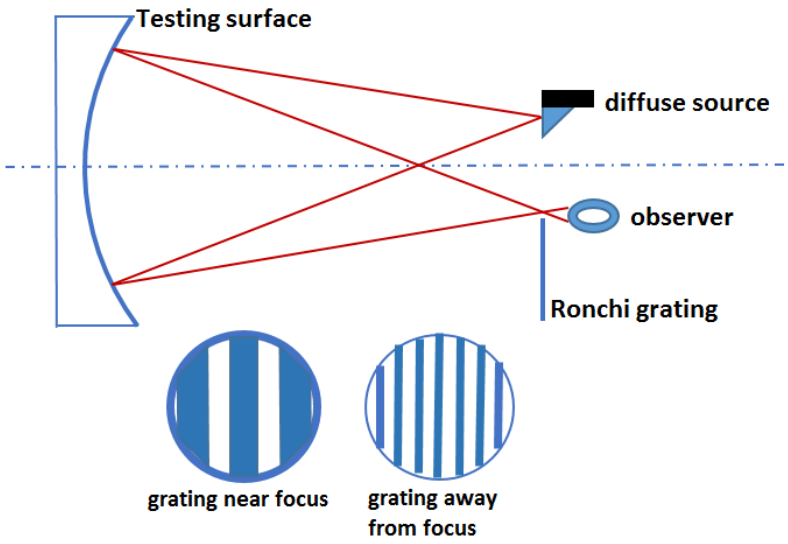

Figure 2-16 Ronchi Test

The advantages and disadvantages of the Ronchi test are listed below.

Advantages

- Ronchi test is simple to conduct.
- Diffuse light source such as white light can be used.

Disadvantages

- The phenomenon of diffraction can affect the measurement accuracy.

2.3.5.4 Software Configurable Optical Testing System (SCOTS)

SCOTS is a useful and powerful tool to measure the multiple lens without additional complex hardware configurations. The SCOTS utilizes the similar principle of Shack-Hartmann test, yet the experimental layout is reverse. Basically, the SCOTS uses a LCD screen which generates multiple dark and bright stripes

to illuminate the testing surface [80, 81]. A CCD camera is also used to capture the reflected or refracted image so that the wavefront slope variation information can be calculated [81].

When a reflective mirror is being tested, a LCD screen is placed face to the surface under testing (Figure 2-17). The position of the LCD screen is close to the centre of curvature of the surface under testing. When a pixel of the LCD screen is illuminated the light ray from this pixel is reflected by the testing surface and captured by the CCD camera. Based on the coordinates of illuminated pixel of the screen, coordinates of the CCD camera and testing surface we can calculate the surface slope. With the surface slope information and Zernike polynomial the final surface form can be reconstructed.

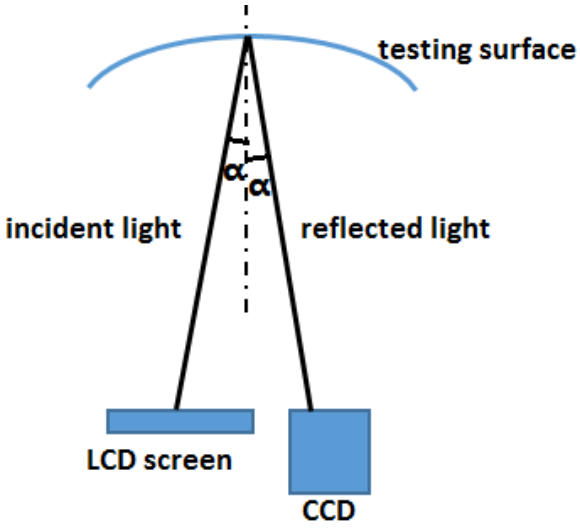

Figure 2-17 Geometry of SCOTS

2.4 Comparison and Contrast of Current Surface Metrology Methods

Methods	Advantages	Disadvantages
Contact Stylus Technique [31]	-Normally easy to use -Direct measurement method -Adaptive on hard and soft surfaces	-Potentially damage the testing surface -Potentially damage the stylus

	-Measure rough and specular surfaces	-Inability to measure surface features smaller than stylus radius -Only 2-D surface profile
Non-contact Stylus Technique [31]	-No damage on the surface -Fast measurement	
Coordinate Measurement Machine (CMM) [30,35,36]	-Long life time -High accuracy -Direct measurement	-Expensive instrument -Additional components required to measure structural surfaces -Not mobile
Swing Arm Profilometer (SAP) [37,38]	-Measure large optics -SAP can be integrated with the fabrication platform to achieve in-situ measurement	-Physical contact between the stylus and testing surface can cause scratches on testing surface -Surface reconstruction algorithm is required to get the final 3-D error map
Phase Shift Interferometer (PSI) [13,60]	-Fast measurement -High measurement accuracy ($\lambda/100$)	-Sensitive to the lab environment -Inability to measure steep surface
Sub-aperture Stitching [61,62]	-Can measure large optics -High measurement accuracy	

Deflectometry Method [64,65]	-Larger tolerance of testing surface dynamic range -Better tolerance to lab environment -No damage on testing surface	-Inability to measure rough surface -Transparent surfaces should be blacken
Computer Generated Hologram (CGH) [54,55,56]	-High accuracy in measurement of aspheric surfaces ($\lambda/100$) -Easy to implement	-Test plate with high transmissive material is expensive
Shack-Hartmann (S-H) Sensing Technique [75,76,77]	-Easy to configure -High dynamic range -High measurement accuracy	-Accuracy is limited by alignment -Expensive (High resolution CCD camera)
Foucault Test [13]	-Simple to conduct -No additional optics are needed -Sensitive	-Not quantitative
Ronchi Test [78]	-Simple to conduct -White light source	-Diffraction limits the accuracy
Phase Diversity (PD) and Wavefront Curvature Sensor Method [79,80,81]	-Less detector pixels needed -Simple light path layout -No reference point light resource is needed	-Smaller dynamic range than S-H -Algorithm is complex and long computation time
Shearing Interferometers Method [82]	-No reference wavefront is needed -Low cost and easy to make	

	-Measure large aperture optics	
Software Configurable Optical Testing System (SCOTS) [82,83]	-Easy to set up -Low cost -High accuracy rival interferometers -Adaptive to measure any form of specular surfaces	-Inability to measure rough surface

2.5 Recommendations

This chapter introduced a series of surface metrology methods for different size of optic components with flat, spherical and aspherical surface form. Currently, both contact and non-contact methods are widely used in optic metrology. Both contact and non-contact surface metrology methods have their own advantages and disadvantages.

In order to meet the future requirements in the field of surface metrology for large size optics, new surface metrology instruments are expected to have the following capabilities:

- No surface damage to testing surface during measurement.
- Can measure both ground and shiny surfaces.
- Can measure optical component with an aperture of 1 meter.
- Measurement instruments are integrated with optic fabrication stage in order to achieve in-situ measurement.
- Can complete surface measurement in fast (less than 1 hour).

No surface metrology methods introduced in this chapter can satisfy all the above requirements.

A pragmatic method which used a high precision non-contact chromatic probe (resolution: 20nm) which was mounted on the terminal of an ABB industrial robot combined with a rotary table was put forward. The existing mechanical air-bearing rotary table can be used for both surface fabrication and measurement. This

integration of both optic fabrication and metrology can definitely improve efficiency. This method is nominated as Swinging Part Profilometer (SPP) and its principles are explained in chapter 3.

Chapter 3 Development of Swinging Part Profilometer (SPP) System

3.1 Introduction

After reviewing most of the major surface metrology methods in Chapter 2 it is necessary to introduce the principles of Swinging Part Profilometer (SPP). An ABB industrial robot is performed as a versatile instrument to provide two functions, one is automating currently-manual functions on a Zeeko CNC polishing machine (or grinder), and the other one is providing its own right as an intermediate smoothing process between CNC grinding and polishing [6, 8, 83].

SPP was designed as the surface metrology instrument to support this intermediate surface smoothing process (Figure 3-1). The introduction of SPP can enhance the capabilities of an industrial robot. This has led us to consider a new surface-metrology device, the "Swinging Part Profilometer" (SPP) for in-situ measurement. The instrument is functionally a reversed version of a Swinging-Arm Profilometer (SAP) [37, 42, 84-86].

The SPP mechanical platform uses a 1.2 meter diameter air-bearing rotary table with an ABB motor which can spin the rotary table. The measurement principles of the SPP determines that it can provide the topography of the following forms of optic components:

- Flat optics;
- Spherical concave optics.

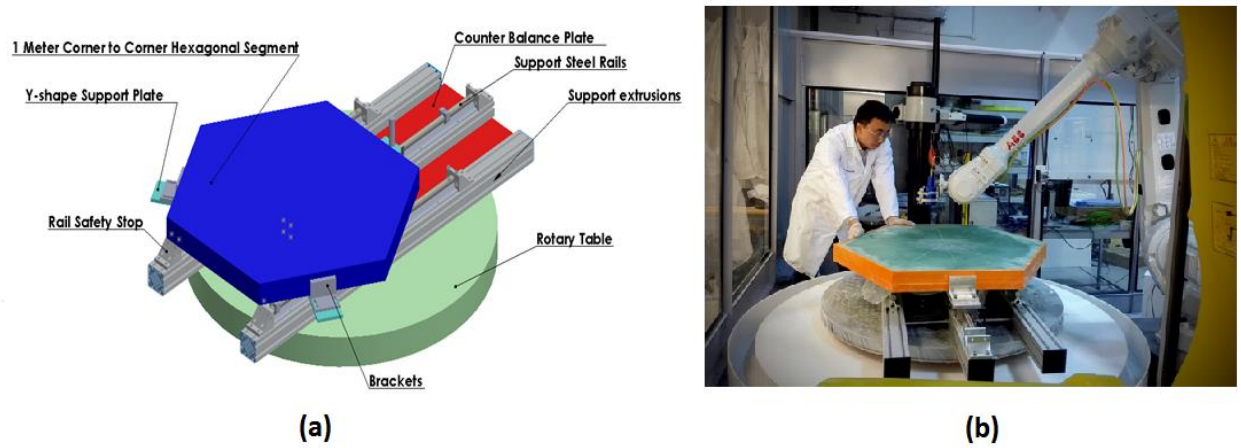

Figure 3-1 General assembly of the SPP

3.2 Basic Swinging Part Profilometer (SPP) Configuration

The SPP consists of a 1.2 meter diameter air-bearing rotary table which locates on top of the large square shape granite basement (Figure 3-2), which was originally built for measuring Wolter-type X-ray mirrors and mandrels, and kindly provided to us by Brera Observatory. The rotary table is powered by an ABB motor and the turntable belt rotary drive-system so that the table can be rotated with full revolutions or specified angle at a specified speed.

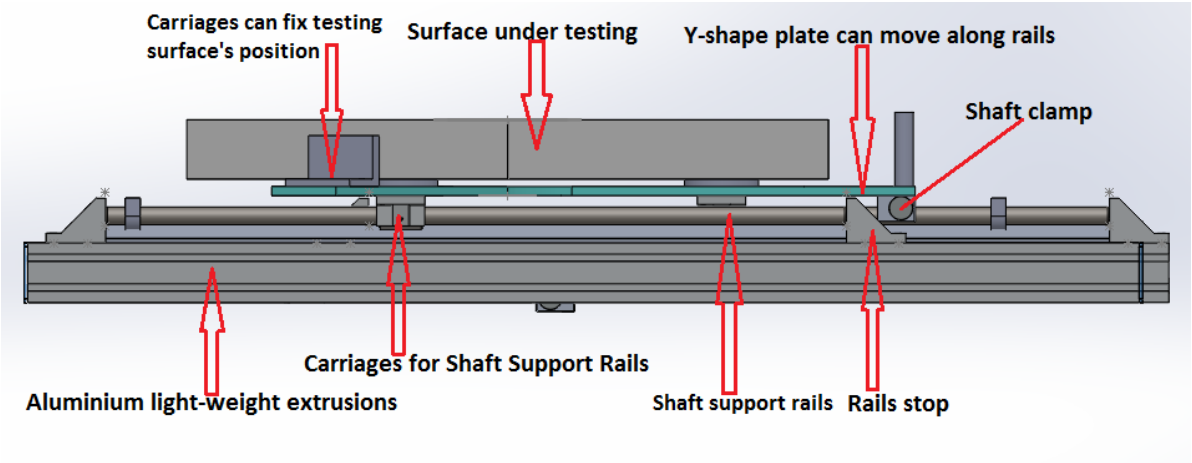

Figure 3-2 SPP Support and Sliding System

- Three light-weight design aluminium extrusions (1.5 meter length) mounted on the surface of the rotary table (Figure 3-2). The extrusions were used to enhance the stiffness of the shaft support rails which were mounted on tops of the light-weight design aluminium extrusions.

- Three hardened and ground carbon steel shaft rails were mounted on top of the aluminium extrusions. The three steel rails enable the testing surface to slide with the help of carriages (Figure 3-2).
- There is a Y-shape plate with three carriages so that the Y-shape plate can move along the support rails (Figure 3-2). The Y-shape plate was designed to load the surface under testing.
- A shaft clamp was mounted underneath the Y-shape plate so that the testing surface can stop at a specified position when a hand bar was pressed down (Figure 3-2).
- Each carbon steel rail accompanied one pair of aluminium made rails stops which were placed on the two terminals of the rail. These rail stops can guarantee that the motion of a surface under testing can be defined with a limited range (Figure 3-2).
- Three aluminium clamps were installed at the end of three branches of the Y-shape plate in order to fix the position of a testing surface (Figure 3-2).

3.3 The Principles of the SPP Operation

The SPP operates by positioning the measurement probe normal to the surface under testing and remain static. Then power the ABB motor which was integrated with rotary table. The motor was manipulated by the Matlab so that the testing surface can be rotated with one full revolution.

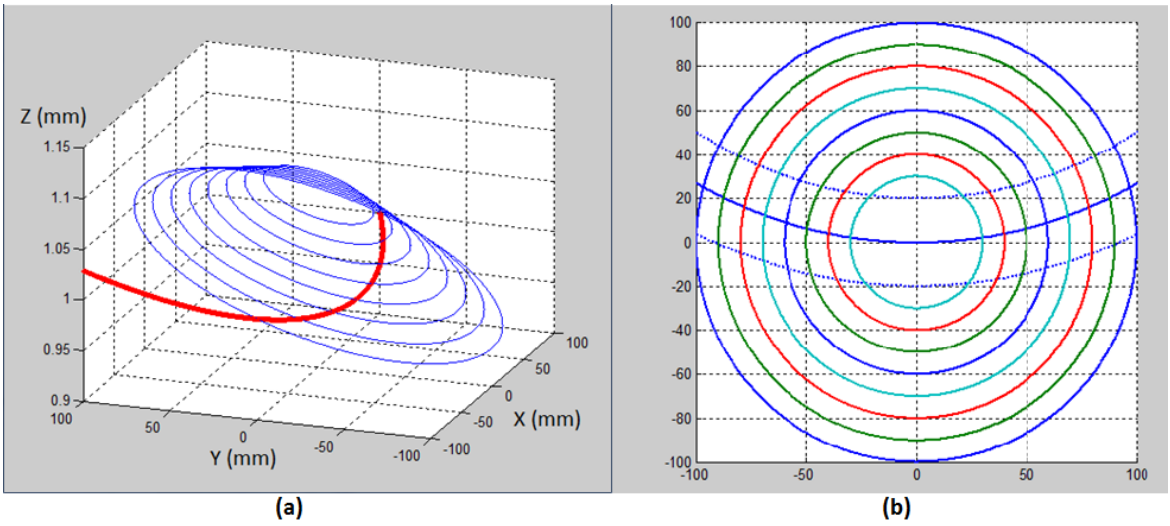

Figure 3-3 SPP Measurement Principles

- Align the position of a testing surface so that its centre coincides with the rotation axis of the ~~air-~~ air-bearing rotary table.
- Conduct outermost circular scan on the surface under testing. Move the non-contact metrology probe which was mounted on the end of ABB industrial robot arm. The first circular scan should be as close as possible to testing surface's edge. This step can make the surface measurement cover more area.
- Repeat the previous step so that a series of concentric scans can be made (Figure 3-3). Use Matlab software to control rotary table to spin with 360 degree. Metrology probe can collect the height data during table's rotation.
- An arcuate scan which passes through all the concentric scans was necessary to make the data stitching after the con-centric profiles are collected. When conducting the concentric scans the surface under testing remains static the metrology probe was manipulated to move with a specified distance. This probe's movement will cause the relative height of adjacent circular scan data cannot accurately reflect the testing surface (Figure 3-3). Therefore an arcuate scan which passes through all the circular scans can determine the relative height of all the concentric scans (Figure 3-3). The work-piece is moved with a specified distance with the sliding rail system. Control of the rotary table rotate through a certain angle so that an arc profile can swing across the work-piece. The arc profile was defined by both the work-piece decentering distance and profiling start point. Repeat the above step with different off-axis distance so that the other two arc scans are measured.

3.4 The Synchronization for Rotary Table with Metrology Probe

The whole Swinging Part Profilometer (SPP) surface metrology instrument consists of an air-bearing rotary table, ABB industrial robot, metrology probe, a motor which was installed underneath the rotary table and a computer (Figure 3-4).

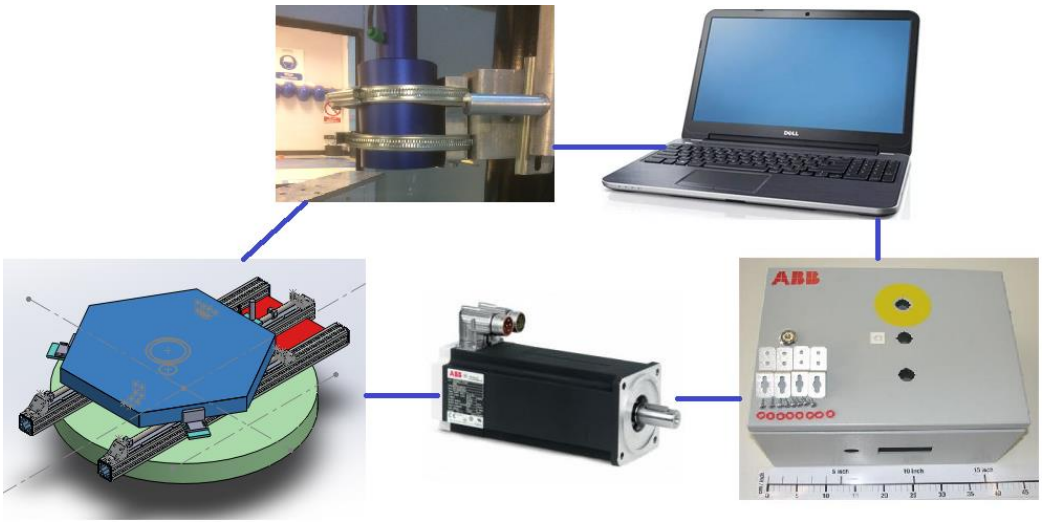

Figure 3-4 SPP System Diagram

It is necessary to synchronize the air-bearing rotary table with the metrology probe so that the rotary table rotation and metrology probe's data collection can be executed simultaneously. The Matlab software was used as the platform to establish the connection between rotary table and metrology probe. In other words the probe traverse data collection and rotary table motion must be started simultaneously. The steps of conducting the synchronization for rotary table with metrology probe are introduced below:

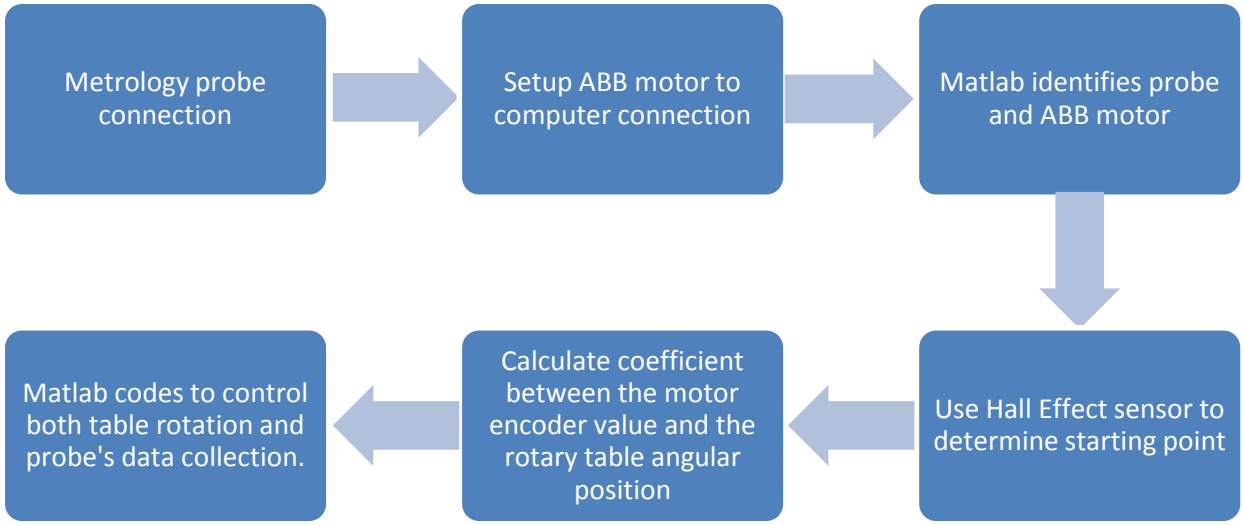

Figure 3-5 Synchronization for Rotary Table with Metrology Probe

- Connect metrology probe to the computer;
- Connect ABB motor control box to the computer with the Ethernet cable;

- Establish the connection between Matlab and metrology probe. Use the ‘instrfind’ command in Matlab to read serial port object which was connected with metrology probe from memory to Matlab workspace;
- Use the Hall Effect sensor which was installed underneath the rotary table for sensing the starting position of the rotary table. This step can guarantee that the rotary table can start its motion from the same angular position (starting position) when the measurement is conducted;
- Calculate the coefficient between the motor encoder value and the rotary table angular position. This step is the foundation for controlling rotary table to rotate as a specified angle. First use Matlab to control the rotary table to rotate its original point by reading the Hall Effect sensor output. Record the motor encoder value by reading ABB motor motion control software. After that program the rotary table continuous motion until it stops as its original position again. The Hall Effect sensor will trigger the ‘stop’ command to the motor. Record the motor encoder value for the second time. Finally, based on the motor encoder values and rotary table’s diameter the coefficient can be calculated. Therefore the rotary table’s angular position can be determined.
- Programming in Matlab in order to control the rotary table to rotate as a specified speed. This program enables the rotary table to spin with a full revolution or any specified value of angle. When the preset value is achieved the Matlab program will send command to the ABB motor to trigger the ‘stop’ function so that the rotary table can stop.
- Both the rotary table’s angular position and metrology probe’s data were recorded when the table was spinning as a specified speed.

3.5 Metrology Probe Mounted on Cast Iron Arm or ABB Robot Arm

The metrology probe remains static during the whole surface measurement. There were two options available to hold the metrology probe, manual cast iron arm and ABB robot arm (Figure 3-6). The drawback of mounting the probe on the end of the cast iron arm is that positioning the probe tip to the specified point

on the testing surface is difficult. The absence of motor and encoder makes it impossible to precisely control the movement of the prove tip.

The ABB industrial robot can overcome this shortcoming. The ABB Teach Pendant allows the probe tip to move along the testing surface with the increment of 0.1 millimetre. Based on the above consideration the metrology probe was finally mounted on the terminal of the ABB robot arm.

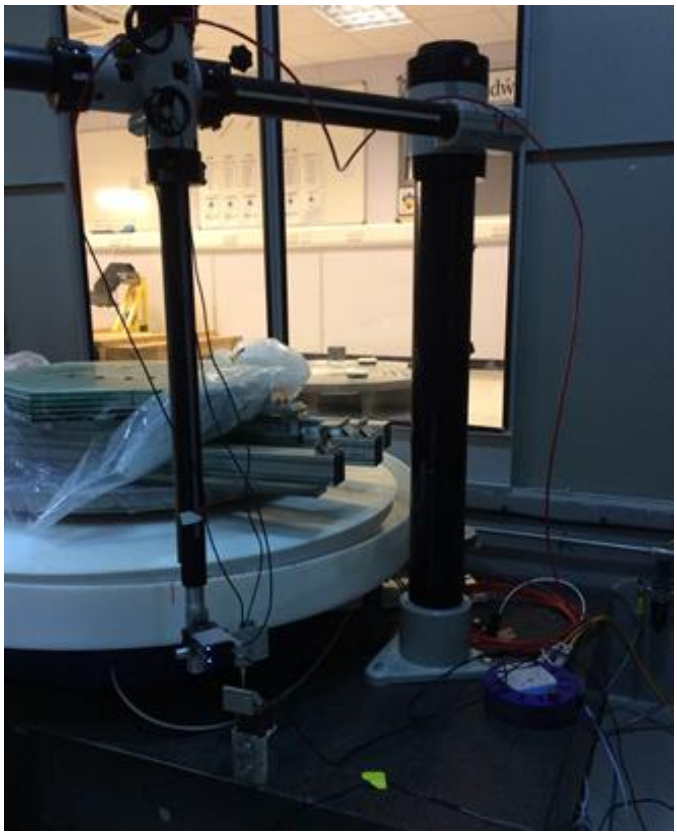

Figure 3-6 Metrology Probe Mounted on Cast Iron Arm

3.6 Metrology Loop Test and Environment Characterization

The effects of lab temperature variations on the dimensional relationship between probe and work-piece is potentially an important term in the overall metrology error budget. During the surface measurement by SPP the metrology probe remained static. Therefore, it is necessary to test metrology probe's data variation when the probe was mounted on the terminal of an ABB robot arm (Figure 3-7).

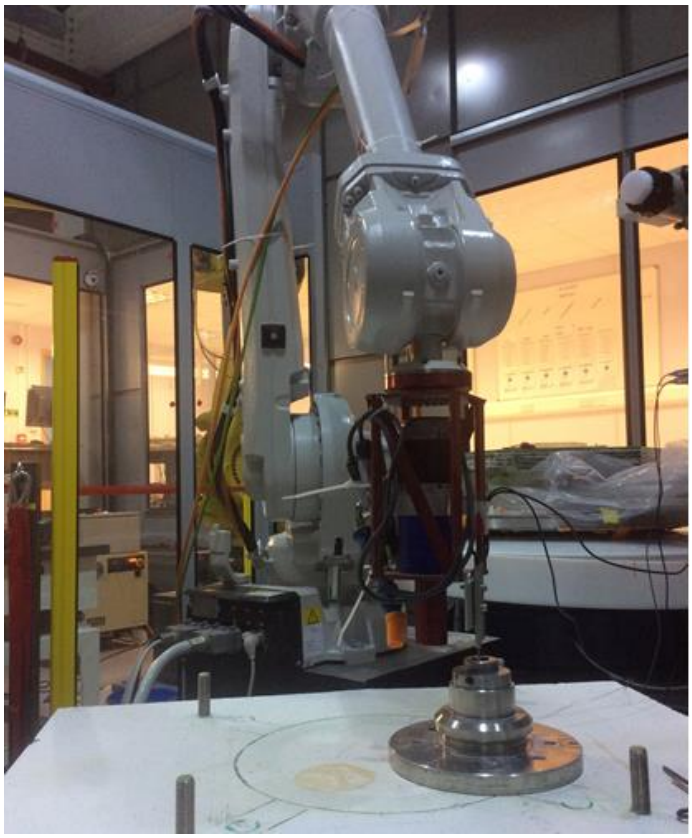

Figure 3-7 Probe Mounted on ABB Robot

To explore this, the probe and work-piece were left in contact but undisturbed for 18 hours, and probe-data collected and plotted (Figure 3-8). A periodic variation in both the probe's readings and temperature log were observed: the lab temperature cycling over +/- 1 ^{o}C with a 30 minutes period. The probe data (red line in (Figure 3-8) followed a similar pattern. Therefore, the periodic variation is attributed to thermal expansion effects, in particular of the ABB robot arm. In practice, the probe is required to remain at a fixed vertical relationship with respect to the work-piece during only a single scan. The typical single-scan time as currently configured is 150 seconds (full rotation of turntable). The typical slope in the probe-data of Figure 3-8 is then 3 microns/ ^{o}C. From this, we estimate that the measurement height-error introduced by such a temperature excursion during a single scan, is 0.6 microns.

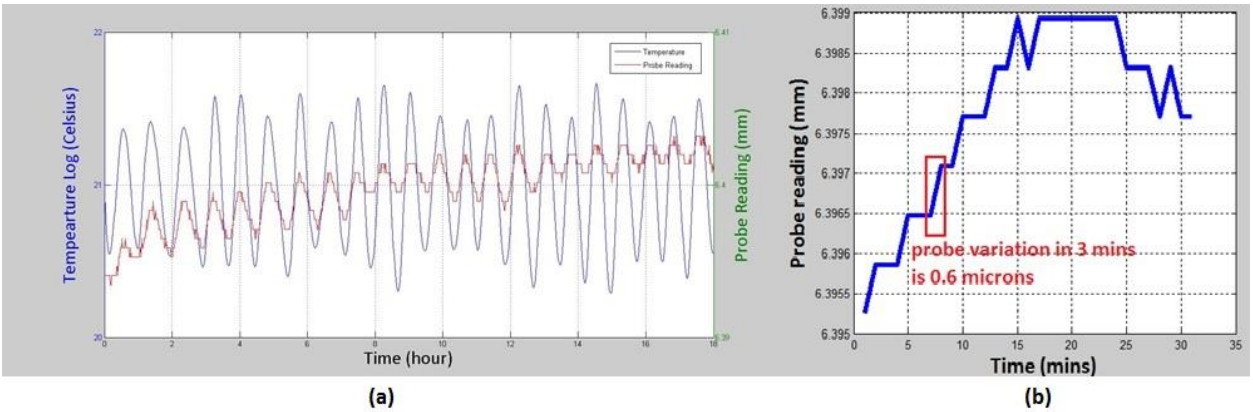

Figure 3-8 Environment characterization test within 18 hours

3.7 ABB Robot Arm Characterization

Next we consider in more detail the stability of the robot-mounted measurement probe during the period of each measurement scan. Given the 150 second typical rotation time of the rotary table, we have collected static probe data over 3 minute periods. The probe data variation, attributed to vibration, was 0.6 μm PV (Figure 3-9), although this is clearly close to the resolution of the probe used (probe resolution: 300nm). The value of the probe data variation during 3 minutes (full rotation of rotary table) is consistent with the thermal drift (Figure 3-8).

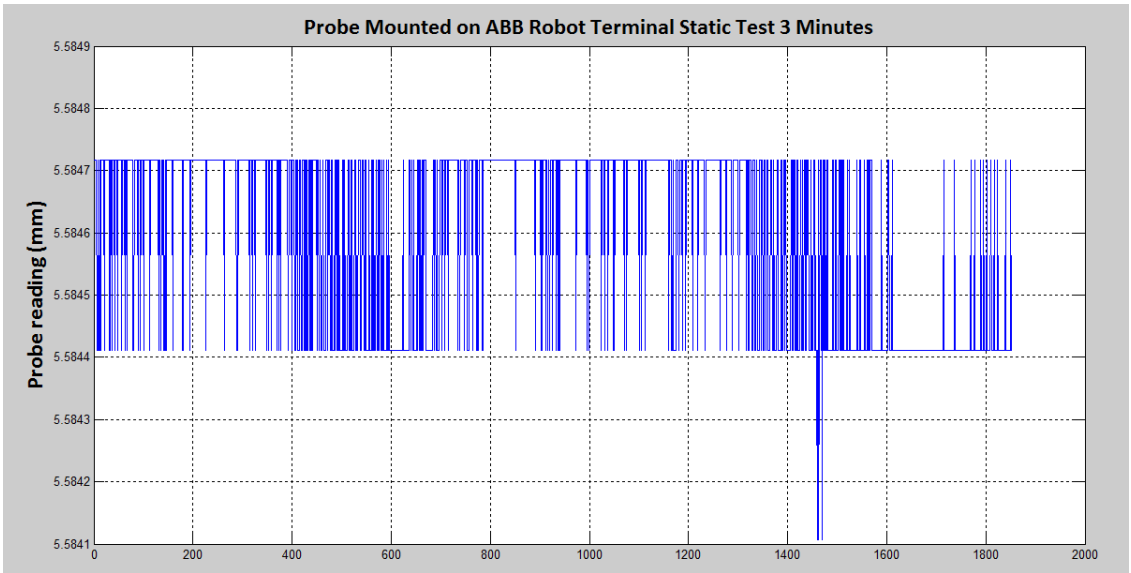

Figure 3-9 ABB Static Test in 3 Minutes

3.8 Matlab Graphical User Interface (GUI) Design

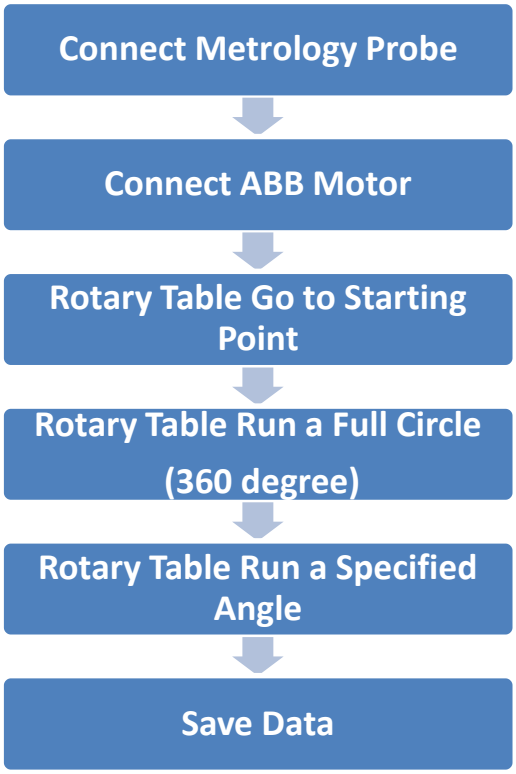

Figure 3-10 Matlab GUI for SPP Control

This section is focusing on developing a Matlab Graphical User Interface (GUI) to control both the ABB motor and Solartron pneumatic contact probe or Armstrong Precitec optical non-contact probe. The ABB motor was installed underneath the rotary air-bearing table. A metrology probe was also controlled by this Matlab GUI to collect s testing surface data.

A Matlab GUI can provide a point-and-click control of software application without learning a new program language. The Matlab GUI contains controls such as menus, toolbars, buttons and sliders. Developers can design their own applications and functions in GUI for other users to use.

The Matlab GUI specifically developed for SPP control and surface data collection contains four main functions (Figure 3-11).

- Initialization-This includes identify the metrology probe and set up a connection through a USB cable. Then GUI will establish a communication through an Ethernet cable. This Matlab GUI is

capable of controlling the motor so that the rotary air-bearing table can spin clockwise or anti-clockwise.

- Circle data logging-When user pressed the button named ‘One Full Circle’ on the Matlab GUI the Matlab will execute a command which can make the rotary air-bearing table spin for 360 degree.
- Arc data logging-The user was required to type in the angle value (degree) which an arc scan will scan. After that when the button named ‘Arc Scan’ on the Matlab GUI was pressed the rotary air-bearing table would spin the angle which was specified before.
- Data saving-When all the concentric scans and arc scan data were collected it was necessary to save them in TXT file. Each TXT file contains two columns, the first one is the rotation angle of the rotary table and the second one is the metrology probe’s data.

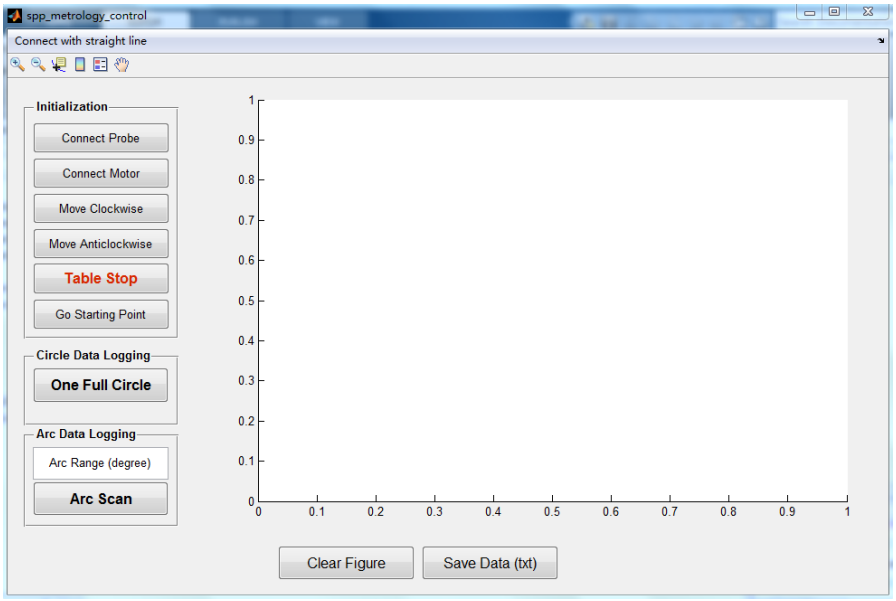

Figure 3-11 Matlab GUI for SPP Operation Control

3.8.1 ABB Motor Motion Control

In order to obtain a series of concentric scans and one arc scan the rotary air-bearing table was required to spin with pre-determined angle and a direction of clockwise or anti-clockwise. Therefore, a series of command were need to execute so that the rotary table can rotate as specified.

Mint™ is a language which was developed for motor motion control applications. In the case of SPP surface metrology the motor was required to run with simple and basic functions such as enabling motor axes, motor motion with different directions, motor motion with specified speed and motor stop. A number built in motion specific keywords were used to control the motor.

- Enabling motor axes-Before motor motion can be executed on an axis, it was required to be enabled. In order to activate the enable output the 'DRIVENABLE' keyword was used. After that the motor was ready to run.
- Motor motion speed control-The ABB motor can spin with different speed as specified. The 'JOG' keyword can enable the motor to run.
- Motor motion stop control-The 'STOP' keyword can perform a stop function on the motor.

3.8.2 Rotary Table Go to Starting Point

The rotary table was designed to spin from the same starting point for all concentric scans measurement. This starting point was marked by a Hall Effect sensor which was installed underneath the rotary table (Figure 3-13).

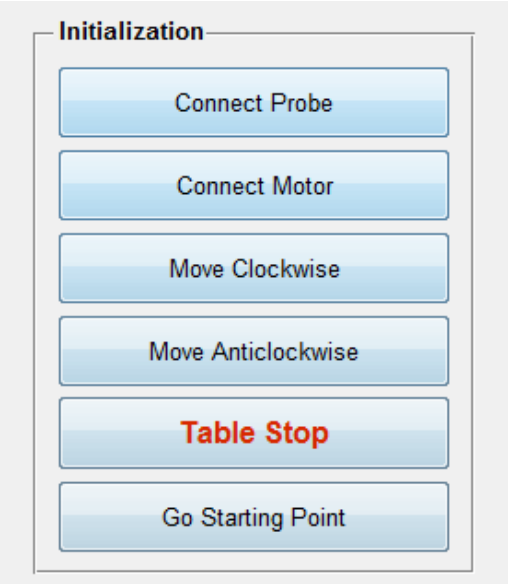

Figure 3-12 Matlab GUI Rotary Table Go to Starting Point

Matlab software can read the current value of the Hall Effect sensor (responding time: 100A/μ S) and this value was marked as 'x_0'. Then the command 'invoke (h, 'jog', 0, 20)' can power the motor to spin continuously with a constant speed. As the rotary table spinning the Matlab was obtaining the value of Hall Effect sensor and its output was marked as 'x_1'. When the magnet was moved just above the Hall sensor where was determined as the starting point, in the Matlab codes the judgement 'if (x0==0&x1==0)' was made, the motion stop command 'invoke (h, 'DoStop', 0)' was triggered.

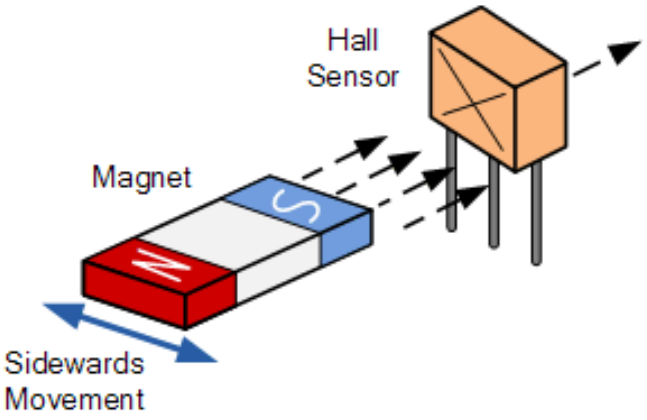

Figure 3-13 Hall Effect Sensor Working Principle

The Hall Effect sensor uses the principles of Hall Effect. The Hall Effect is when a conductor or semi-conductor with current flowing in a straight direction, the straight current flowing direction will be disturbed if this conductor or semi-conductor located in a magnetic field. A voltage difference which is perpendicular to the current flowing direction can be detected. The Hall Effect theory was discovered by Edwin Hall in 1879 [87].

The SPP used a Hall Effect sensor (Table 3-1) which was installed on the outer side of the rotary table's basement and the magnet was installed underneath the rotary table. The magnet will move in a circular path when the rotary table is rotating. The starting position of the SPP was defined when the magnet was on top of the Hall Effect sensor. Therefore, when the magnet is on top of the Hall Effect sensor again the rotary table was rotated with a full circle (360 degree).

Table 3-1 Hall Effect Sensor specifications

Type	NJK - 5002C
Appearance	M12mm cylinder
Output	NPN three wire normally open type
The detection distance	10 mm
Supply voltage	5-24VDC,6-36VDC
Output current	200 mA
Objects can be detected	permanent magnets
Switching frequency	320 KHz
The shell material	copper
Thread Length	50 mm

Based on the specifications above (Table 3-1) the Hall Effect sensor has a switching frequency of 320 KHz. It means the Hall Effect sensor can switch from its on-state to off-state for once with the time of 1/320000 seconds. The rotary table can rotate with a full circle (360 degree) in 2 minutes and 30 seconds. Therefore, during the tiny period of 1/320000 seconds for Hall Effect sensor switching its state of on and off the rotary table can rotate with an angle of:

$$\theta = \frac{360}{150} \times \frac{1}{320000} = 7.500000000000000e^{-6}(deg) \quad (3\text{-}1)$$

When the rotary table was rotated with a full revolution (360 degree) the metrology probe's collected data varied since the rotary table's rotation axis was tilted. The maximum probe data's variation was 1.791915893554688e^{-05} mm when the metrology probe traverse the largest circle with a radius of 100 mm. Therefore, when testing a flat surface the Hall Effect sensor can cause the maximum metrology probe's data variation of 17.92 nm.

3.8.3 Rotary Table Full Circle Scan

When the rotary air-bearing table was moved to the starting point the table was about to spin for 360 degree in order to obtain the circular scan data. The positional encoder installed underneath the rotary table was

compulsory to get the table position information. In order to obtain rotary table position information the coefficient between the encoder output and rotary table's rotation angle was firstly calculated. At the starting point the output of the encoder was marked as 'E_0'. Then command the rotary table to spin a little so that the Hall sensor was moved ahead of the magnet. Stop the motion of the rotary table. After that press the button 'Go Starting Point' once in Matlab GUI to perform the rotary table to move to its starting point again. Until now the rotary table was rotated for one circle and the encoder output was marked as 'E_1'. Therefore the coefficient between the encoder output and the rotary table's rotation angle was described as:

$$\mathrm{k} = \frac{E_1 - E_0}{360} \tag{3-2}$$

After determining the coefficient it was time to conduct the coding for rotary table 360 degree motion. Firstly, the rotary table was performed to run as a steady speed and mark the initial output of the encoder. Then a 'while' loop was executed repeatedly and a 'if…else' condition at the end of the 'while' loop can stop the loop execution. When the rotary table's rotation angle was greater than or equal to 360 degree the 'while' loop stopped. Finally, a stop command was executed to stop the motor motion.

Besides controlling the rotary table's motion the metrology probe's data was required to collect. Both rotary table's rotation angle and probe's data were required to log. The table's current rotation angle (degree) can be determined as:

$$\text{Current angle} = (Encoder_{current} - Encoder_{original}) \times \mathrm{k} \tag{3-3}$$

The rotary table's rotation angle was stored in a variable named 'current angle' and metrology probe's data was stored in a variable 'probe data'. Then both 'current angle' and 'probe data' were stored in a TXT file as two columns (Table 3-2). Table 3-1 is an example which illustrates data collected by the chromatic probe is stored in a TXT file. Each rotary table's real-time rotation angle has one corresponding probe's data. The rotary table's current rotation angle was calculated by the initial encoder value and current encoder value.

Table 3-2 Collected Data in Two Columns

Rotation angle (degree)	Probe data 'Z' direction (mm)
2.6968307e-02	6.0351563e+00

4.2699820e-02	6.0351563e+00
1.0787323e-01	6.0357666e+00
1.9327287e-01	6.0351563e+00
2.4720948e-01	6.0351563e+00
2.7642515e-01	6.0357666e+00
2.8541459e-01	6.0357666e+00

3.9 Chromatic Probe Calibration

Normally, a metrology probe should be calibrated by another device with known accuracy[88]. The SIOS miniature interferometer with reflective mirror is a precision length, displacement measurement instrument. During measurement experiments all of the interferometer laser sensor head, aluminium coated mirror and testing optical probe will be aligned on the same straight line (Figure 1-1). The lateral position of the mirror can be slightly repositioned with the X-Y stage (Figure 3-14). This tiny displacement can be measured by both SIOS interferometer and Armstrong optical probe. The resolution of the SIOS laser interferometer is 20pm (0.02 nanometre) which is much higher than the probe's resolution. Therefore, the accuracy of the optical probe can be measured and determined by the laser interferometer.

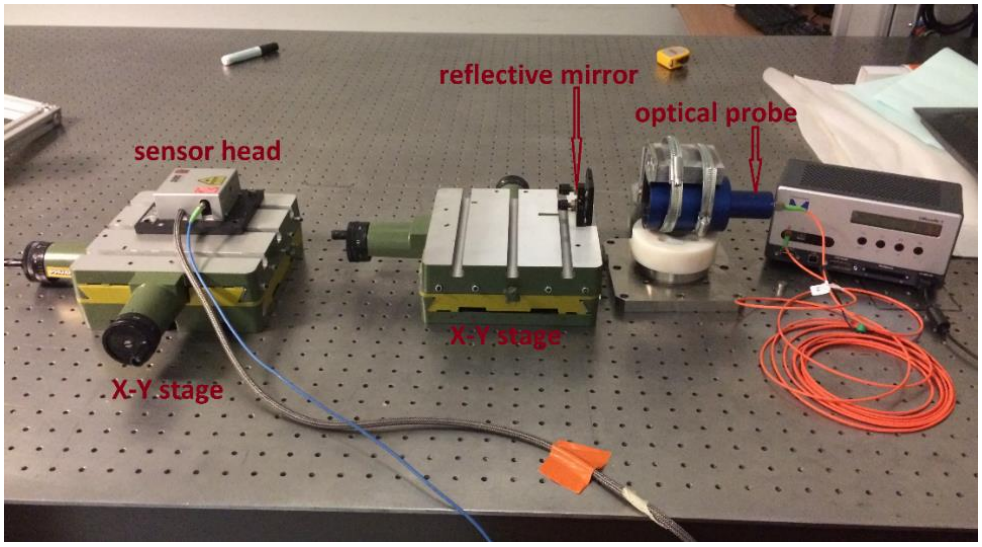

Figure 3-14 Armstrong Chromatic Probe Calibration

3.9.1 Experiment Procedures

- Connect all the SIOS laser interferometer components: laser sensor head, optical fibre, power supply and modular data processing unit (Figure 3-14).
- Align the laser sensor head with the reflective mirror. The alignment must be conducted so that the direction of the reflected laser by the mirror will coincide with the measurement axis. The alignment can be operated by either adjust the sensor head by using adjustment screws or positioning the reflective mirror. The alignment can be completed when the reflected laser spot is just on the centre of the alignment target spot on the sensor head.
- The motion of the reflective mirror can be controlled by utilizing rack and pinion of the X-Y stage. Using the adjustment screw for the measurement axis direction so that the mirror can be moved with the increment of 10 μm, 100 μm or 500 μm. Each time the mirror displacements can be recorded by both laser interferometer and optical probe. The two readings are recorded separately in an Excel file (Figure 3-15).
- The measurement experiments can be divided into three groups by different measurement range: 100 μm, 1000 μm and 8000 μm. The accuracies of the optical probe in different measurement range can be determined. This accuracy value is one of critical component of the Swinging Part Profilometer metrology uncertainty budget.

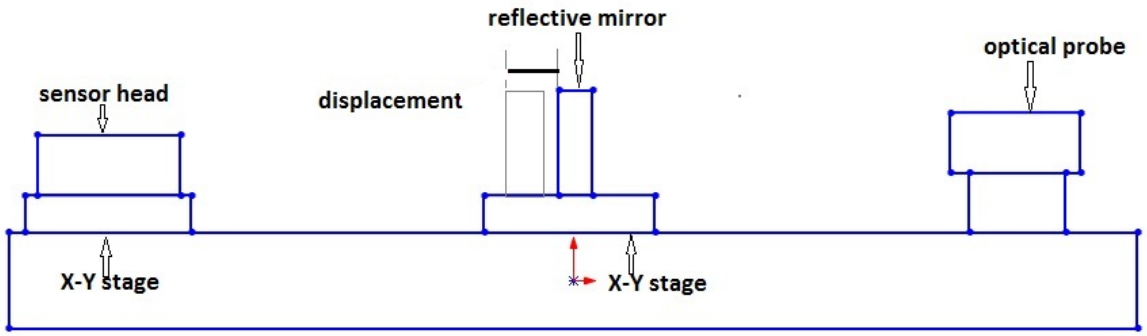

Figure 3-15 Experiment Principles

3.9.2 Data Processing

The mirror displacement measurement range was configured as 0.1 millimetre, 1 millimetre and 8 millimetre. The optical probe will be used for measuring flat and spherical surfaces. When measuring the flat surface the peak-to-valley (PV) value won't be exceed to 1 millimetre. Similarly, the PV for spherical surface will be within 8 millimetre when the surface curvature of radius (RoC) is 3 metres.

When conducting the experiment of 1 mm range, first set up the laser interferometer so that the initial value is zero. After that repositioning the X-Y stage with the increment of 0.1 mm. This displacement can be measured by laser interferometer as d1 and updated distance between mirror and probe can be measured by optical probe as d2. Repeat the above procedure so that we get another pair of readings d3 and d4. Totally ten pairs of readings can be collected. Then we subtract d2 from d1 we get δ1. Ten differences from δ1 to δ10 can be calculated. The Matlab was needed to process all the data. We used the Curve Fitting Tool in Matlab to find the best fitting line for all the differences value δ1 to δ10.

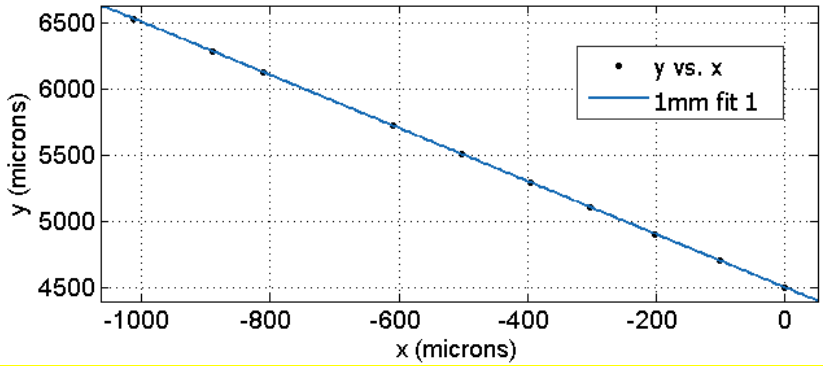

Figure 3-16 Best fitting line of collected data

In the figure above (Figure 3-16), Y axis refers to δ value and X axis is the mirror displacements from 0 to 1 millimetre. In the ideal circumstances all the δ values can be linked to a straight and smooth line. Actually, the ideal straight and smooth line cannot be drawn since the accuracy of the optical probe is below the laser interferometer. With the recorded interferometer data and optical probe readings, the best fitting straight line can be generated by Curve Fitting Tool.

For each the collected chromatic probe readings, there is a difference called between probe reading and best fitting point (Figure 3-17). This difference value can be regarded as the accuracy of the chromatic probe within specified measurement range. This residual can be plotted and calculated by Matlab Curve Fitting Tool.

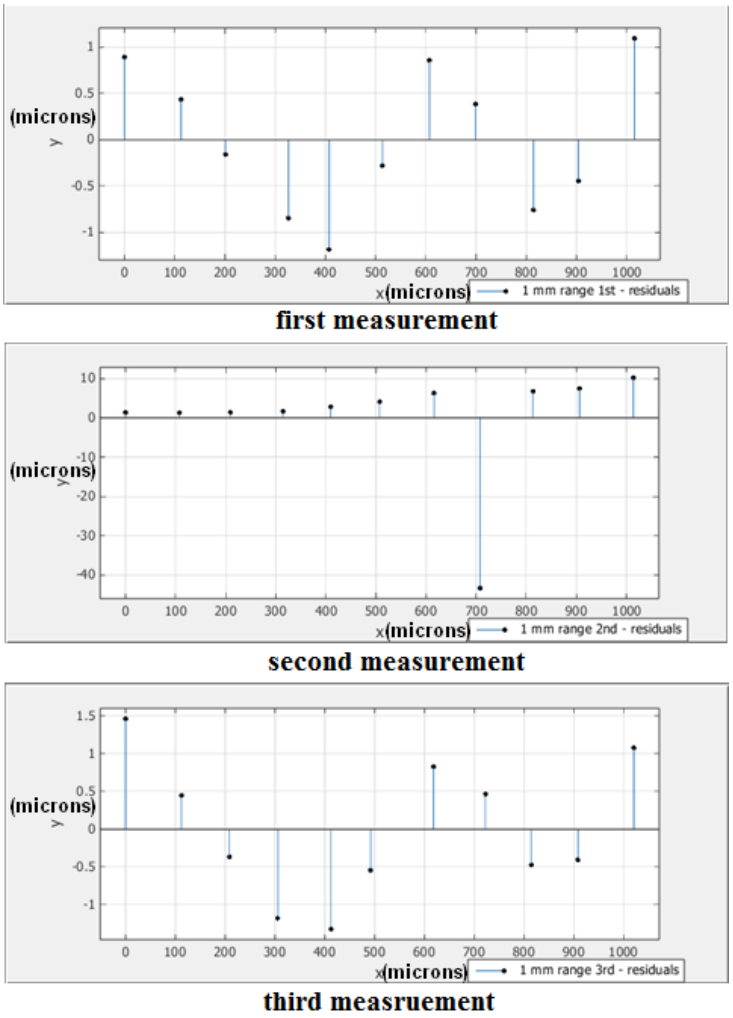

Figure 3-17 Residuals for the best fitting line

During the first measurement test with the range of 1 millimetre the root-mean-square error (RMSE) of 11 logged data is 0.8197. All the RMSE are listed in the table below (Table 3-2).

Table 3-3 RMSE with best-fitting line within different measurement range

RMSE (Root mean square error)	0.1mm range	1.0mm range	8.0mm range

RMSE	0.2256	0.8197	3.641
RMSE	0.1741	15.47	3.546
RMSE	0.1287	0.9640	3.473

It can be noticed that the second RMSE in 1 millimetre measurement range is 15.47 which significantly larger than the other two 0.8197 and 0.964. Therefore, this result was abandoned. Based on the theory of uncertainty the probe accuracy with 8 millimetre range is: 2*3.641=7.282 (μm). The probe accuracy will increase with measurement range (Table 3-4).

Table 3-4 Chromatic probe accuracy within different measurement range

	0.1 mm	1.0mm	8.0 mm
Probe accuracy (μm)	0.4512	1.9280	7.2820

3.10 Summary

- In this chapter the measurement principles of SPP were introduced.
- The synchronization between the chromatic probe and the rotary table was conducted. This synchronization was necessary since this step can guarantee that both the table rotation and metrology probe's data collection can be started simultaneously.
- Two options of holding the metrology probe were compared by testing the probe for 18 hours. Based on the experiment data the ABB industrial robot was chosen to host the chromatic probe for surface measurement since it had better stability compared with the cast iron arm.
- A Matlab based programme was developed by the thesis author. The Matlab programme was specifically used to control both the rotary table's rotation and probe's data collection.
- The chromatic probe's accuracy with different measurement range was tested. It can be seen that when increase the measurement range the probe's accuracy decreased.

Chapter 4 System Test on Flat Surface

4.1 Introduction

After designing all components of Swinging Part Profilometer (SPP) and installing them properly it is necessary to test the operation and performance of the SPP. A hexagonal flat mirror was chosen as a testing surface. The mirror has a dimension of corner to corner 300 millimetre and a flat back surface. The testing mirror's upper surface was measured by SPP and all the collected scan data was stitched to a 3D surface form. The procedures of testing a flat surface by SPP was stated below (Figure 4-1):

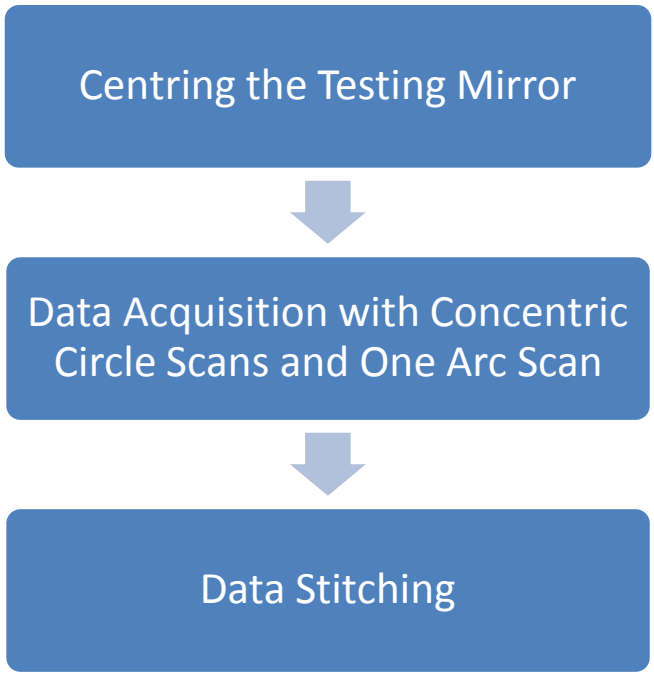

Figure 4-1 SPP measurement procedures

4.2 Centring the Testing Mirror

As mentioned in previous chapter the surface measurement was conducted by rotating the 1.2 meter air-bearing table and a metrology probe remained static. Therefore the first step should be position the testing mirror so that its geometric centre coincides with the air-bearing table's rotation centre (Figure 4-2).

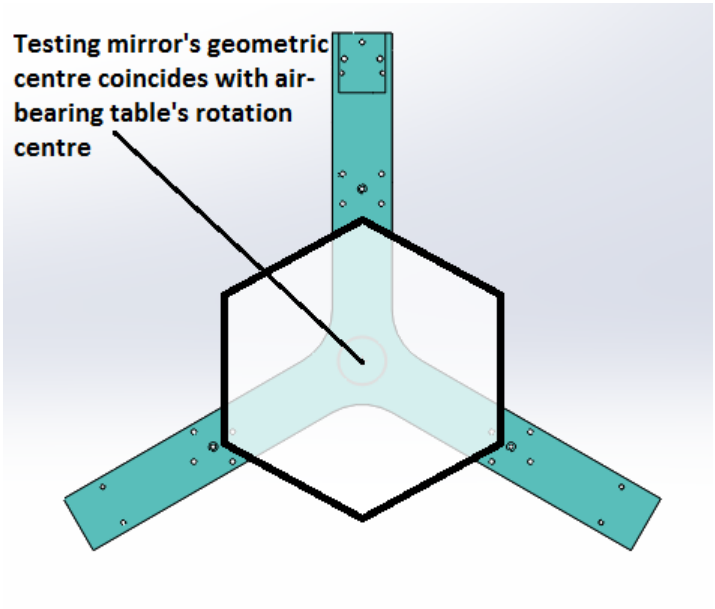

Figure 4-2 Centring the Testing Mirror

- Attach a mark pen on the terminal of an ABB robot arm and align the pen so that it is perpendicular to the testing mirror. Control ABB robot arm to move the mark pen until its tip touched the Y-shape plate.
- Program the Matlab software to control air-bearing table to rotate for 360 degree. The mark pen drew a full circle since it remained static during table's rotation. The centre of this circle is the air-bearing table's rotation centre.
- Position the testing mirror so that its geometric centre coincides with table's rotation centre.

4.3 Test the Hexagonal Mirror

4.3.1 Data Acquisition

After centring the testing hexagonal mirror a metrology probe mounted on the terminal of an ABB robot arm was controlled to move downward to testing surface. The non-contact probe uses the chromatic aberration principle by which testing mirror can be detected when it was located within the probe's working distance (70mm). A tiny and sharp bright light spot will be shown if the probe is placed properly.

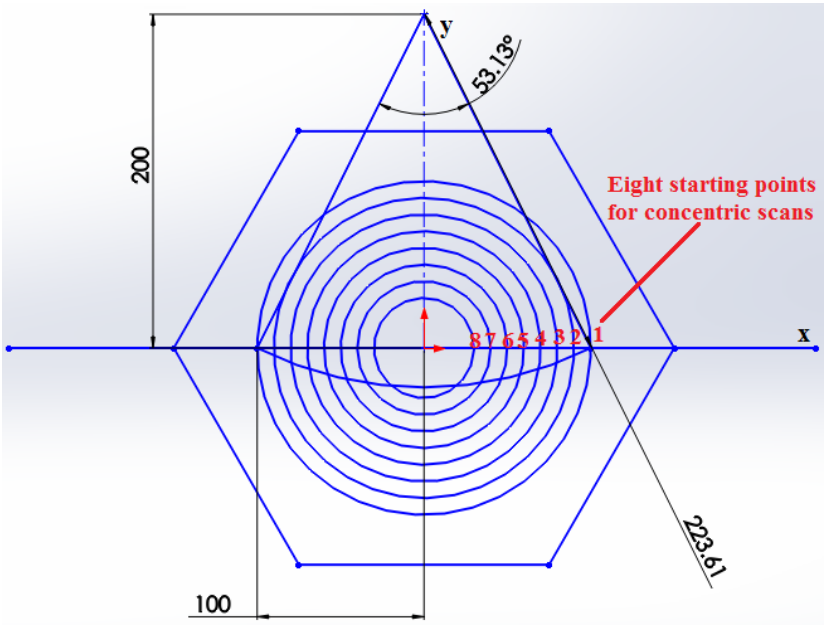

Figure 4-3 SPP Measurement Layout

As mentioned the previous chapter a series concentric scans will be measured in the first place. Based on the scale of the hexagonal testing mirror a circular scan with a radius of 120 millimetre should be the outermost among all the concentric scans (Figure 4-3). In order to indicate the specified starting point of each circular scan a ruler was used. The ruler was positioned from the testing mirror's geometric centre and pointing to a hexagonal corner. The ruler's scale was used to determine each circular scan's radius. The radius of all concentric scans were listed in the table below (Table 4-1):

Table 4-1 Circular and Arc Scan Scale

Radius (mm)	100	90	80	70	60	50	40	30
Arc scan radius (mm)	223.6			Arc central angle (degree)		53.13		

The next step is conducting an arc scan which passes through all concentric circles. Move the Y-shape plate on which was the testing mirror along the sliding rails with a distance of 200 millimetre (Figure 4-3). Press down the shaft clamp hand bar so that Y-shape plate cannot be moved during the table rotation. The arc scan was determined to start at the intersection point between the outermost circular scan and X axis (Figure

4-3). Based on the geometry the minimum arc central angle should be 53.13 so that this arc can pass through all concentric circles (Figure 4-3) (Table 3-2).

4.3.2 Data Stitching

It is necessary to conduct the data stitching process after all the concentric scans and arc scan are measured. When the outermost circular scan measurement was completed the testing mirror remained static and the metrology probe was controlled to move to the second starting point (Figure 4-3). Therefore distance between the metrology probe and the testing mirror varied during probe's movement. Consequentially, the relative height of all concentric scans cannot reflect testing surface form (Figure 4-4).

The arc scan which passes through all concentric circles can be used as the datum data to stitch. When arc scan intersects with concentric circles there will be points of intersection. Both concentric scans and arc scan pass these points of intersection, therefore probe's collected data on these intersection points on both arc and circular scan should be equivalent. The arc scan data can determine the relative height among all circular data. A specific Matlab programme was coded in order to load raw probe data, calculate coordinates of points of intersection, stitch all concentric scans and finally generate a 3-D surface error map (Figure 4-4).

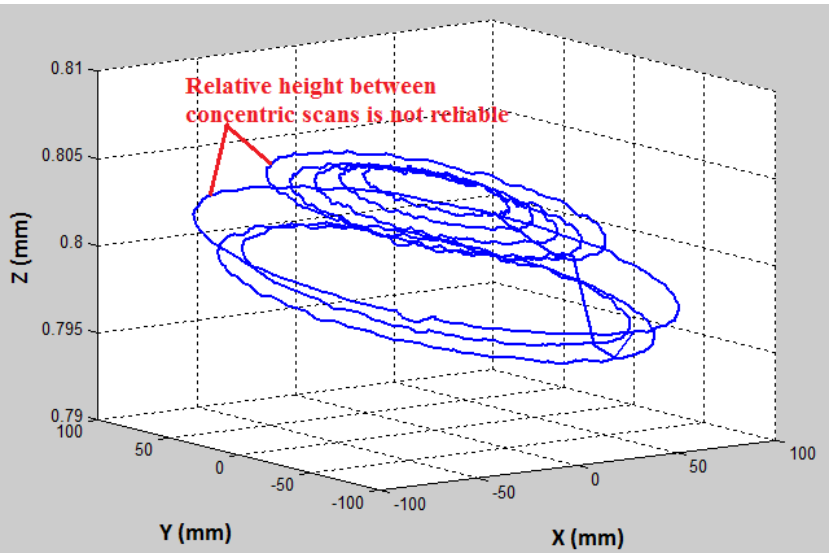

Figure 4-4 Concentric Scans Raw Data

4.3.3 Data Stitching Algorithm

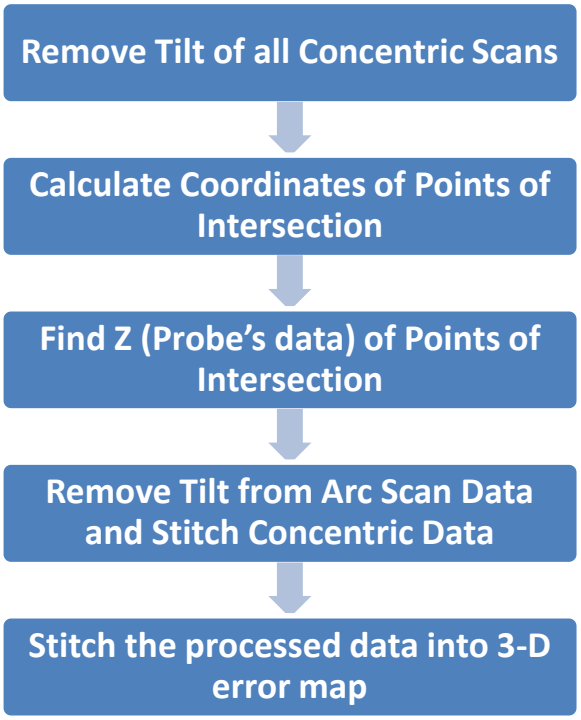

Figure 4-5 SPP data stitching algorithm

4.3.3.1 Remove Tilt of all Concentric Scans

The air-nearing table's rotation axis is tilted which can be noticed from the raw circular scan data (Figure 4-6 (a)). The first step of data stitching process should be remove the tilt of all concentric scans data (Figure 4-6). Here a 'Least Square Method' was used to find the 'best-fit plane' of all concentric scans and calculate the residual value above or below the reference plane.

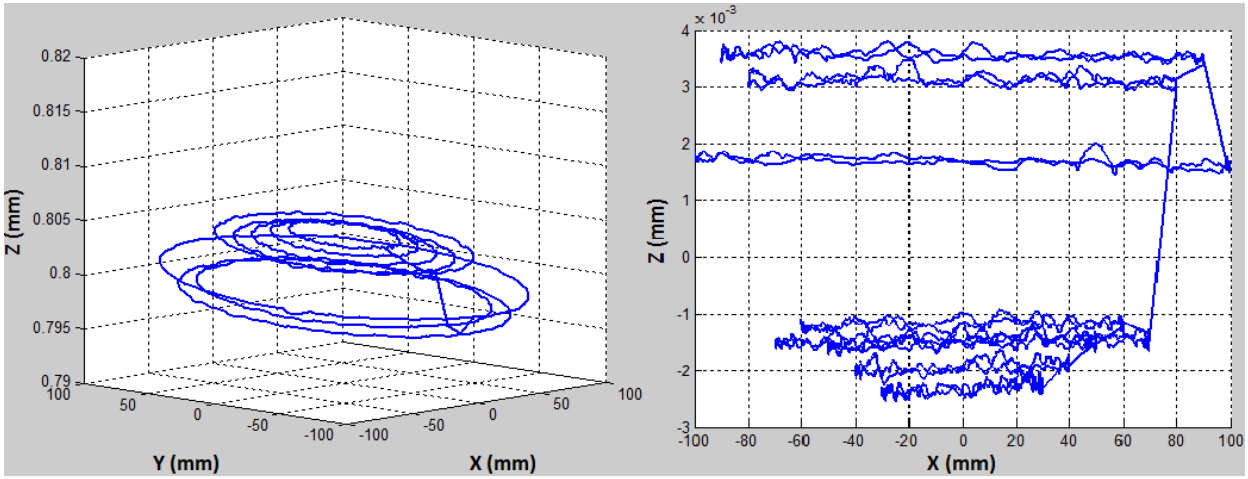

Figure 4-6 Remove Concentric Scans Tilt

4.3.3.2 Calculate Coordinates of Points of Intersection

Coordinates (x, y) of all points of intersection between arc scan and concentric scans should be calculated after removing the tilt of all concentric scans. A Cartesian coordinate system was set up on which centre of all circles was determined as the origin point. Based on Cartesian coordinate system all the concentric circles and an arc curve can be described as the equations below:

$$x^2 + y^2 - (Circle\ Radius)^2 = 0 \quad (4\text{-}1)$$

$$(y + Arc\ off\ axis\ distance)^2 + x^2 - (Arc\ radius)^2 = 0 \quad (4\text{-}2)$$

In above equations ((4-1), (4-2)) radiuses of all concentric circles were imported and stored by Matlab data stitching programme (Figure 4-10). Arc off-axis distance was the length between the Y-shape plate was moved from centre to a specified position. All the calculated coordinates (x, y) based on the above equations were used as the index value to locate the corresponding probe's data on both circular and arc scan.

4.3.3.3 Find Z (Probe's data) of Points of Intersection

All coordinates of points of intersection on X-Y plane can be used as the index to locate its corresponding Z data. The outermost circular scan and an arc data were used as an example to illustrate. Firstly, each circular scan contain 1000 or more data points. It is possible that for a certain point of intersection ($X_{intersection}$, $Y_{intersection}$) there is no corresponding data point (X_{circle}, Y_{circle}) of a circular scan. In this case

among all data points of a single circular scan the nearest one to the intersection point ($X_{intersection}$, $Y_{intersection}$) was selected as the index value to locate the corresponding point of a circular scan (Figure 4-7).

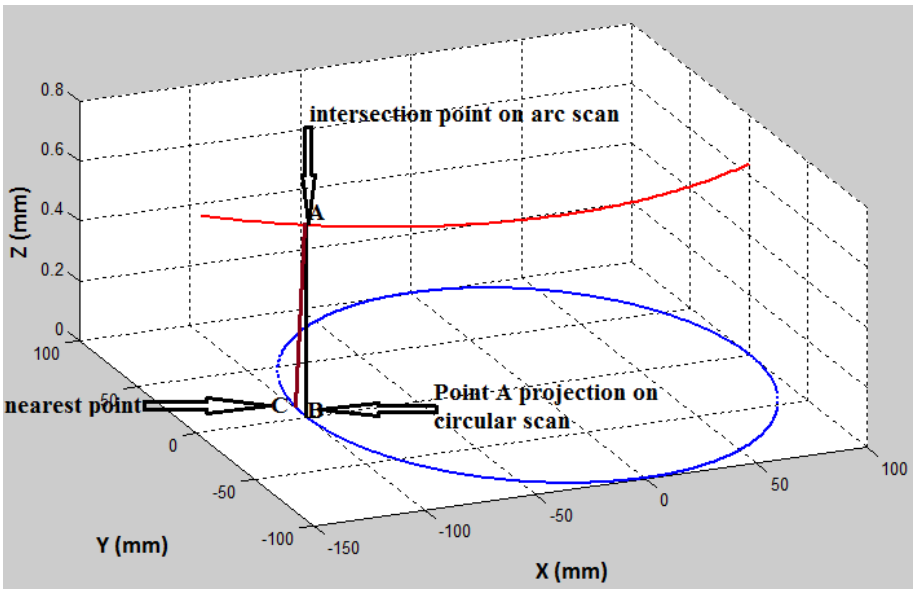

Figure 4-7 Locate Point of Intersection between a Circle and an Arc

4.3.3.4 Remove Tilt from Arc Scan Data and Stitch Concentric Data

The air-bearing table's rotation axis is tilted based on the concentric scans data (Figure 4-6(a)). Therefore the arc scan was also tilted. It is necessary to remove the tilt of this arc scan data (Figure 4-8).

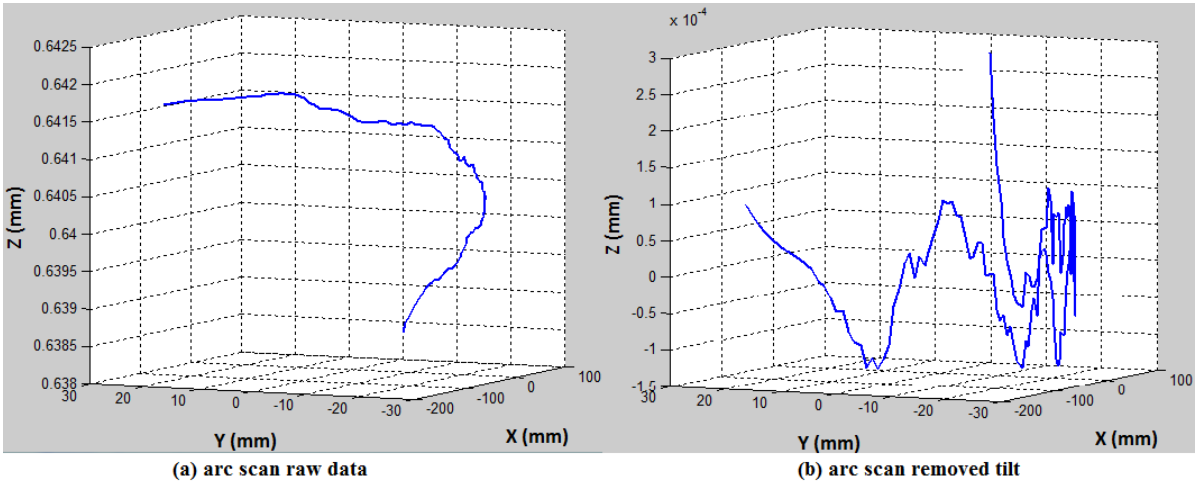

Figure 4-8 Remove Tilt from Arc Scan Data

The same 'Least Square Method' mentioned to remove tilt of all circular scans data was also used to flatten this arc scan.

After flattening the arc scan a vertical distance between each circle and an arc should be calculated. For a certain point of intersection there are two corresponding points on an arc scan and a circular scan, $Z_{intersection\_arc}$ and $Z_{intersection\_circle}$. Coordinate $Z_{intersection\_circle}$ was determined in the above section. This vertical distance H should be calculated as below (4-3):

$$H = Z_{intersection\_circle} - Z_{intersection\_arc} \tag{4-3}$$

Based the measurement layout (Figure 4-3) the arc scan can intersect each circular scan twice. Therefore there are two vertical distance H_1 and H_2 for each pair of arc and circular scan. In this case the mean value of H_1 and H_2 was used as the final vertical distance H_{final}. Then move each circular scan along the Z axis based on the final vertical distance H_{final} (Figure 4-9).

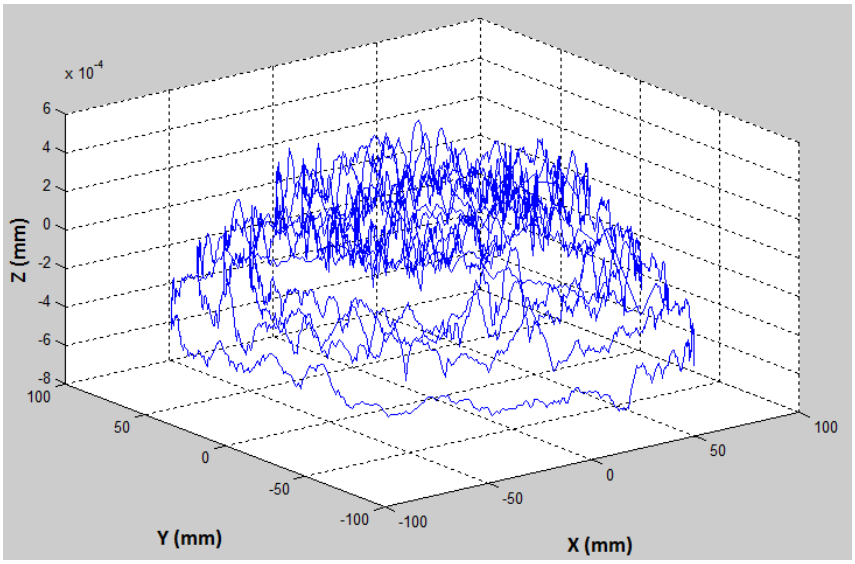

Figure 4-9 Stitched Concentric Scans

After removing the tilt of the single arc scan and the tilt of all concentric circular scans, all the concentric scans data can be stitched together. In the Matlab Data Stitching programme that I developed, the Matlab 'griddata' function was used to fit a surface based on all the existing concentric circle data and the interpolation method was determined as 'cubic' method. The 'cubic' method is Triangle-based cubic interpolation. The final stitched surface can be regarded as the surface error map of the testing mirror. The Matlab Data Stitching programme (Figure 4-10) can also calculate the PV and RMS value of the concentric scans and the PV and RMS value can be considered as the testing mirror's surface topography information.

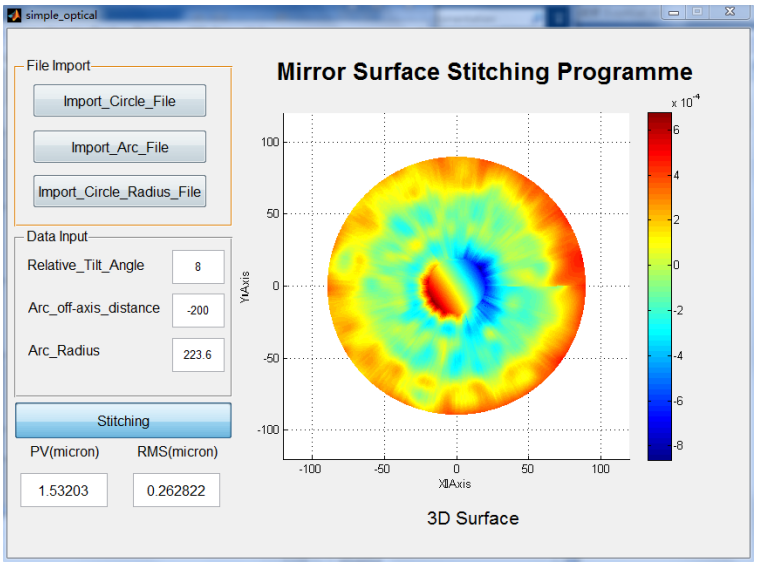

Figure 4-10 Final stitched 3D surface error map of the testing mirror

The testing flat mirror was measured by a 4D interferometer after tested by the SPP. The interferometer surface error map was shown below (Figure 4-11). It can be seen that the SPP result showed that the testing mirror had a PV of 1.532 μm and a RMS of 0.263 μm. The 4D interferometer calculated the testing mirror had a PV of 0.19 μm and a RMS of 0.03 μm (Table 4-2).

The circular 'ripple' pattern in the SPP stitched error map was introduced in the data stitching process. It is possible that for a certain point of intersection there is no corresponding data point of a circular scan. The Matlab Data Stitching programme was designed to locate the nearest point to the crossing coordinates. The second error source of the surface error map was the distance which the testing mirror was moved from the centred position to a specified de-centred position. This distance was determined manually by a steel ruler which was installed on the aluminium extrusion. A 0.5mm de-centred error can contribute 3nm rms error to the final stitched surface.

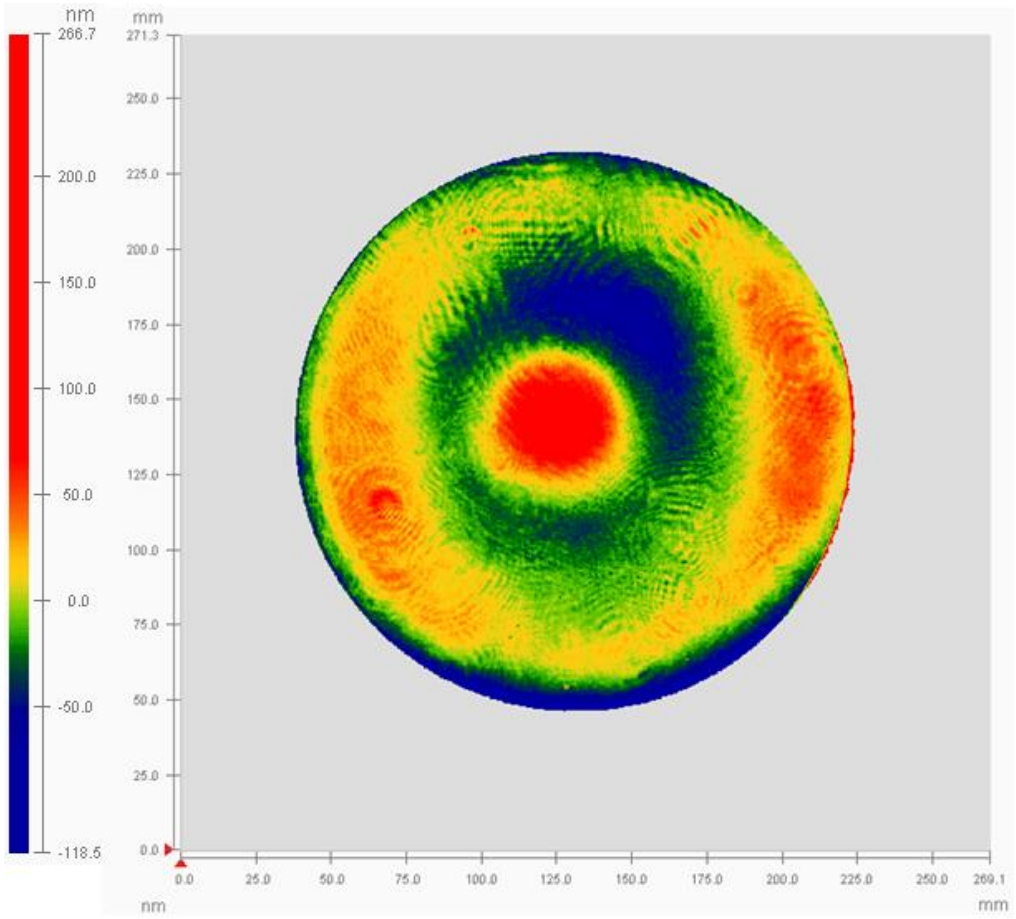

Figure 4-11 4D interferometer surface error map of the testing mirror

Table 4-2 SPP and 4D interferometer PV&RMS

	SPP Result	4D Interferometer Result
PV (μm)	1.532	0.263
RMS (μm)	0.19	0.03

4.4 Theoretical Data Stitching Error Analysis

It is compulsory to conduct a Matlab based simulation to confirm the data stitching algorithm validation. Theoretically, if an ideal flat surface is being measured by the SPP with a series of concentric scans and one arc scan, the stitched surface should be an ideal flat surface. The stitching algorithm should eliminate the tilt error caused by rotary table. The PV and RMS of the stitched error map should be zero.

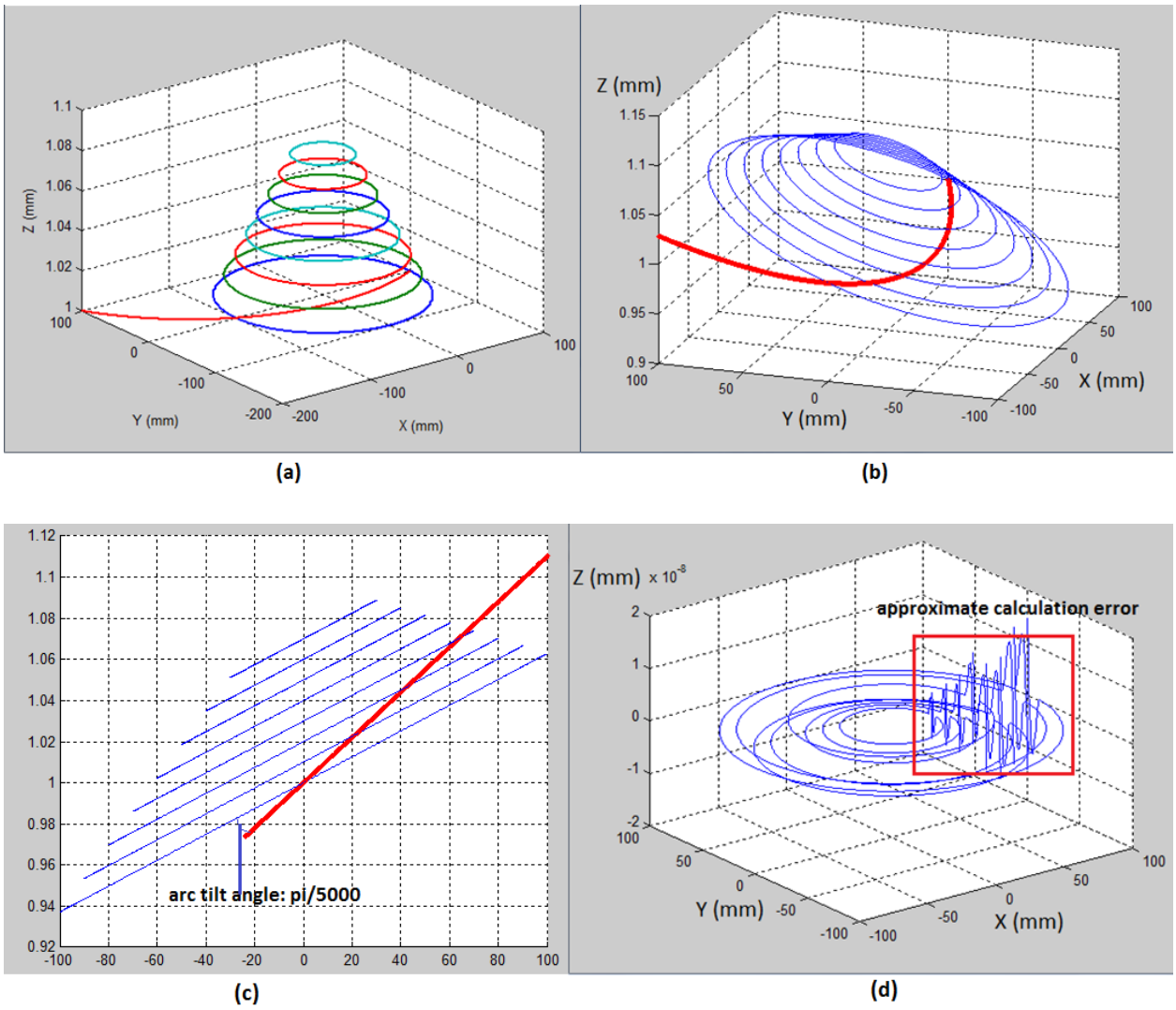

Figure 4-12 Data stitching algorithm ((a), (b), (c), (d))

- Firstly, eight horizontal concentric circles with different 'Z' values were generated by Matlab (Figure 4-12(a)). The concentric scans were measured in an experiment by moving the chromatic probe. The radius of each circle was determined by the probe light spot's position on the testing mirror.
- All the generated concentric circles were rotated with 'X' axis with a specified angle. Let the angle be $\pi/5000$ (Figure 4-12(b) (c)). It has been found that there was wobble error for the rotary table. Therefore, all the measured concentric scans were tilted.

- Similarly, a tilted arc profile data is also generated since the sliding rails will be bended slightly (48μm) when testing mirror is moved with 200mm. Let's assume that the arc scan has a tilted angle of π/5000+ π/10000 (Figure 4-12 (c)).
- Based on the data stitching algorithm, the tilt errors of both concentric scans and an arc scan were removed. Then the 'Z' coordinates of all intersections points between concentric circles and one arc curve were calculated. After that, based on these 'Z' coordinates all the concentric circles were translated along the Z axis and 'landed' on the arc scan profile. The error of each circle profile and their relative height information determine the final error map of the testing mirror (Figure 4-12(d)).

The calculated final stitched result is: root mean square (rms) is 1.27279×10^{-6} μm and peak-to-valley (p-v) is 4.07745×10^{-6} μm (Figure 4-13). The unit scale is 10^{-6} μm is 0.001 nm which is extremely close to the ideal flat surface. The existence of nonzero rms and p-v error is because the approximate calculation by Matlab software. This calculated surface error map can confirm that the data stitching algorithm is right and can be used to conduct the data analysis.

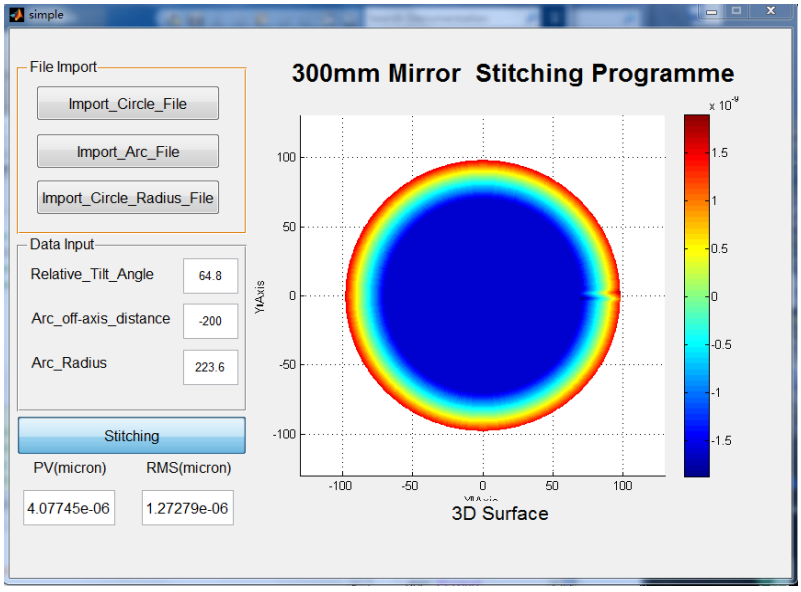

Figure 4-13 Validation of data stitching algorithm

Since the air-bearing rotary table's rotation axis was not ideally perpendicular to the horizontal plane. The rotary table has wobble error. This wobble error can cause the tilt error for all concentric scans and arc scan. Different values of tilt errors can cause the variations of the final stitched surface error map. Therefore it is

reasonably to use Matlab to generate both concentric scans and arc scan with different tilt error. These tilt errors were specified as: π/2000, π/3000, π/4000, π/5000. Then, run the Matlab based data stitching programme to compare the difference (Figure 4-14).

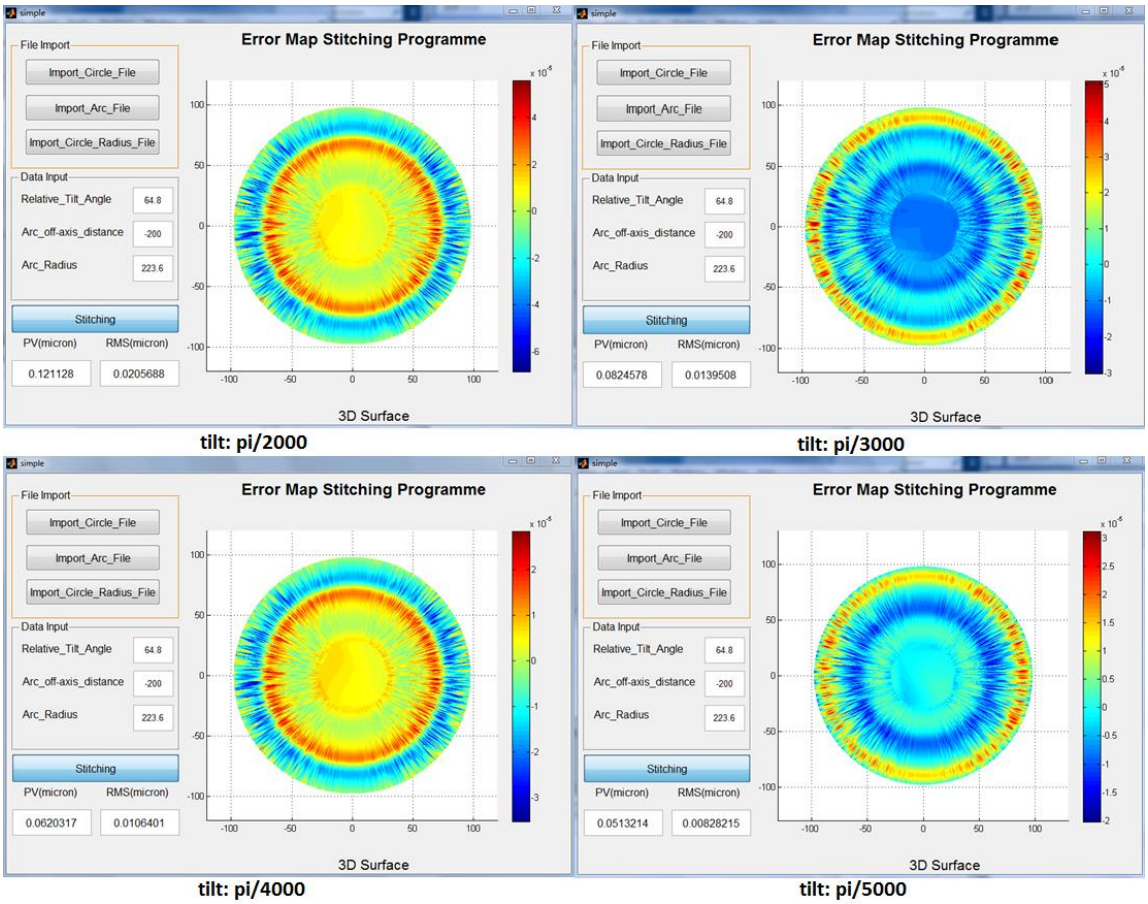

Figure 4-14 Matlab simulation results with different tilt error

The results can be summarised as below (Table 4-3):

Table 4-3 Simulation results with different tilt error

	Circles tilt: pi/2000 Arc tilt: pi/2000+pi/1000	Circles tilt: pi/3000 Arc tilt: pi/3000+pi/1000	Circles tilt: pi/4000 Arc tilt: pi/4000+pi/1000	Circles tilt: pi/5000 Arc tilt: pi/5000+pi/1000
PV (μm)	0.121	0.082	0.062	0.051
RMS (μm)	0.021	0.014	0.011	0.008

It can be seen from the table 4-3 above that as the tilt error increase the final stitched surface error map's PV and RMS value also increase. This can be explained as the tilt error increase the metrology probe's vertical measurement range will be extended. When the petrology probe measure the arc scan which across all the concentric scans the probe's vertical measurement distance will be also extended. This can cause the probe's vertical measurement accuracy compromised. The experiment results regarding spherical mirror in chapter 5 can confirm this explanation.

4.5 Conclusion and Summary

In this chapter the procedures of testing a hexagonal flat mirror by the SPP was firstly introduced. The measurement principles of the SPP was introduced. A specific Matlab based data loading and stitching programme was developed by the thesis author. This programme can load collected data, stitch data and calculate PV and RMS of the final stitched surface error map.

The final stitched surface error map of the testing mirror was compared with the 4D interferometer error map. Possible error sources of the two surface metrology methods (SPP and 4D interferometer) were analysed.

Chapter 5 System Test on Concave Spherical Surface

5.1 Introduction

A flat hexagonal mirror with a 300 millimetre corner to corner was tested by Swinging Part Profilometer (SPP) in the previous chapter. The final stitched 3-D surface error map was generated and then compared with a result obtained by 4D interferometer. After testing a flat mirror by SPP a hexagonal concave spherical mirror was also measured by SPP in this chapter. The testing mirror was measured with series of concentric scans and one arc scan. All the circular data and arc scan data were collected and stitched to a 3-D surface error map. This stitched error map was compared with an interferometer result. The procedures of measuring a spherical mirror by SPP are shown below:

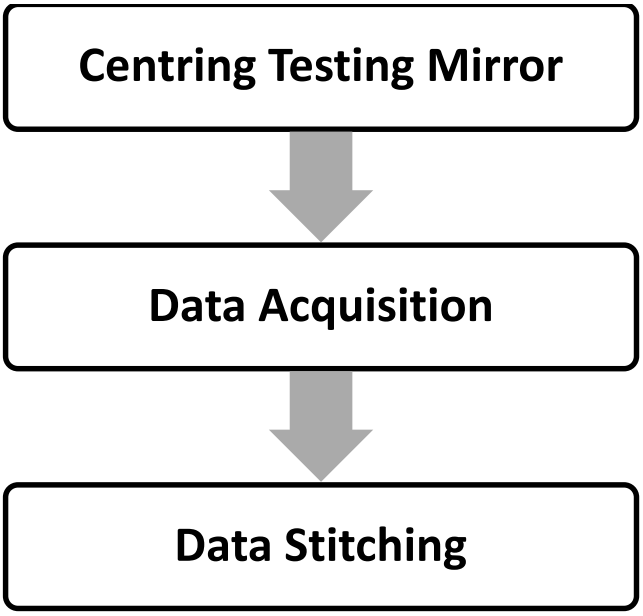

Figure 5-1 SPP measurement procedures for a spherical mirror

5.2 Solartron Pneumatic Probe and Armstrong Optical Probe

The metrology probe plays an important role in the whole Swinging Part Profilometer (SPP). Two types of probes, contact and optical one were selected to meet the requirements of measurement projects. Among current available contact probes a Solartron@ pneumatic probe DP/10/P was selected as the metrology

probe. The Solartron@ DP/10/P probe has a vertical measurement range of 10 millimetre (Table 5-1), therefore a spherical mirror with a sagitta (SAG) up to 10 millimetre and a flat mirror can be measured. Considering a pneumatic contact probe will exert a force on a testing surface, this force can damage the testing mirror if the mirror's material is aluminium. Therefore, it is essential to choose a non-contact probe to measure an aluminium testing surface. In the SPP an Armstrong Precitec Optical probe RB 200 071 accompanied a CHRocodile optical sensor were finally selected as the metrology probe. Armstrong Precitec optical probe has a vertical measurement range of 10 millimetre and vertical resolution of 300 nanometre (Table 5-2). The measurement theory in the application of Armstrong Precitec optical probe is based on chromatic aberration theory.

Table 5-1 Solartron Pneumatic Probe Specifications

Model	Solartron Pneumatic Probe DP/10/P
Operation Temperature	+5 °C ~ +80 °C
Resolution	0.05 μm
Measurement Range	10 mm
Reading Rate	3906 readings per second
Air Supply	0.7 bar
Probe Diameter	8.6 mm
Length (fully extended/retracted)	123.4mm/112.4mm

Table 5-2 Armstrong Precitec Optical Probe Specifications

Model	RB 200 071
Applications	Thickness and distance
Measurement range (vertical)	10 mm

Working distance	70 mm
Spot diameter	24 µm
Lateral resolution	12 µm
Dimensions	Length: 146 mm Diameter: 65mm
Weight	721 gram

Table 5-3 CHRocodile Sensor Specifications

Model	CHRocodile S
Applications	Thickness and distance
Operation temperature	+5 ºC ~ +50ºC
Dimensions (W*H*D)	200*100*93 (mm)
Weight	1.1 kilogram
Interfaces	USB, RS 232, RS 422,
Resolution	0.003% of measurement range
Transfer Rate	USB: 921600 Baud
System Voltage	90~264 V AC power
Optical fibre length	5 metre

5.2.1 Optical Probe Distance Measurement Principle

The Armstrong optical probe distance measurement is based on chromatic aberration principle. A white light source is emitted from CHRocodile@ sensor to illuminate a testing surface with an optical fibre. This white light beam travels through the optical fibre and then to the optical probe. Based on chromatic aberration principle lenses have different refractive indices for different wavelength of light. The white light travels through the lens inside an optical probe will be separated and then focused on different position based on different wavelength. During a distance measurement mode white light will be focused on the

testing surface. Then reflected light is maximized for the wavelength in focus on the testing surface. Based on the wavelength of reflected light a distance measurement can be conducted up to 66000 times per second. The vertical measurement range (10 mm) is determined by the optical probe.

5.2.2 Air Supply for Solartron Pneumatic Probe

A continuous and steady air supply was compulsory in order to maintain the pneumatic probe work properly. The Solartron pneumatic probe DP/10/P required the air supply of 0.7 bar based on its manual. In the case of pneumatic probe measurement the air pump-in for the air-bearing table was used to provide the air flow for the Solartron pneumatic probe. The air pressure for air-bearing table was 3.7 bar which significantly larger than the requirement of pneumatic probe (Table 5-1). This high pressure of air flow can damage the pneumatic probe. In order to overcome this problem an air regulator with gauge was used. A tee pipe fitting was used to divide air flow from the main air supply which was used for rotary air-bearing table (Figure 5-2 Air Flow Control for Pneumatic Probe).

The air regular was connected to the pneumatic with a plastic pipe (Figure 5-2). When the air regulator was switched off and locked there was no air flow to the pneumatic probe, generating a vacuum environment which can retract the stylus of the pneumatic probe. When the air regulator was switched on and set as 0.7 bar based on its gauge the probe's stylus was pushed outward.

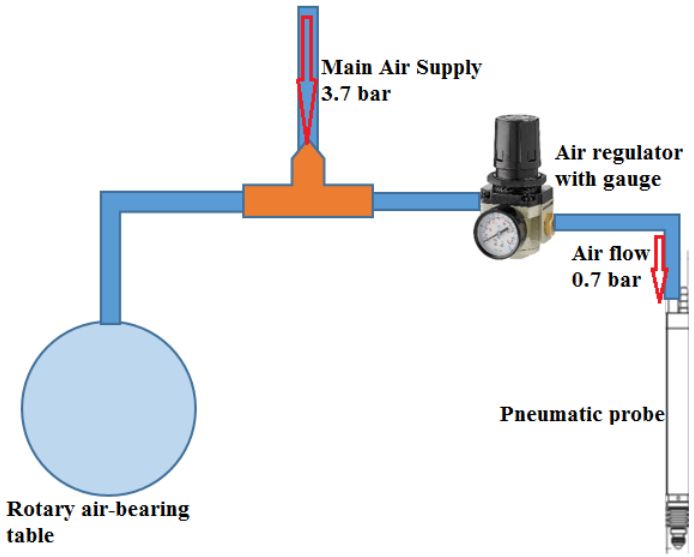

Figure 5-2 Air Flow Control for Pneumatic Probe

5.3 Test Hexagonal Concave Spherical Mirror

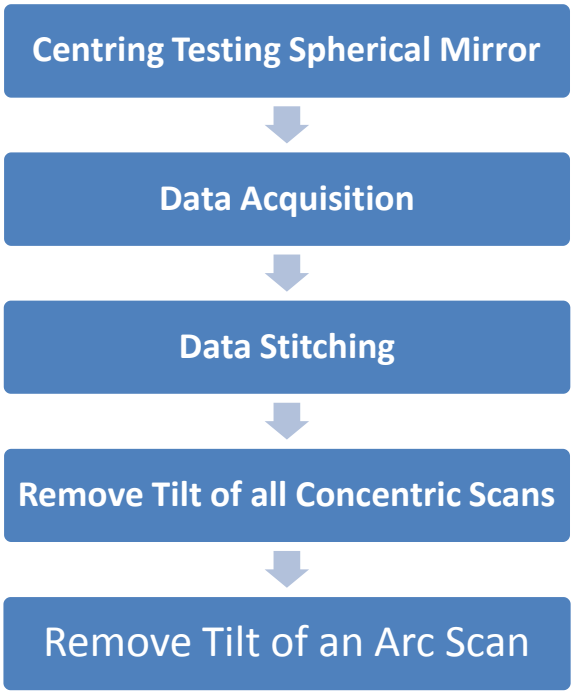

Figure 5-3 SPP data acquisition and data stitching

5.3.1 Centring Testing Spherical Mirror

The aim of centring a testing spherical mirror is to make sure its geometrical centre coincides with the rotation axis of the air-bearing table.

- Attach a permanent mark pen to the terminal of an ABB industrial robot arm. Make sure the mark pen is perpendicular to the Y-shape plate. Use 'teach pendant' to control the ABB robot arm so that the mark pen's tip touch the Y-shape plate.
- Use Matlab software to control the motor which was installed beneath the air-bearing table. The motor was connected to the rotary table by an Ammeraal Beltech@ TGE4RQ belt with high friction at process side so the motor can power the rotary table's rotation. Control the rotary table with Matlab to rotate with 360 degree. Since the mark pen remained static during table's rotation a circle was drawn on top of the Y-shape plate. The centre of this drawn circle is the rotary table's rotation centre.

Draw a straight line from corner to the opposite corner on the back of testing mirror. Draw a second straight line connects two opposite corners. Since the testing hexagonal mirror is symmetrical the point of intersection of two straight lines is mirror's geometrical centre. Position the testing mirror to make sure its geometrical centre coincides with the centre of the drawn circle (previous step).

5.3.2 Data Acquisition

After positioning the testing spherical mirror on top of the Y-shape plate it is time to conduct the probe data acquisition procedure. In order to conduct the data acquisition procedure properly, a Matlab Graphical User Interface (GUI) programme was developed. With this GUI programme the air-bearing table can be rotated with 360 degrees or any specified angle. It can identify the metrology probe and a motor which can power the table's rotation. This GUI programme is capable of spinning table to a specified measurement starting point determined by Halls Effect Sensor which was installed underneath the table.

Totally eight concentric scans and one arc scan were needed to conduct in order to stitch the final surface error map (Figure 5-4).

- Control the ABB industrial robot arm on which a non-contact probe was mounted. Move the non-contact probe slowly to make sure the light spot emitted from probe was properly focused.
- As the measurement layout regulates all the starting points of concentric scans share the same straight line. This straight line originates from testing mirror's geometrical centre and pointing to mirror's corner (Figure 5-4). Move the probe until its emitted light spot coincides with one of eight starting points, for example point 8 for outermost circular scan (Figure 5-4).
- Use Matlab software to control the air-bearing table to rotate for 360 degree. Move the probe to make sure its light spot was moved from point 8 to point 7 (Figure 5-4). Repeat this step so that all concentric scans were conducted.
- An arc scan was necessary in order to stitch all circular scans data. This arc scan passes through the centre of all concentric scans (Figure 5-4). The testing spherical mirror was de-centred with 250 millimetre distance by moving the Y-shape plate by 250 millimetre (Figure 5-4).

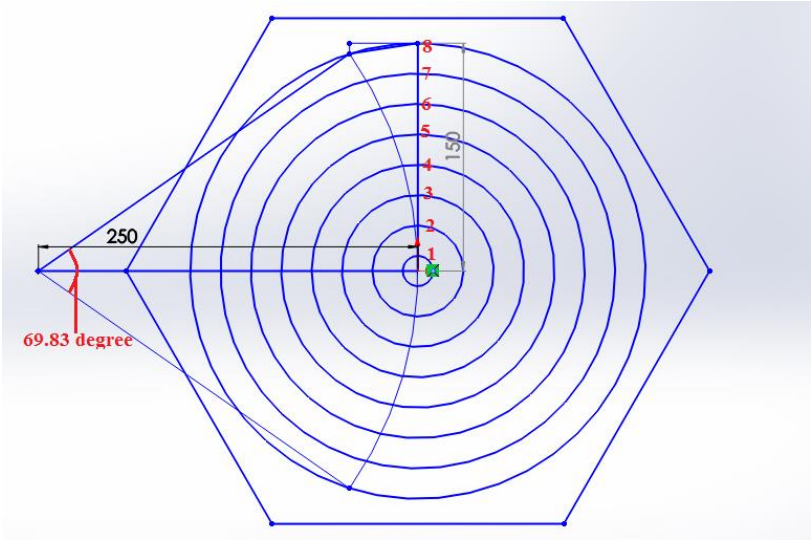

Figure 5-4 SPP Spherical Mirror Measurement Layout

5.3.3 Data Stitching

It is necessary to stitch all the circular scans data together based on the arc scan data. When conducting the measurement of all concentric scans the metrology probe was moved one starting point to its next one. The probe's movement can cause the relative height between adjacent circular data are not reliable (Figure 5-5). The concentric scans data alone cannot reflect the testing mirror surface form (Figure 5-5). Therefore an arc scan was compulsory in order to determine all concentric scan's relative vertical position.

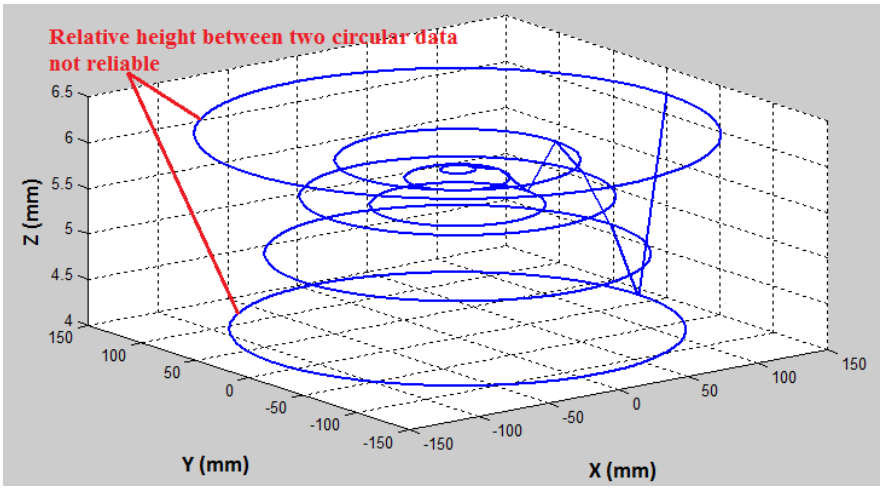

Figure 5-5 Relative height between Two Circular Data

The basic principle of stitching is probe's data on a specified point should be equivalent even the measurement path is different. In this SPP spherical mirror measurement case an arc scan will pass through eight concentric scans. Totally sixteen points of intersection were generated. When the probe scanned with circular or arc path the probe's data on intersection point should be equivalent. This point of intersection can be used as the datum to adjust the vertical position of a circular data. Similarly, all the concentric scans data can be adjusted based on their point of intersection data.

Eight circular scans and one arc scan contain thousands of data. In order to process data accurately and conveniently a Matlab data stitching programme was developed. This GUI programme is capable of importing concentric scans data, arc scan data and calculating coordinates of all points of intersection. It can calculate the 'best-fit sphere' as a reference and then calculate the testing mirror's surface error map.

5.3.4 Remove Tilt of all Concentric Scans

Since the rotation axis of air-bearing table was not perfectly vertical. This can cause all concentric scans were tilted. A mathematical approach called 'Decentre-Introduced Tilt' as used to remove this tilt of all circular scans data (Figure 5-6). All concentric scans share the same tilt angle since the testing mirror was centred previously.

A 'best-fit plane' for all circular scans data was found and the residual value of each circular data to this plane was calculated. The residual value was considered as the new circular scans data.

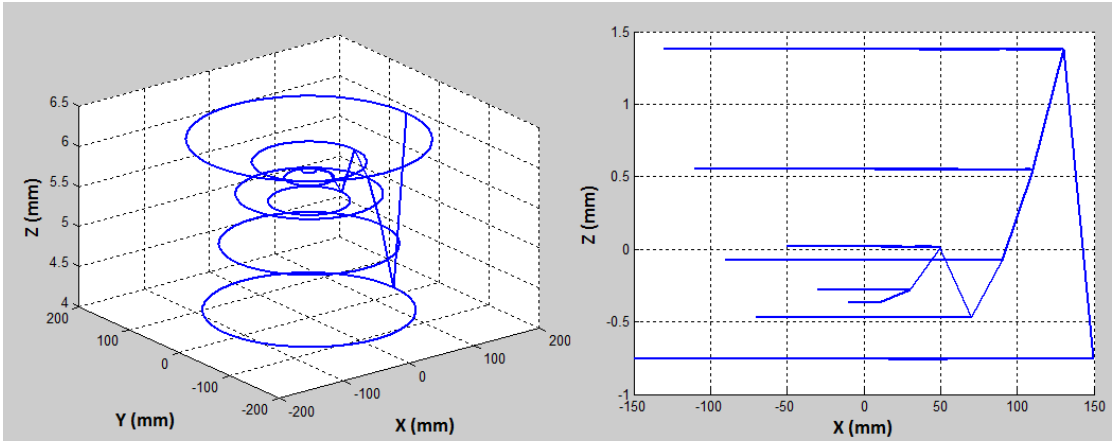

Figure 5-6 Remove Tilt of all Concentric Scans

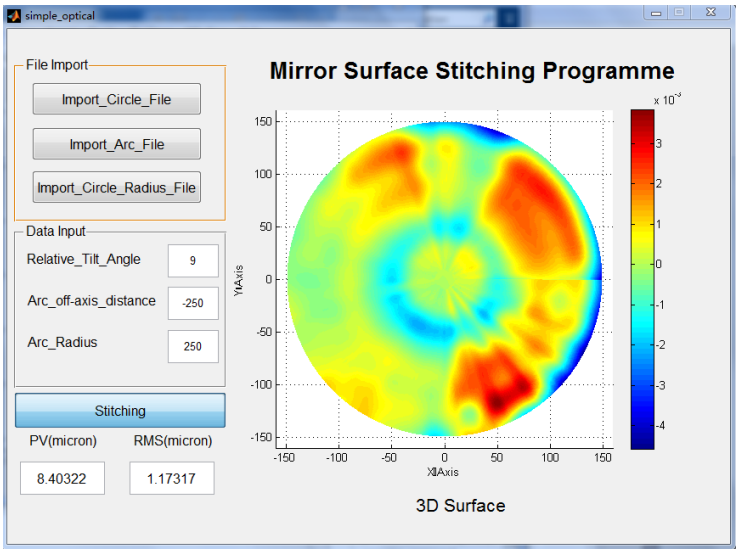

Figure 5-7 SPP stitched surface error map

After removing the tilt of all the concentric scan data and the tilt of the arc scan, the circular scans data were stitched together and use Matlab to interpolate a 3D surface error map (Figure 5-7).

The SPP accuracy of testing the spherical mirror is larger compared with the testing a flat surface (Figure 5-7). This difference is caused by the measurement of the single arc scan. When measuring both flat and spherical mirrors the single arc scan is compulsory so that the arc scan is used as the datum to stitch all the concentric scan data. Therefore, the accuracy of this arc scan can determine the accuracy of the final stitched surface error map. When the chromatic probe traverse the testing spherical mirror to conduct the arc scan it will cover the full sag (6.67mm) of the spherical mirror. However, when it measure the flat surface this sag will be zero. Based on the experiment of probe calibration in Chapter 3 section 3.9 the chromatic probe's vertical accuracy will be worse when its vertical measurement range increases. The probe's vertical accuracy is 7.2820 μm when its vertical measurement range is 8.0 mm. Therefore, when the probe measures an arc scan of a spherical mirror its measurement accuracy will be compromised compared with the measurement of a flat surface.

5.4 Summary

In this chapter the SPP was used to test a spherical concave mirror. The experiment procedures were stated and the SPP measurement principles were introduced. A hexagonal spherical concave mirror was tested by

the SPP and its 3-D stitched error map was generated by using a Matlab based data stitching method developed by the thesis author. This Matlab data stitching programme contains concentric scans and arc scan data loading, data stitching and PV and RMS calculation. It significantly improve the experimental data analysis efficiency. It was concluded that the measurement error from the arc scan contribute the most significant error for the SPP measurement result. The reason can be attributed that when the vertical measurement is large (6.67mm) the chromatic probe's vertical accuracy will be decreased.

Chapter 6 Aspherical Mirror Mid-spatial Frequency Feature Testing by SPP

6.1 Introduction

6.1.1 Introduction of LOCUS Telescope Mission

The detailed chemistry processes taking place in the Mesosphere Lower Thermosphere (MLT) region which located between about 60 kilometres and 110 kilometres in altitude were rarely observed. Observations conducted in the MLT are a critical indication for climate change.

LOCUS is a Low-Earth orbit satellite which was designed to measure atomic oxygen, the thematically linked trace gases CO, CO_2, NO, O_3 and OH [89]. These measurements are conducted both in the THz frequency region and in a photometric narrow band near and middle-infrared channels. The LOCUS mission can provide a complete picture of mesospheric transport and thermal structures. The LOCUS is capable of scanning the atmosphere as often as possible within the region of 50 kilometres to 150 kilometres altitude. The LOCUS will make 75 observations with 3 seconds integration times which can bring a 2 kilometres spatial resolutions.

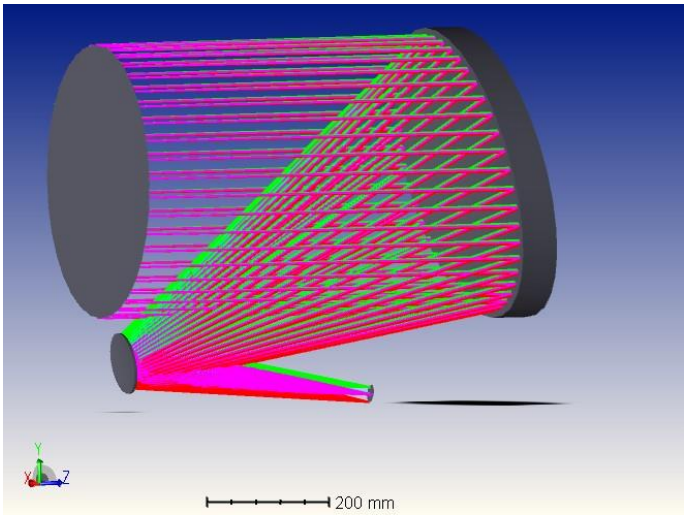

Figure 6-1 LOCUS Optimal Design

The challenge of the LUCUS mission is to design a Cassegrain type telescope which will meet the load requirement of small satellite (150 kilograms) (Figure 6-1). In order to achieve the light-weight design target the material for telescope was chosen as aluminium. Besides the total weights limitation the space requirements for LOCUS telescope are also need to consider so the telescope can be inserted into the limited space of satellite. Therefore the Cassegrain configuration was finally adopted in LOCUS telescope optimal design. The basic optical specifications for LOUCS telescope are shown as follows (Table 6-1):

Table 6-1 LOCUS Telescope Mirrors Specifications

Mirror	Dimensions (mm)	Conic constant	Distance (mm)	R_C (mm)
Primary M1	480 x 495 ellipse off-axis concave parabola	1.000	M1 to M2: 650.0	1557.227
Secondary M2	Diameter 110 mm off axis convex hyperbola	3.497	M2 to focus: 425.0	368.567

6.1.2 Mid-spatial Frequency (MSF) Errors

Optical surfaces errors are normally classified into three categories, low spatial frequency errors, mid-spatial frequency (MSF) errors and high spatial frequency errors according to power spectral density (PSD) [90]. In details, based on the ISO 10110 standards low spatial frequency errors with spatial frequencies smaller than $0.0303/mm^{-1}$, MSF errors with spatial frequencies between 0.0303 and $8.33/mm^{-1}$ and high spatial frequency errors with spatial frequencies larger than $8.33/mm^{-1}$ [91-93].

The primary mirror M1 in LOCUS project was concave off-axis parabolic surface form and it has been polished with Zeeko IRP 1200 computer numerical controlled (CNC) polishing machine. The mirror surface was required to conduct a measurement to test whether a MSF error was presented after processed

by Zeeko CNC polishing machine. The contact stylus Taylor Hobson profilometer was not suitable to test this aluminium mirror since the contact stylus tip can damage the mirror's surface. If an interferometer is used to test the mirror's surface the alignment procedures of measuring an off-axis aspherical mirror was complex and time-consuming. Based on the above considerations an optical contactless chromatic probe integrated with a SPP was adopted to test the MSF errors on this primary mirror (Figure 6-2).

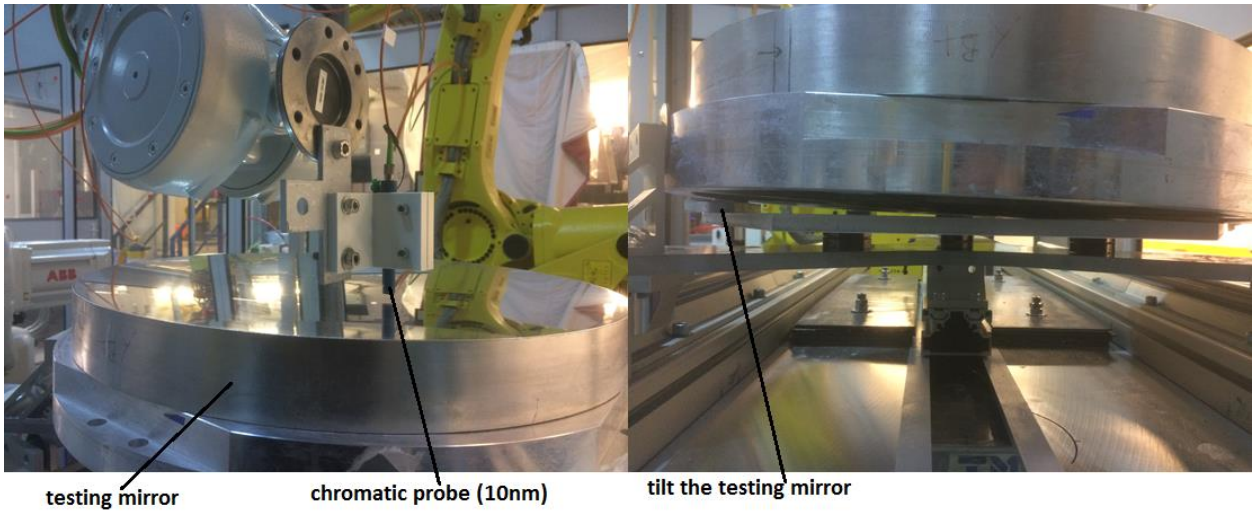

Figure 6-2 MSF Errors Test by SPP and Chromatic Probe Setup

6.2 Experiment Setup

Currently, three metrology probe are available to use in the Robot Lab, Solartron contact pneumatic probe, Armstrong Precitec non-contact chromatic probes with vertical resolution of 10 nanometre and 300 nanometre. Firstly, considering the local height of MSF errors are normally 200 nanometres the chromatic probe with 300 nanometre resolution is incompetent to test the MSF errors. Therefore, an Armstrong Precitec non-contact chromatic probe with 10 nanometre resolution was adopted to test MSF errors. Secondly, the contact Solartron pneumatic probe with diamond tip and 0.7 bar air pump-in will harm the testing aluminium surface.

Considering the vertical measurement range of Armstrong Precitec chromatic probe with vertical measurement range of 2 millimetre which was significantly smaller than testing mirror's SAG (10 millimetre), the measurement traverse path can cover a local area at the bottom of the testing mirror. In

order to extend the measurement path length the testing mirror was required to tilt (Figure 6-4). In the following illustration (Figure 6-4) the orange curve line should be the measurement path to measure.

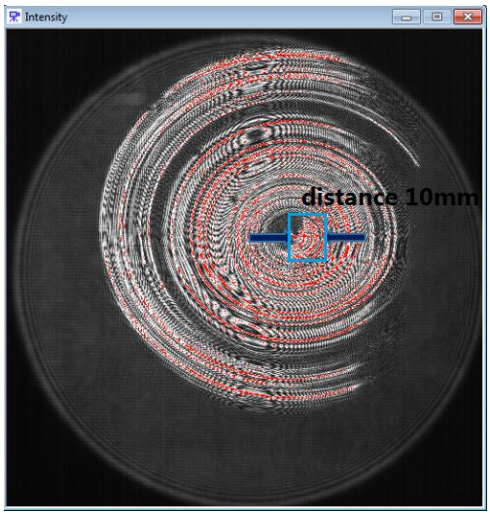

Figure 6-3 Observation of Fringe Pattern

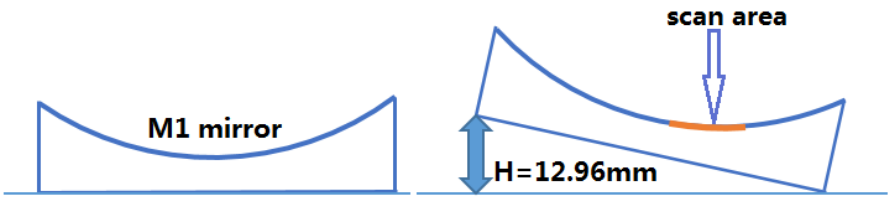

Figure 6-4 Testing Mirror Tilt Determination

Based on the observation of the fringe pattern obtained by FISBA interferometer a series of concentric ripples of MSF errors were available on the testing surface. The local area which starting from the mirror's centre with a distance of 10 millimetre was the target that was to be measured. The short axis of the testing primary mirror was 480 millimetre. According to ratio between observed fringe pattern and testing mirror's dimensions the pre-determined measurement length was:

$$\frac{55}{240} = \frac{10}{Length} \tag{6-1}$$

Where length is 43.6364 millimetre. The dimensions of testing off-axis parabolic mirror were shown below (Figure 6-5):

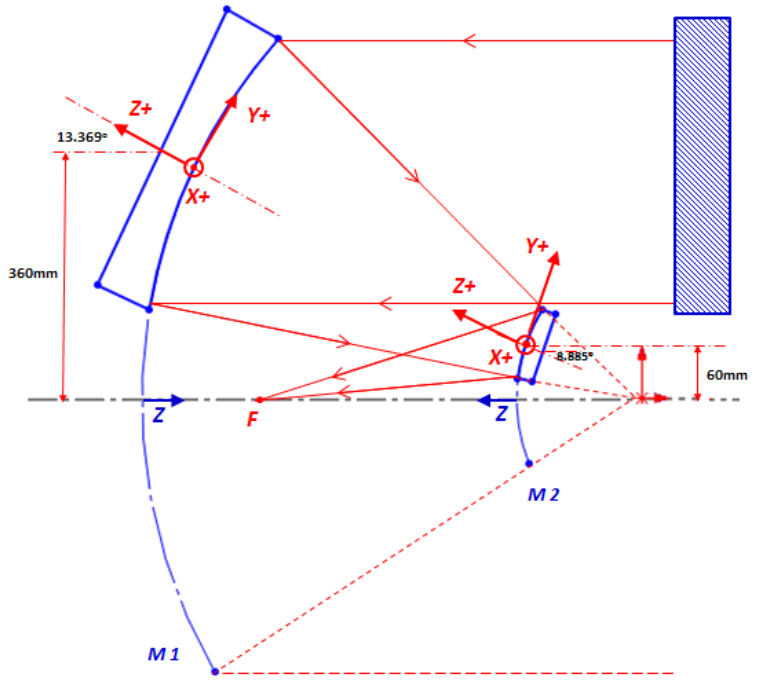

Mirror	Dimensions (mm)	Conic constant	Distance	Rc
Primary M1	480 x 495 ellipse off-axis concave parabola	1.000	M1 to M2: 650.0 mm	1557.227
Secondary M2	Diameter 110 mm off axis convex hyperbola	3.497	M2 to focus: 425.0 mm	368.567

Figure 6-5 Testing Off-axis Parabolic Mirror Dimensions

According the parabolic curve geometry features the tilt angle of testing mirror should be obtained by:

$$\tan\Theta = \frac{92.2181-92.1642}{44-42} = 0.0269 \text{ rad} \quad (6\text{-}2)$$

$$\delta H = 480\times\tan\Theta = 12.96 \text{ mm} \quad (6\text{-}3)$$

Where δH in (6-3) was the height which should be used to tilt the testing mirror.

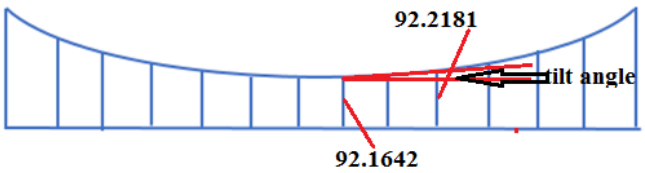

Figure 6-6 Tilt angle calculation

6.3 MSF Features Tested by SPP

Use Matlab program which was developed specifically for controlling SPP operation including rotary table's rotation and metrology probe's data collection. The testing mirror was initially rotated with 0.8 degrees. Normally, testing surface was rotated on top of Y-shape plate several times in order to determine a suitable rotation angle. Based on the data collected within first 0.8 degree rotation it was decided to continue to rotate for another 1.5 degrees.

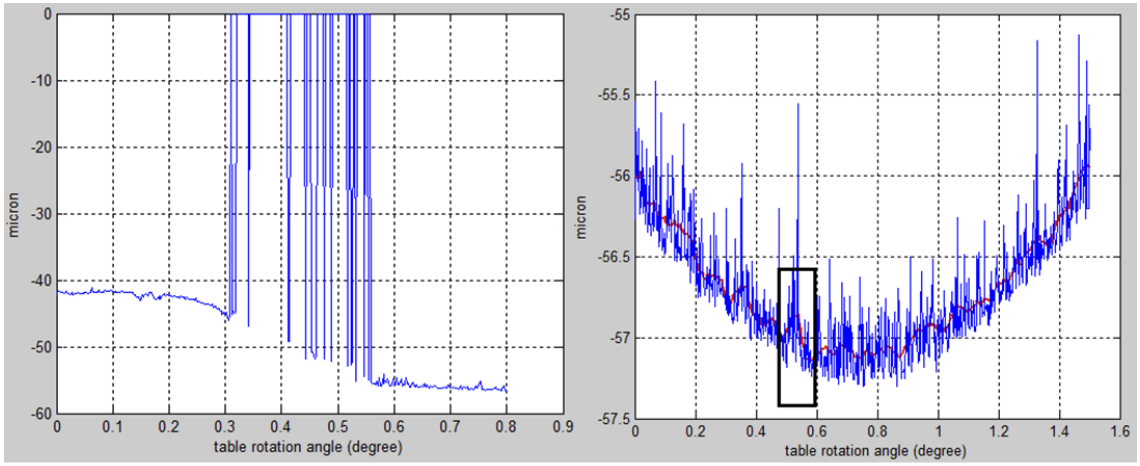

Figure 6-7 MSF Errors Test Data

The blue line in the above graph shows there is noise in collected raw probe data. Therefore, a noise filter Matlab program was used to remove the noise. The red curve was the filtered data. It can be shown in the above graph that there was MSF errors presented on the testing mirror (Figure 6-7). The scale in 'Z' direction is 0.5/3 μm (166 nm). The MSF features occurred at the position where the rotary air-bearing table was rotated with 0.8+0.5=1.3 degree. This test has been repeated twice in order to confirm the existence of MSF errors (Figure 6-8).

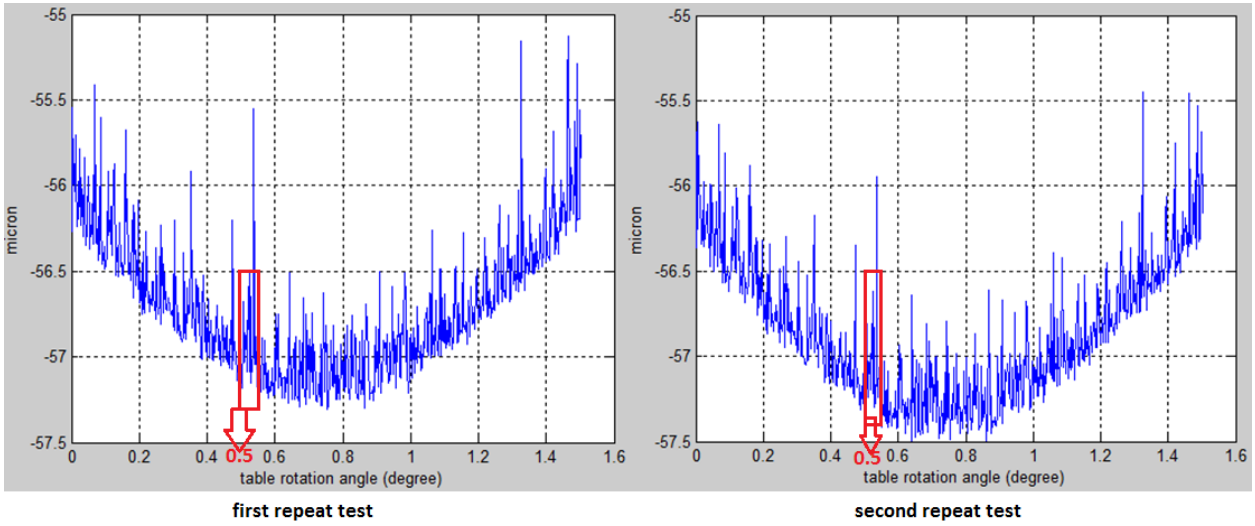

Figure 6-8 Repeat MSF Errors Test

Based on the graph above (Figure 6-7) the assumed MSF feature occurred on the position when the rotary table was rotated with an angle of 1.3 degree. It is necessary to conduct a repeatability test to confirm the assumed MSF feature do occur on the position when the rotary table was further rotated with 0.5 degree (Figure 6-8). This repeatability test was conducted by the thesis author, the original SPP instrument under the identical lab condition. During this repeatability test the testing aluminium mirror remained its origin position on top of the rotary table without any movement. It can be seen that the assumed MSF feature occurred on the position when the rotary table was rotated with an angle of 1.3 degree (0.8+0.5=1.3).

6.3.1 First Confirmation Test of MSF Errors

The previous experiments showed that MSF errors presented on the testing primary aluminium mirror. Within the 43.6364 millimetre measurement path the MSF errors located on the position where the rotary table was rotated for 1.3 degrees. It is necessary to conduct confirmation tests regarding MSF errors to show that the 'bump' feature occurred in the collected data represented the MSF errors on testing mirror (Figure 6-7).

In the first MSF errors confirmation test, in principle the measurement path still coincided with the previous measurement path. However, the whole measurement path was divided into two different sections compared with the previous measurement (Figure 6-9). In details, the testing mirror was initially rotated

for 1.0 degree and then rotated for 1.4 degree (Figure 6-9). During the first test the testing mirror was firstly rotated for 0.8 degrees and then for another 1.5 degrees.

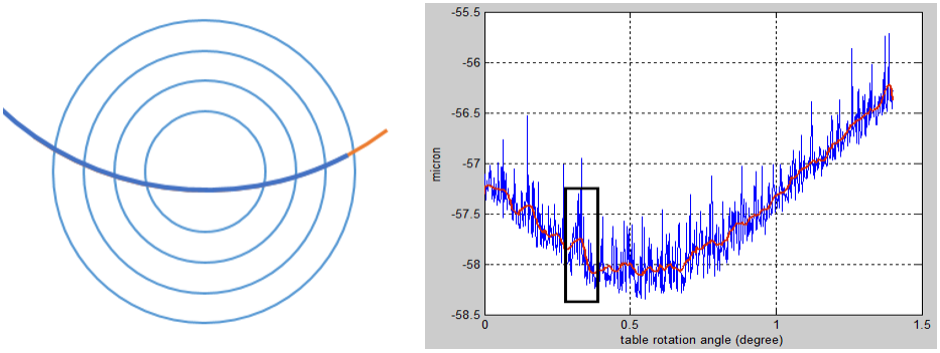

Figure 6-9 MSF Errors First Confirmation Test

It can be shown in the above graph the MSF feature occurred at the position where the air-bearing table was rotated with 1.3 (1.0+0.3=1.3) degree. This results showed that MSF feature occurred at the same position compared with the first MSF errors test.

6.3.2 Second Confirmation Test of MSF Errors

The second MSF errors confirmation test was also conducted afterwards. In principle, the testing mirror was moved along the steel sliding rails with a tiny distance (0.5 mm). Considering the testing mirror's motion distance is so small that the 'bump' feature will occur at the same position if the MSF errors do exist on testing mirror (Figure 6-10).

Move the testing mirror along the sliding rails with a distance of 0.5 millimetre and remain the Armstrong chromatic probe static (Figure 6-10). Then control the rotary table to rotate with 0.8 degree and continue to rotate with 1.5 degree.

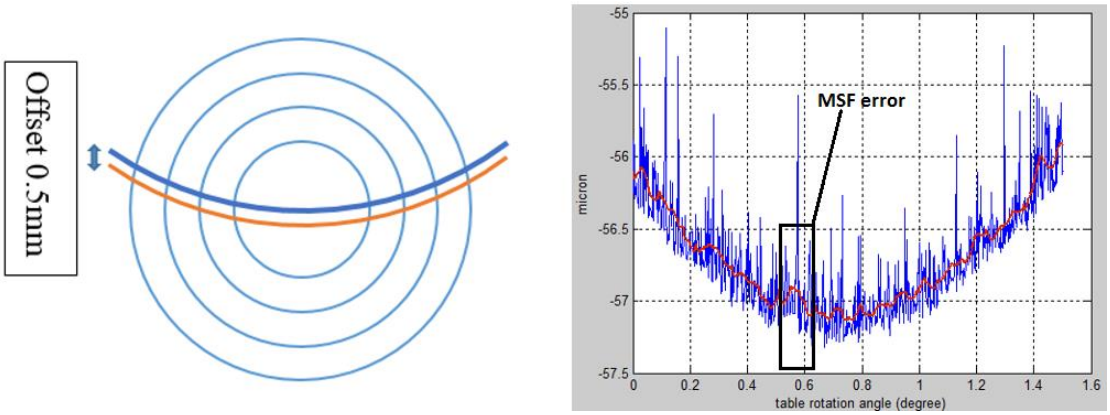

Figure 6-10 MSF Errors Second Confirmation Test

The above figure confirmed that the MSF feature occurred at the position where the air-bearing table was rotated with 1.3 degree (0.8+0.5=1.3). The scale of MSF error in 'Z' direction was 166 nm which coincides with first MSF errors test experiment.

6.4 Conclusions

The two confirmation tests showed that MSF errors presented on the testing aluminium mirror. The concentric ripples in the observed fringe pattern (Figure 6-3) represented the MSF errors on top of the testing primary mirror.

Based on data collected the local height of MSF feature within the 43.6364 millimetre measurement oath was 166 nm. The MSF errors on top of the testing mirror were left by the previous grinding operation. During the grinding operation a single edge of the 'cup wheel' physically touches the aluminium mirror surface. This small contacting area and vibration of the grinding tool could introduce the MSF features.

Chapter 7 Uncertainty Budget of the Swinging Part Profilometer (SPP)

There are many sources of measurement error which can determine certainty of measurement. In the case of surface metrology by using SPP, error sources may come from rotary table's radial runout error, rotation wobble error, sliding rail's bending error and metrology probe's error. The purpose of this chapter is to find out all the possible error sources and quantify them.

7.1 Sliding Rails Stiffness Test

In the Swinging Part Profilometer (SPP) mechanical system, the aluminium Y-shape plate, carbon steel rails and aluminium extrusions are mounted on top of the rotary air-bearing table by M6 bolts (Figure 7-1). On top of the aluminium Y-shape plate there is a five layers 'sandwich' hexagonal glass segment. This segment has the dimensions of corner to corner 1 metre and total thickness of 10 centimetres. The glass segment weights 70.0 kilograms. When conducting the surface measurement by moving the testing surface from centre position to a specified de-centred position the weight (70.0 kg) of hexagonal segment may cause bending or deformation on the aluminium extrusions.

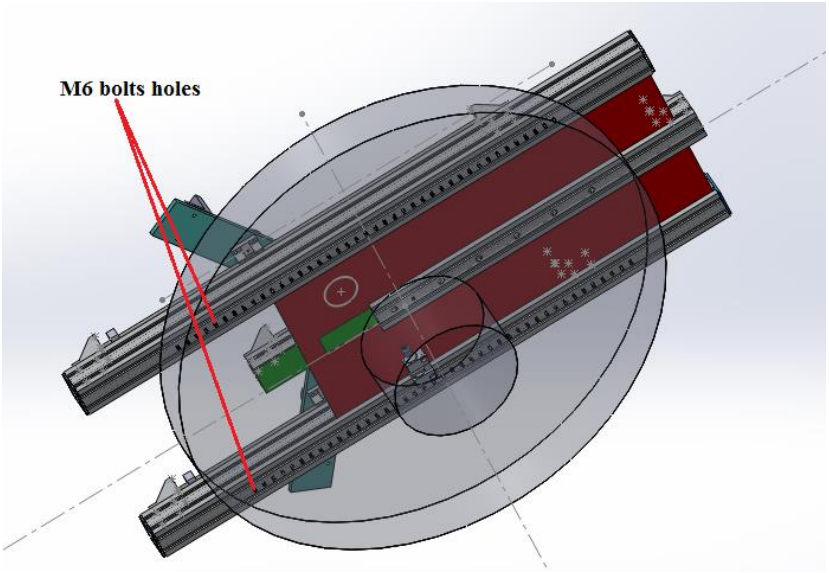

Figure 7-1 SPP Sliding Rails Instalment

7.1.1 Experiment Setup

When the SPP is operated to conduct the surface measurement the air pump in for air-bearing table remained switched on. A thin film of pressurized air (2.7 bar) was provided inside the rotary table to make sure two surface did not touch each other. The use of air-bearing will provide a very low friction between surfaces. In the case of rotary air-bearing table its upper circular flat surface will not touch the basement when rotary table is being rotated. The rotary table's upper surface was floating above the basement with the help of air-bearing. Therefore, the hexagonal segment's surface will be tilted when the segment is moved from centre position to a specified de-centred position along sliding rails.

There are two possible reasons which can cause the change of the segment's upper surface. The first one is the existence of air-bearing inside the rotary table. The 70.0 kilograms segment may cause one end of the aluminium extrusion downward and the opposite end upward. The second reason is when the segment is moved to a de-centred position its weight can cause the bending of aluminium extrusions. It is necessary to quantify the scale of aluminium extrusions bending and variation of segment's floating. A micron dial indicator gauge and an Armstrong Precitec chromatic probe were used to record the data. The configuration is shown below (Figure 7-2):

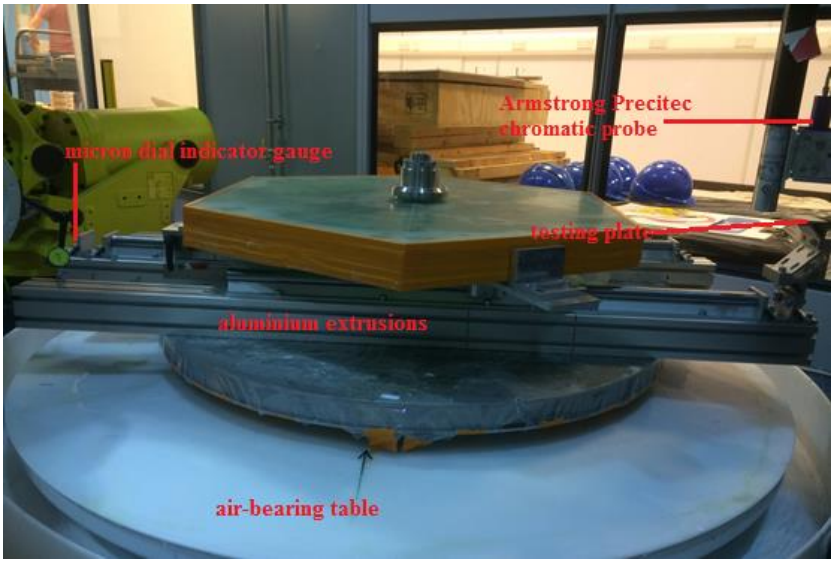

Figure 7-2 Sliding Rails Stiffness Test Configuration

Firstly, the air supply for the rotary table was switched off. Then segment was moved along the sliding rails with an increment of 5 centimetres each time and record the readout for both the micron dial indicator and chromatic probe. When the air pump-in was switched off the rotary table will be attached to table's basement and cannot be rotated. Therefore, the change of the segment's upper surface caused by air-bearing can be excluded. Each time the segment was moved long the sliding rails with a distance of 5 centimetres and locked on the rails, record the readouts on micron dial indicator gauge and chromatic probe. The maximum de-centred length was 25 centimetres and then the segment was moved back to its original position with an increment of 5 centimetre.

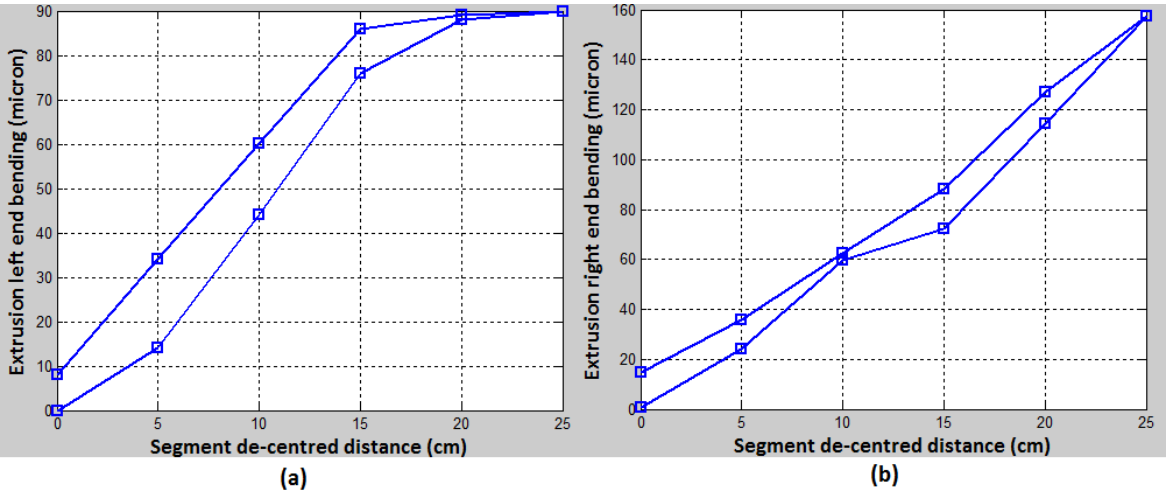

Figure 7-3 Aluminium Extrusion Two Terminals Variations

During the test the air pump-in was switched off so the circular pad beneath the aluminium extrusions was attached to the table's basement and remained static. It can be shown from the figure above (Figure 7-3) the maximum extrusion bending occurred on the position when the segment was moved to its maximum de-centred position of 25 centimetres. On the right side the extrusion's terminal bended with 157 microns and on the left side the extrusion's end pointed upward with 90 microns. Therefore, during the segment motion along the sliding rails which is essential to conduct an arc scan measurement the aluminium extrusions will bend due to the weight of glass segment.

7.2 Rotary Table Motion Radial Runout

Radial runout is defined as the total indicted reading of the horizontal movement of the rotary table. When using the SPP to conduct a surface measurement a series of concentric circles are required to measure. The rotary table will be controlled by a Matlab programme to rotate with 360 degree in order to complete a circular scan on a testing surface.

7.2.1 First Experiment Setup

Firstly, a Solartron Pneumatic Probe DP/10/P was used to quantify the rotary table's radial runout error. The probe was placed horizontally and perpendicularly touching the outer wall of the rotary table (Figure 7-4).

Figure 7-4 Rotary Table Radial Runout First Test

It can be shown from the figure that the Solartron pneumatic probe was mounted on switchable magnetic base with M8 mounting hole. The two magnetic bases were attached to a circular iron basement. This mechanical configuration will make sure that during the rotary table's rotation the pneumatic probe can remain static. A Matlab program was used to control both pneumatic probe and rotary table so that probe's data collection and table's rotation can be executed simultaneously.

This test targeted on the rotary table's outer wall by pneumatic probe has been conducted for eight times (Figure 7-5). The maximum probe data difference within eight test was 258.8 microns (Figure 7-5). The probe's data variation has two sources. One is the real rotary table's radial runout error, the other one comes from the testing rotary table's outer wall. The testing outer wall was not machined with ultra-precision so that its surface cannot be regarded as a reference surface. However, it can be concluded that the rotary table's radial runout was less than 258.8 microns.

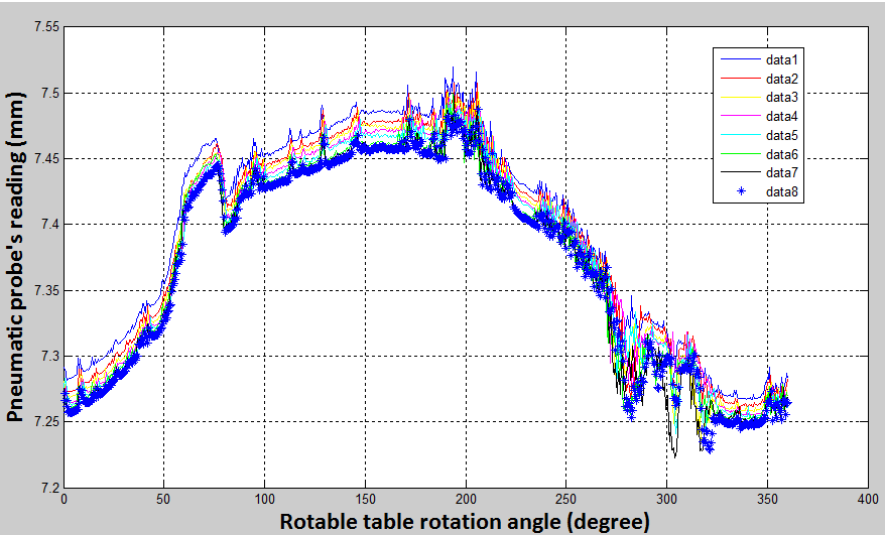

Figure 7-5 Rotary Table Outer Wall Eight Tests

7.2.2 Second Experiment Setup

During the first experiment on testing rotary table's radial direction runout the cylindrical testing surface was not machined perfectly, therefore this cylindrical testing surface cannot be treated as a reference surface. This cylindrical testing surface finish error, rotary table's radial direction runout error and rotation axis wobble error were combined. The testing cylindrical surface roughness was unknown. Therefore, based on the first rotary table's radial direction runout experiment it is essential to conduct another experiment to quantify the rotary table's radial runout.

In the second test a second testing by using a calibration master ball and a XY translation stage was conducted (Figure 7-6). This calibration ball was made of high carbon chrome steel which showed excellent hardness, wear resistance, surface finishing and dimensional stability.

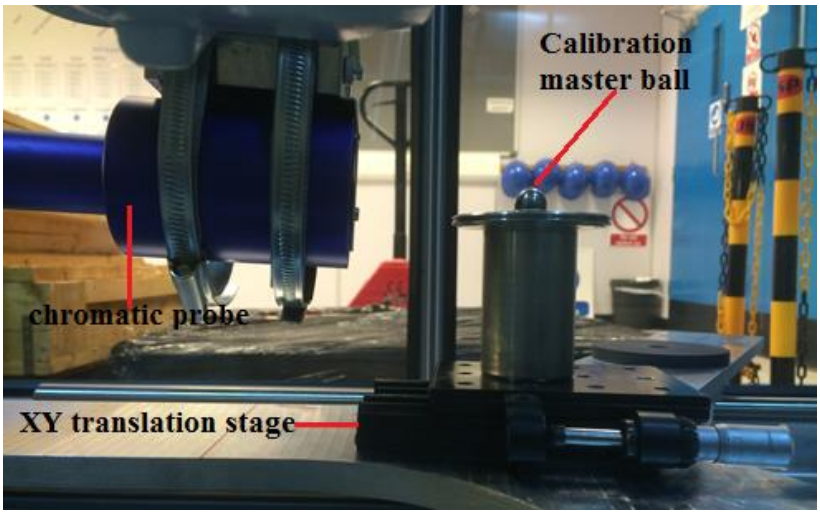

Figure 7-6 Rotary Table Radial Runout Test by Using Master Ball

Firstly, it is essential to place the calibration master ball on the table's rotation centre. An Armstrong Precitec chromatic probe was used to help position the calibration master ball (Figure 7-6). The XY translation stage was mounted on top of Y-shape plate by a M6 bolt. Control the rotary table to rotate for a full circle (360 degree) and figure out the de-centre direction based on chromatic probe's data and its relevant table's rotation angle. Adjust the XY translation stage after rotating rotary table with one circle. After that, adjust the height of the chromatic probe to make sure the light spot from the probe focused on the master ball's most outer edge.

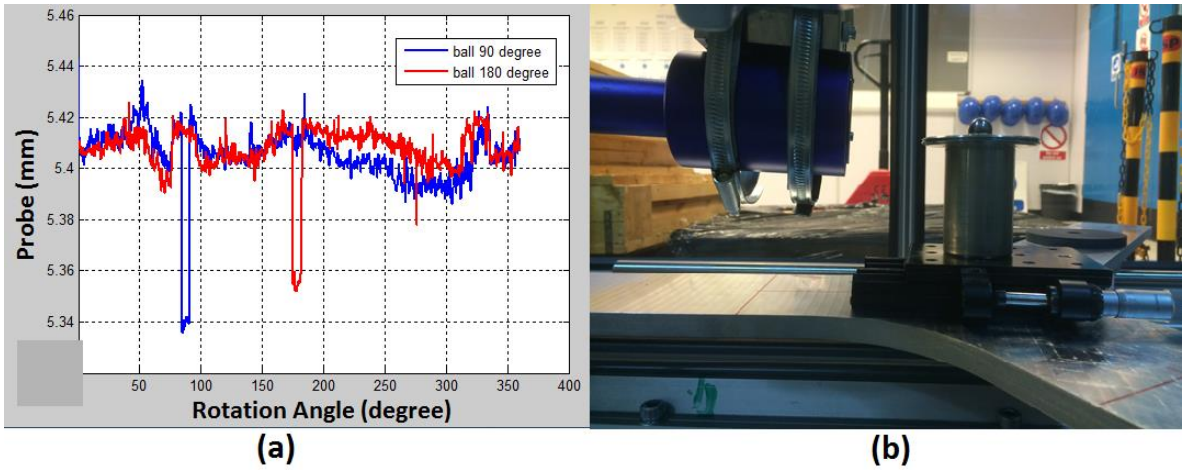

Figure 7-7 Rotary Table Radial Runout Error Test

It can be shown from the graph above (Figure 7-7) the maximum variation of the testing master's surface was 30 microns. The calibration master ball was fixed to the Y-shape plate so the master ball's variation

can represent the rotary table's radial direction runout. In order to confirm this result, a permanent mark pen was used to make a vertical mark on master ball's surface. Rotate the testing master ball with 90 degrees and test it again. After rotating the master ball it is necessary to re-centre the master ball since its original position was changed. According the graph (Figure 7-7) the maximum rotary table's radial runout occurred on the position when rotary table was rotated 70 and 300 degree (Figure 7-7).

7.3 Rotary Table's Wobble Error Test

The rotary table's wobble error was defined as the angular error between the actual axis of rotation and the theoretical axis of rotation (Figure 7-8). The rotary table's wobble error will affect the accuracy when conducting the concentric scans on surface measurement.

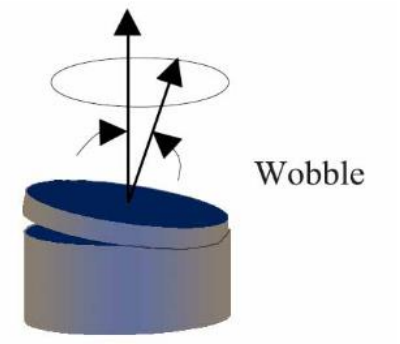

Figure 7-8 Rotary Table Wobble Error

The same calibration master ball was used as the testing reference surface and a XY translation stage can help centre the master ball. After centring the calibration precision ball on top of the Y-shape plate the metrology probe's data collection should be conducted. Control the rotary table to rotate for a full circle (360 degree) and the chromatic probe collect the position variation of the master ball simultaneously.

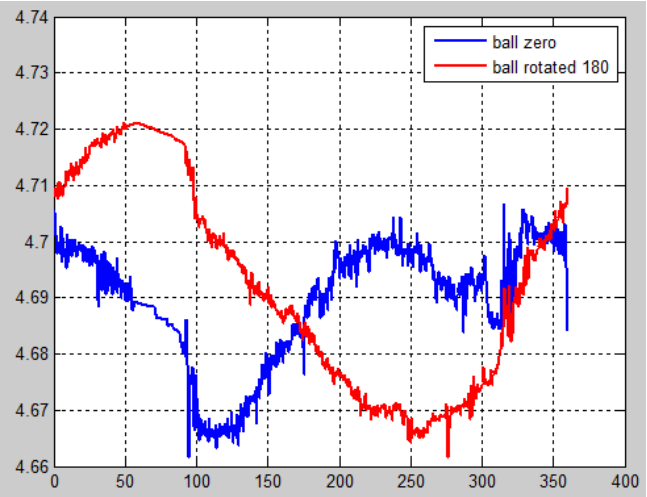

Figure 7-9 Rotary Table's Wobble Error Test

According the graph (Figure 7-9) the rotary table's rotation axis swung during a full circular rotation and it swung most when the rotary table rotated 100 degrees. The zero degree position of the rotary table was defined by Hall Effect Sensor installed beneath the rotary table. In order to confirm the result of rotary table's wobble error test a confirmation experiment was conducted.

Reverse the calibration master ball (180 degree) and re-centre it with the help of XY translation stage and chromatic probe. It was assumed that if the rotary table swung most at the rotation angle of 100 degree, when the testing calibration master ball was reversed by 180 degree the rotary table should be swung most at the rotation angle of 280 degree (100+180). It can be shown from the graph above (Figure 7-9) the 'valley' position transferred from 100 degree to 280 degree. This confirmation test confirmed the rotary table wobble error's position.

Another test should be conducted to confirm the scale of rotary table's wobble error. A cylindrical steel block was placed underneath the calibration ball and attach to which to vary the testing master ball's height. The master ball was need to re-centre since the introduction of a steel block. The confirmation test result was shown below:

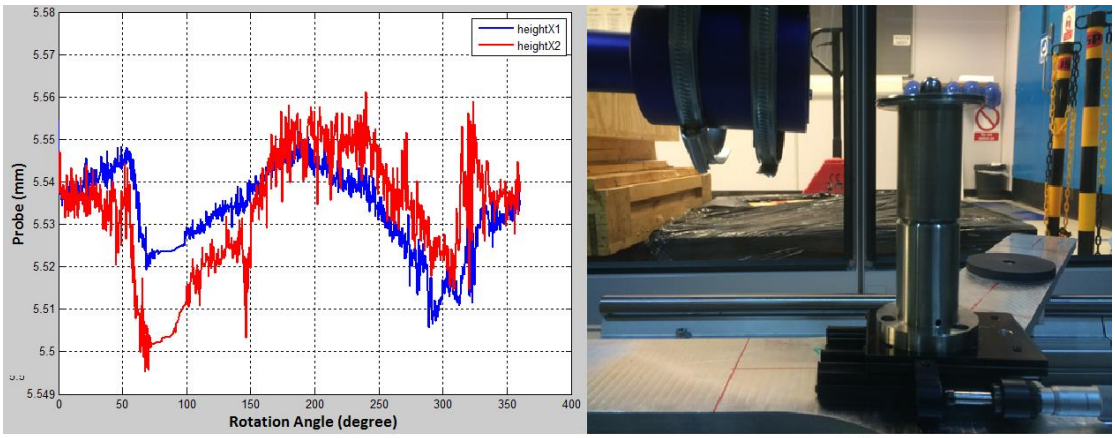

(a) (b)

Figure 7-10 Confirmation Test of Rotary Table Wobble Error

It can be shown from the graph (Figure 7-10) that when the total height of testing master ball has been doubled, the maximum variation of chromatic probe's data was also doubled.

7.4 Summary

In this chapter, the error sources of the SPP have been identified. The SPP uncertain budget contains sliding rails stiffness, the rotary table's radial runout and its wobble error. Based on data collected it can concluded that the air-bearing rotary table contributed the major error source of the whole SPP measurement system. Based on a series experiments increase the pressure of the air supply of the rotary table can improve the rotary table's rotation stability.

Chapter 8 Chromatic Probe Maximum Measurement Angle to Surface

8.1 Introduction

In the Swinging Part Profilometer (SPP) surface metrology system, chromatic probes with different resolutions (20nm/300nm) produced from Precitec Group were used in order to gain surface profile information. With different surface quality left by 'pre-polishing' on Zeeko IRP polishing machine, the maximum measurement angle to surface of the chromatic probe should be varied. The chromatic probe adopted in SPP used the principle of chromatic aberration [47, 49]: a white light beam will be split into different color light beams based on their own wavelength. When a testing surface is presented within the probe's measurement range the only corresponding wavelength will be focused on the testing surface and then reflected into the probe's optical system.

When measuring spherical or aspherical surfaces the probe will not be always normal to a testing surface. The chromatic probe will have an angle to the testing surface. When the probe is placed normal to the testing surface most of reflected light beam can be gathered by its own optical system. However, if the probe is tilted to the testing surface when measuring spherical or aspherical surfaces some of the reflected light beam will be scattered. The probe's optical system won't gain the scattered light and then the position of the testing surface along 'Z' axis cannot be determined in the measurement range.

The aim of this chapter is figuring out the maximum measurement for chromatic probes with different resolutions (20nm/200nm) when illuminating different surface quality. For each surface quality finished by Zeeko IRP polishing machine the maximum measurement angle for each chromatic probe was determined based on experiments data. This will find out the probe's measurement capability.

8.2 Experiment Procedures

In the experiments, a piece of square BK7 glass was used as the testing surface (Figure 8-1). During the experiments the BK7 testing sample was placed normal to a high precision rotary mount (Figure 8-1). This

Edmund@ rotary mount has continuous 360 degrees scale with 1 degree increment. This rotary mount was fixed on top of a circular matrix board with three clamps (Figure 8-1). Since the texting surface was positioned vertically to the matrix board, the chromatic probe was aligned horizontally with the matrix board. Initially, the chromatic probe was perpendicular to the testing surface (Figure 8-1).

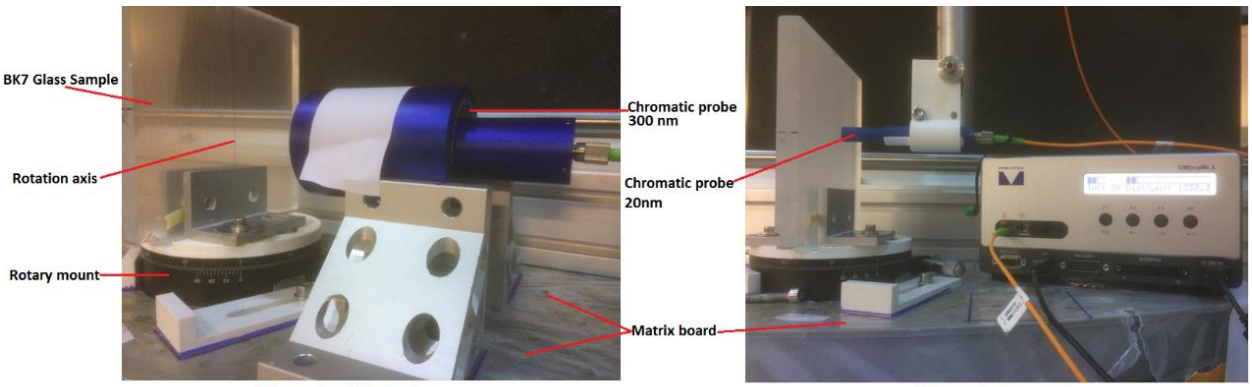

Figure 8-1 Experiment setup

Before conducting experiments the testing BK7 sample was smoothed for 20 minutes with cerium oxide (CeO_2) in order to remove other surface scratches such as mid spatial frequency (MSF) feathers left by previous fabrication process. Aligned the chromatic probe back and forth until the focused light spot on the testing surface was sharp and illuminated. Make sure the focused light spot was located on the rotation axis line marked on the testing surface (Figure 8-1). Make sure the rotation axis line coincides with the symmetrical line of the testing sample.

This step can guarantee that the chromatic probe could measure the same point of the testing surface during experiments.

Then record the probe's reading when probe was normal to the testing surface. In this experiment configuration when probe was placed normal to the testing surface the measurement angle to surface was defined as 0 degree (Figure 8-2). When the probe was parallel to the testing surface the measurement angle to surface was defined as 90 degree (Figure 8-2).

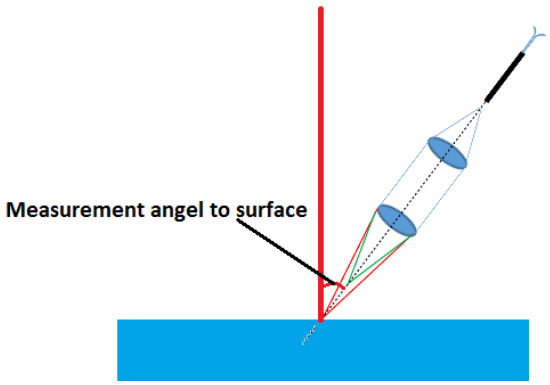

Figure 8-2 Measurement angle to surface definition

Rotate the rotary mount with an increment of 1 degree and record the probe's reading and rotary mount's rotation angle value. Repeat the above step until the chromatic probe was unable to record any data. When the probe cannot record any data the corresponding rotation angle of the rotary mount stage can be considered as the maximum measurement angle to surface. This maximum measurement was corresponding the initial surface quality.

After testing the first surface quality of the testing sample, the testing sample was transferred to conduct the polishing process by Zeeko IRP polishing machine in order to get a different surface quality (Figure 8-3). The polishing process took 16 minutes and totally nine polishing process were conducted (Figure 8-3).

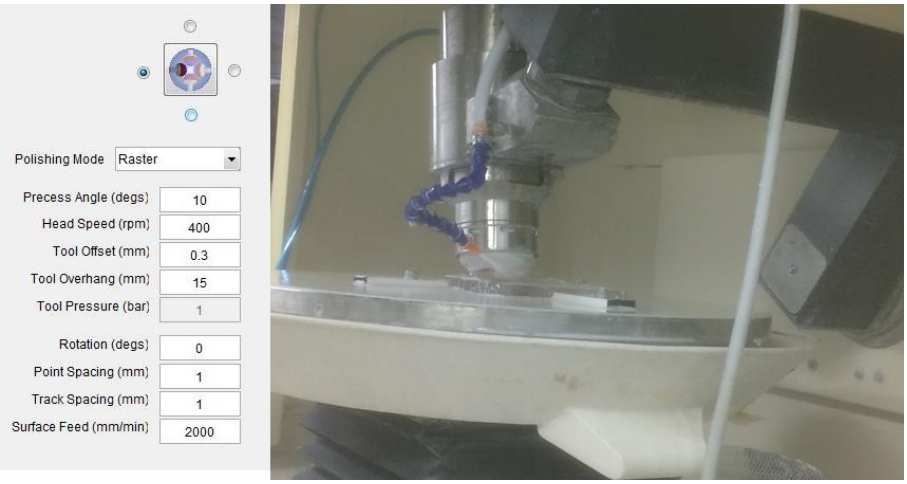

Figure 8-3 Polishing with Zeeko IRP 600

Each time when the testing surface was polished it was then transferred to conduct the surface texture measurement. The surface texture measurement was carried out by Nikon ADE MicroXam Optical Surface Profiler. This surface profiler has a height resolution of 0.1 nm and a footprint of 1mm×1mm (Figure 8-4).

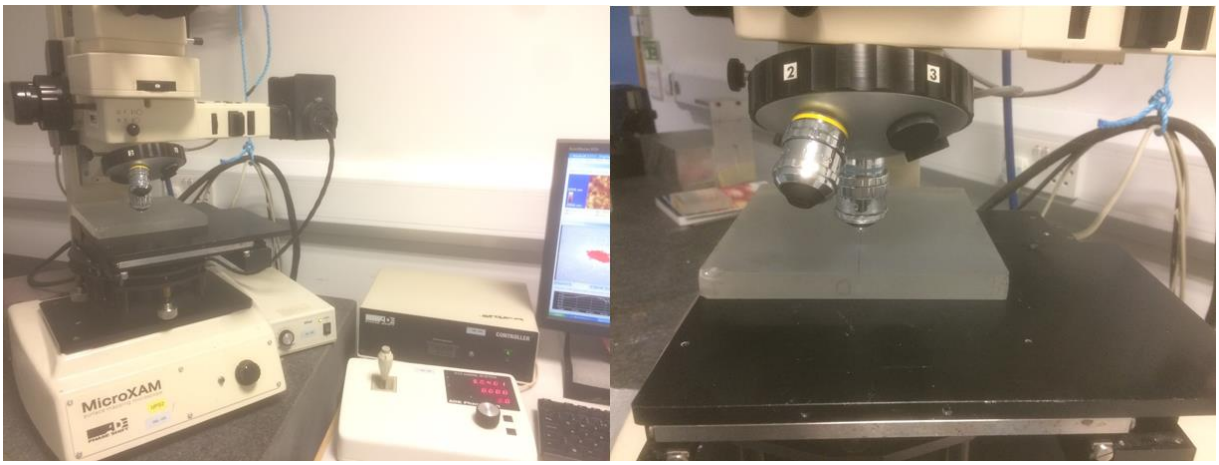

Figure 8-4 Nikon ADE MicroXam Optical Surface Profiler

8.3 Maximum Measurement Angle to Surface Corresponding to Surface Quality

Each time when the testing sample was processed by polishing then it was conducted by surface measurement to gain the surface quality data. After that, the testing sample was placed back on top of the rotary mount to find out the maximum measurement angle to surface. Each time both chromatic probe and rotary mount remained static. The above procedures were conducted for two chromatic probes with different resolutions (20nm/300nm).

Based on the collected experiments data the maximum measurement angle to surface after each time polishing were shown in table below:

Table 8-1 Maximum Measurement Angle to Surface for 300nm Chromatic Probe

300nm Chromatic probe Maximum Measurement Angle to Surface										
Polish	Before polish	1st polish	2nd polish	3rd polish	4th polish	5th polish	6th polish	7th polish	8th polish	9th polish

Angle (°)	65	61	59	48	47	46	43	38	20	15

Table 8-2 Maximum Measurement Angle to Surface for 20nm Chromatic Probe

20nm Chromatic probe Maximum Measurement Angle to Surface										
Polish	Before polish	1st polish	2nd polish	3rd polish	4th polish	5th polish	6th polish	7th polish	8th polish	9th polish
Angle (°)	20	19	18	16	15	13	12	11	10	6

Based on the data collected graphs can be plotted to show the relations between the maximum measurement angle to surface and surface quality. It can be shown from the graph below as the testing sample was polished the maximum measurement angle to surface declined gradually (Figure 8-5). For 300nm chromatic probe the maximum angle declined from 65 degree to 15 degree. For 20nm chromatic probe the maximum angle decreased from 20 degree to 6 degree (Figure 8-5). Since the testing sample has been polished for nine times the sample's surface was becoming smoother. Therefore, as the testing sample's surface was getting smoother the chromatic received less backscattered light. The reduced received backscattered light weakened the chromatic probe's performance.

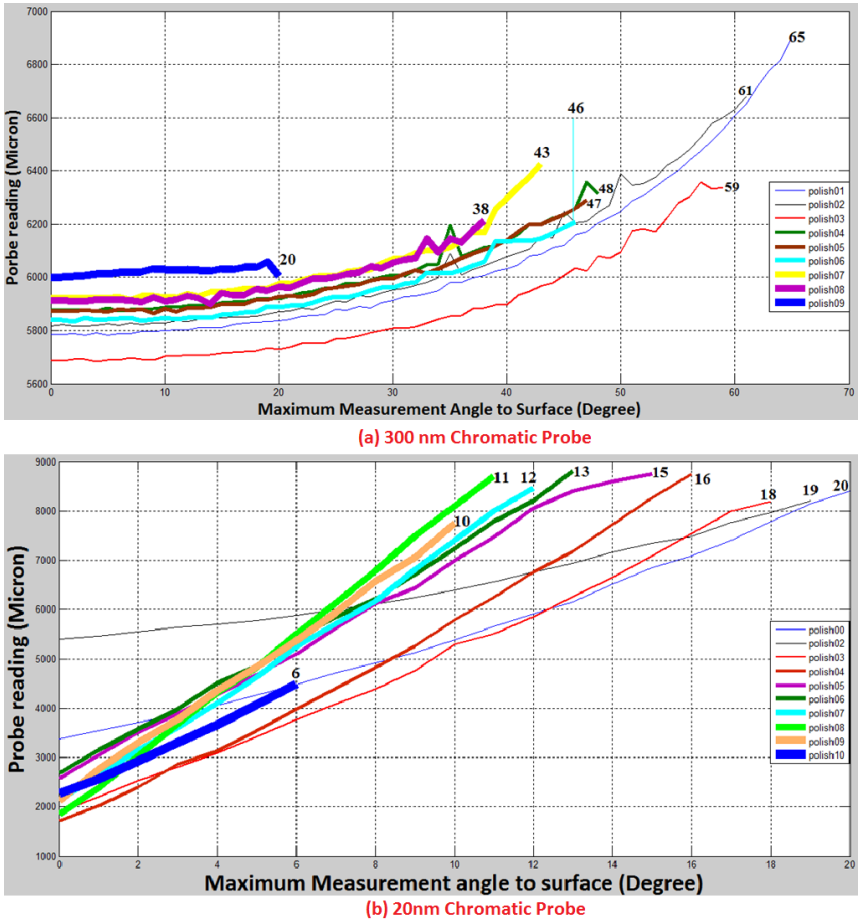

Figure 8-5 Maximum measurement angle to surface

A Nikon ADE MicroXam Optical Surface Profiler was used to measure the sample's surface texture. When both the chromatic probe and testing sample were aligned properly the position of the focused light spot was marked. Each time this marked spot was measured by surface profiler. This surface profiler can give the local surface texture map (Figure 8-6). It can be shown from the graph below initially as the influence of chemical mechanical planarization [94] (combination of chemical etching and abrasive polishing) many surface scratches were available. After the testing sample has been polished time by time these scratches were becoming less until finally only a few scratches can be found (Figure 8-6).

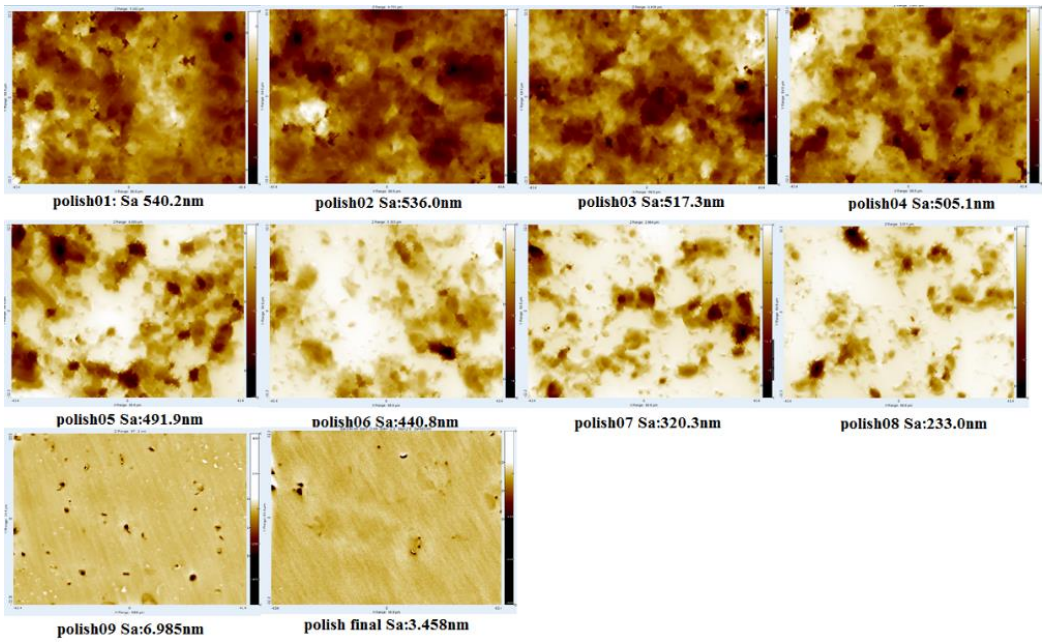

Figure 8-6 Surface texture result

Finally, based on all the surface quality data and maximum measurement angle to surface for two chromatic probes (20nm/300nm) a graph was plotted below (Figure 8-7). It can be concluded from the graph that the probe with 300nm resolution has larger maximum measurement angle to surface than 20nm probe when measuring the same surface.

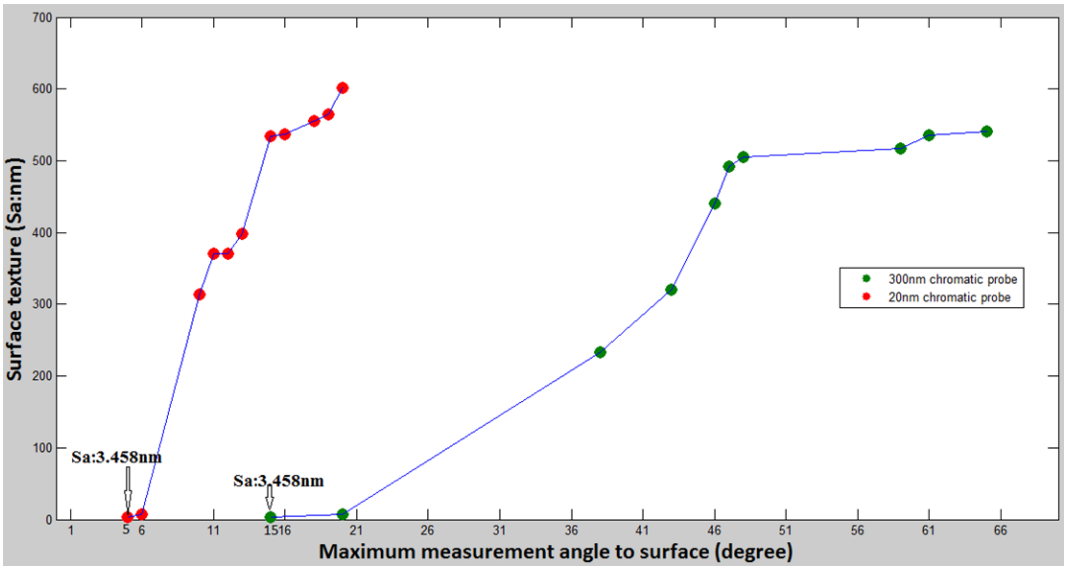

Figure 8-7 Maximum measurement angle to surface corresponds to different surface texture

8.4 Summary

In this chapter, the maximum measurement angle to grey surfaces has been determined. When the SPP is utilised to measure surfaces the chromatic probe remains still. If the testing surface is flat the chromatic probe will be positioned normal to the testing workpiece. However, if the testing mirror is spherical or aspherical the probe cannot be always perpendicular to the testing workpiece. Therefore, it can be concluded that the probe will not receive any data when the testing spherical surface is moved to a certain position. Furthermore different surface texture quality can also cause the probe's data recording performance. It is necessary to figure out the chromatic probes (300nm/20nm) maximum measurement angle to surface. This will help us to determine which probe with a certain vertical resolution should be used when testing a workpiece with a certain surface texture quality.

Chapter 9 Conclusions

This research is aimed at designing, installing and testing an in-situ surface metrology instrument which can bridge the gap between CNC grinding and CNC polishing. The next generation ground-based telescope, E-ELT was determined to adapt segmented mirrors. Each hexagonal segment has a dimension of 1.4 metre corner-to-corner and its fabrication is challenging. The whole fabrication process starts from Cranfield University's BoX™ CNC grinding to Zeeko CNC polishing. In order to speed up the whole segment fabrication process and remove the MSF features left by the grinding process, a 'grolishing' process which was the intermediate process between grinding and polishing was developed. The 'grolishing' process was conducted by a FANUC or an ABB industrial robot. The surface after a 'grolishing' process was unable to be measured by an interferometer and current stylus type profilometer has a maximum measurement range of 300 millimetre. Therefore, a novel surface metrology instrument with can measure large optics (above 500 millimetre) and can measure grey surface was demanded. This surface metrology instrument can also conduct in-situ measurement.

The contributions to this aim of research are listed below:

1. Using Solidworks designed all the components of the SPP (Swinging Part Profilometer).
2. Install all the SPP components together and develop necessary Matlab GUI programme to control both rotary table rotation and metrology probe's data logging.
3. Design a surface reconstruction algorithm for the SPP and develop the relevant Matlab GUI programme to conduct data logging and data stitching.
4. The SPP was used to test a hexagonal flat mirror and a 3D surface error map with PV: 1.532 μm and RMS: 0.19 μm was gathered. This result was compared with 4D interferometer error map (PV: 0.263 μm RMS: 0.03 μm).
5. The SPP was used to test a hexagonal concave spherical mirror with ROC of 3m.

6. The SPP was used to test the MSF errors on the surface of an off-axis parabolic concave aluminium mirror with a 20nm vertical resolution chromatic probe which was mounted on the terminal of an ABB industrial robot arm. The MSF errors can be identified by the SPP.
7. Test the maximum measurement angle to surface of two chromatic probes with different resolutions (300nm/20nm). It can be concluded that the testing surface has been polished over and over again (nine times), the probe's maximum measurement angle to surface declined gradually. For 300nm chromatic probe the maximum measurement angle declined from 65 degree to 15 degree. For 20nm chromatic probe the maximum measurement angle decreased from 20 degree to 6 degree.

9.1 Future Work

The SPP was designed to fill up the gap of surface metrology for large optics which was on the stage between surface grinding and polishing. It was scheduled to provide a method to achieve the in-situ surface metrology method which can significantly improve the efficiency for optical fabrication and metrology. The SPP presented in the thesis was the prototype instrument and some necessary future work could be conducted in order enhance the performance of surface metrology.

- Larger size optical component should be tested by SPP. The largest testing surface has been tested by SPP was the hexagonal spherical concave mirror with a dimension of 400mm of corner-to-corner. Based on the design model of the SPP larger size testing surface with an aperture of 800mm can be measured by SPP.
- Improve the rotation accuracy of the air-bearing rotary table. The SPP used the 1.2m diameter air-bearing rotary table and this table itself was not equipped with an incremental encoder to precisely indicate the table's rotation position. The SPP used a Hall Effect switch sensor and an encoder which can monitor the motor's spinning to calculate the rotary table's angular position. It cannot directly read the rotary table's angular position. This drawback can cause the angular errors for the arc scan on a testing surface.

- Conduct the test for convex spherical mirror. In this thesis both flat and concave spherical mirrors were tested by the SPP. Based on the measurement theory convex spherical mirrors can be measured by the SPP. Therefore, in future convex mirrors should be tested by the SPP to test the performance of the whole system.
- Design a different measurement theory and data stitching algorithm for SPP. The new measurement theory can be, firstly measure a series of arc scans by moving the testing surface with different offset values, then rotate the testing surface with 120 degree and measure another set of arc scans. Finally stitch the two groups of arc scans data together or obtain a 3-D surface error map.

Appendix 1 SPP Control Matlab GUI Codes

This Matlab code was developed by me in order to manipulate the whole system of the Swinging Part Profilometer (SPP). This programme includes connecting metrology probes (Solartron pneumatic probe or Armstrong chromatic probe), connecting motor for powering air-bearing rotary table, controlling air-bearing rotary table to rotate to the specified starting point, collecting probe's data for a circular on a testing surface, collecting probe's data for an arc scan with a specified angle on a testing surface and saving all the collected data.

```
function varargout = spp_metrology_control(varargin)
% SPP_METROLOGY_CONTROL MATLAB code for spp_metrology_control.fig
%      SPP_METROLOGY_CONTROL, by itself, creates a new SPP_METROLOGY_CONTROL or raises the existing
%      singleton*.
%
%      H = SPP_METROLOGY_CONTROL returns the handle to a new SPP_METROLOGY_CONTROL or the handle to
%      the existing singleton*.
%
%      SPP_METROLOGY_CONTROL('CALLBACK',hObject,eventData,handles,...) calls the local
%      function named CALLBACK in SPP_METROLOGY_CONTROL.M with the given input arguments.
%
%      SPP_METROLOGY_CONTROL('Property','Value',...) creates a new SPP_METROLOGY_CONTROL or raises the
%      existing singleton*.  Starting from the left, property value pairs are
%      applied to the GUI before spp_metrology_control_OpeningFcn gets called.  An
%      unrecognized property name or invalid value makes property application
```

```
%      stop.  All inputs are passed to spp_metrology_control_OpeningFcn via varargin.
%
%      *See GUI Options on GUIDE's Tools menu.  Choose "GUI allows only one
%      instance to run (singleton)".
%
% See also: GUIDE, GUIDATA, GUIHANDLES
% Edit the above text to modify the response to help spp_metrology_control
% Last Modified by GUIDE v2.5 16-Dec-2016 21:24:21
% Begin initialization code - DO NOT EDIT
gui_Singleton = 1;
gui_State = struct('gui_Name',       mfilename, ...
                   'gui_Singleton',  gui_Singleton, ...
                   'gui_OpeningFcn', @spp_metrology_control_OpeningFcn, ...
                   'gui_OutputFcn',  @spp_metrology_control_OutputFcn, ...
                   'gui_LayoutFcn',  [] , ...
                   'gui_Callback',   []);
if nargin && ischar(varargin[89])
    gui_State.gui_Callback = str2func(varargin{1});
end


if nargout
    [varargout{1:nargout}] = gui_mainfcn(gui_State, varargin{:});
else
    gui_mainfcn(gui_State, varargin{:});
end
% End initialization code - DO NOT EDIT
```

```
% --- Executes just before spp_metrology_control is made visible.
function spp_metrology_control_OpeningFcn(hObject, eventdata, handles, varargin)
% This function has no output args, see OutputFcn.
% hObject    handle to figure
% eventdata  reserved - to be defined in a future version of MATLAB
% handles    structure with handles and user data (see GUIDATA)
% varargin   command line arguments to spp_metrology_control (see VARARGIN)

% Choose default command line output for spp_metrology_control
handles.output = hObject;

% Update handles structure
guidata(hObject, handles);

% UIWAIT makes spp_metrology_control wait for user response (see UIRESUME)
% uiwait(handles.figure1);


% --- Outputs from this function are returned to the command line.
function varargout = spp_metrology_control_OutputFcn(hObject, eventdata, handles)
% varargout  cell array for returning output args (see VARARGOUT);
% hObject    handle to figure
% eventdata  reserved - to be defined in a future version of MATLAB
% handles    structure with handles and user data (see GUIDATA)
```

```
% Get default command line output from handles structure
varargout{1} = handles.output;



% --- Executes on button press in connect_probe.
% This section can find and set up connection with Armstrong chromatic probe
function connect_probe_Callback(hObject, eventdata, handles)
% hObject    handle to connect_probe (see GCBO)
% eventdata  reserved - to be defined in a future version of MATLAB
% handles    structure with handles and user data (see GUIDATA)
obj1 = instrfind('Type', 'serial', 'Port', 'COM7', 'Tag', '');
if isempty(obj1)
    obj1 = serial('COM7');
else
    fclose(obj1);
    obj1 = obj1(1)
end
set(obj1, 'BaudRate', 921600);
set(obj1, 'InputBufferSize', 4096);
set(obj1, 'OutputBufferSize', 4096);


handles.probe = obj1;
guidata(hObject,handles);
```

```
% --- Executes on button press in connect_motor.
% This section can set up connection with a motor which can power the air-bearing rotary table.
function connect_motor_Callback(hObject, eventdata, handles)
% hObject    handle to connect_motor (see GCBO)
% eventdata  reserved - to be defined in a future version of MATLAB
% handles    structure with handles and user data (see GUIDATA)

pid= 'MintControls5706.MintController.1';
h=actxcontrol(pid);
invoke(h,'setEthernetControllerLink','192.168.0.1');

handles.h = h;
guidata(hObject,handles);



% --- Executes on button press in table_move_clock.
% This section can control the air-bearing rotary table to rotate in a clockwise direction.
function table_move_clock_Callback(hObject, eventdata, handles)
% hObject    handle to table_move_clock (see GCBO)
% eventdata  reserved - to be defined in a future version of MATLAB
% handles    structure with handles and user data (see GUIDATA)

h = handles.h;
invoke(h,'jog',0,-20);% control rotary table to rotate clockwise
guidata(hObject,handles);
```

```
% --- Executes on button press in table_stop.
& This section can stop the air-bearing rotary table's motion.
function table_stop_Callback(hObject, eventdata, handles)
% hObject    handle to table_stop (see GCBO)
% eventdata  reserved - to be defined in a future version of MATLAB
% handles    structure with handles and user data (see GUIDATA)

h = handles.h;
invoke(h,'DoStop',0);% stop the rotary table's motion
guidata(hObject,handles);



% --- Executes on button press in start_point_go.
% This section can control the air-bearing rotary table to rotate to its starting point defined by Hall effect
sensor.

function start_point_go_Callback(hObject, eventdata, handles)
% hObject    handle to start_point_go (see GCBO)
% eventdata  reserved - to be defined in a future version of MATLAB
% handles    structure with handles and user data (see GUIDATA)
h = handles.h;

x0=0;% record the initial value of Hall effect sensor position.
invoke(h,'jog',0,20); % start the rotary table's rotation.
% this while loop can control the rotary table to go back the specified starting point position
```

```
while(1)    x1=get(h,'INX',0);
   if (x0==0&x1==0)
     invoke(h,'DoStop',0)
     encoderoriginal=get(h,'ENCODER',2);
     break
   end
   x0=x1;
end

guidata(hObject,handles);



% --- Executes on button press in one_full_circle.
% This section can control the air-bearing rotary table to rotate with a full revolution (360 degree).

function one_full_circle_Callback(hObject, eventdata, handles)
% hObject    handle to one_full_circle (see GCBO)
% eventdata  reserved - to be defined in a future version of MATLAB
% handles    structure with handles and user data (see GUIDATA)
h = handles.h;
obj1 = handles.probe;

encoder0=get(h,'ENCODER',2); %read and record the initial position of the motor.
encoderoriginal=encoder0;

invoke(h,'jog',0,-100);% control the rotary table to move with a specified speed.
```

```
currentangle=[]; % save all the real-time rotary table's rotation angle with respect to its starting point.
currentangle(1)=0; % define current angle as zero degree when rotary table at its starting point.
current=1;
fopen(obj1)
probedata=[];% save all the metrology probe's data an array.

% this while loop control the rotary table to rotate with a full revolution.
while(1)
    encoder1=get(h,'ENCODER',2); %read and record the initial position of the motor.
    data_ch_f= fscanf(obj1);
    while(length(data_ch_f)~=19);
      data_ch_f= fscanf(obj1);
    end
    data_ch=deblank(data_ch_f(1,1:5));
    probedata(current) = str2num(data_ch)/32768*10;
   currentangle(current,1)=(encoderoriginal-encoder1)*0.002247358942576249;
% calculate the rotary table's real-time rotation angle based on the motor's encoder value
    if(currentangle(current)>=360) % when real-time rotary table's rotation angle equals to 360degree or
is bigger than 360 degree the motor will be stopped.
      invoke(h,'DoStop',0) % stop the motor
      break
    end
    current=current+1;
end

handles.probe = probedata;
```

```
handles.table.angle = currentangle;
guidata(hObject,handles);
update_axes1(hObject, eventdata, handles);



% --- Executes during object creation, after setting all properties.
function axes1_CreateFcn(hObject, eventdata, handles)
% hObject    handle to axes1 (see GCBO)
% eventdata  reserved - to be defined in a future version of MATLAB
% handles    empty - handles not created until after all CreateFcns called

% Hint: place code in OpeningFcn to populate axes1
% currentangle = handles.table.angle;
% probedata = handles.probe;
% plot(currentangle',probedata);
% grid on;
% xlabel('Rotation Angle (degree)','FontSize',12,'FontWeight','bold');
% ylabel('Probe (mm)','FontSize',12,'FontWeight','bold');
% guidata(hObject,handles);

function update_axes1(hObject, eventdata, handles)
currentangle = handles.table.angle;
probedata = handles.probe;
plot(currentangle',probedata);
grid on;
xlabel('Rotation Angle (degree)','FontSize',12,'FontWeight','bold');
```

```
ylabel('Probe (mm)','FontSize',12,'FontWeight','bold');
guidata(hObject,handles);


% --- Executes on button press in save_data.
% This section can save all the collected probe's data and rotary table's position data into a TXT file.
function save_data_Callback(hObject, eventdata, handles)
% hObject    handle to save_data (see GCBO)
% eventdata  reserved - to be defined in a future version of MATLAB
% handles    structure with handles and user data (see GUIDATA)
currentangle = handles.table.angle; % get rotary table's rotation angle
probedata = handles.probe; % get probe's data
data = [currentangle,probedata']; % collected data will be separated into two columns, the first column is
rotary table's real-time rotation angle and the second column is the metrology probe's data
[file,path] = uiputfile('*.txt','Save Filename As');%get file name&path;
str=strcat(path,file);
save(file, 'data','-ASCII');%save data to any name;
guidata(hObject, handles);


% --- Executes on button press in clear_figure.
function clear_figure_Callback(hObject, eventdata, handles)
% hObject    handle to clear_figure (see GCBO)
% eventdata  reserved - to be defined in a future version of MATLAB
% handles    structure with handles and user data (see GUIDATA)
cla; %clear plotted gragh
```

```
guidata(hObject, handles);



% --- Executes on button press in clear_figure.
function pushbutton8_Callback(hObject, eventdata, handles)
% hObject    handle to clear_figure (see GCBO)
% eventdata  reserved - to be defined in a future version of MATLAB
% handles    structure with handles and user data (see GUIDATA)



% --------------------------------------------------------------------
function connect_straight_line_Callback(hObject, eventdata, handles)
% hObject    handle to connect_straight_line (see GCBO)
% eventdata  reserved - to be defined in a future version of MATLAB
% handles    structure with handles and user data (see GUIDATA)
x1 = handles.table.angle;
z1 = handles.probe;
z1 = z1';
[x1,z1]=connect_straight(x1,z1);
handles.table.angle = x1;
handles.probe = z1';
axes1_CreateFcn(hObject, eventdata, handles);



% --- Executes on button press in table_move_anticlock.
% This section can control the air-bearing rotary table to rotate in an anticlockwise direction.
```

```
function table_move_anticlock_Callback(hObject, eventdata, handles)
% hObject    handle to table_move_anticlock (see GCBO)
% eventdata  reserved - to be defined in a future version of MATLAB
% handles    structure with handles and user data (see GUIDATA)
h = handles.h;
invoke(h,'jog',0,20); %control the rotary table to rotate in an anticlockwise direction
guidata(hObject,handles);


% This section can control the rotary table to rotate with any specified angle with respect to its starting point defined by Hall effect sensor.
function edit_arc_range_Callback(hObject, eventdata, handles)
% hObject    handle to edit_arc_range (see GCBO)
% eventdata  reserved - to be defined in a future version of MATLAB
% handles    structure with handles and user data (see GUIDATA)

% Hints: get(hObject,'String') returns contents of edit_arc_range as text
%        str2double(get(hObject,'String')) returns contents of edit_arc_range as a double
arc_range=str2num(get(handles.edit_arc_range,'string'));
handles.arc.range = arc_range;
set(handles.edit_arc_range,'string',arc_range);
guidata(hObject,handles);


% --- Executes during object creation, after setting all properties.
function edit_arc_range_CreateFcn(hObject, eventdata, handles)
```

```
% hObject    handle to edit_arc_range (see GCBO)
% eventdata  reserved - to be defined in a future version of MATLAB
% handles    empty - handles not created until after all CreateFcns called

% Hint: edit controls usually have a white background on Windows.
%       See ISPC and COMPUTER.
if ispc && isequal(get(hObject,'BackgroundColor'), get(0,'defaultUicontrolBackgroundColor'))
    set(hObject,'BackgroundColor','white');
end



% --- Executes on button press in arc_scan.
function arc_scan_Callback(hObject, eventdata, handles)
% hObject    handle to arc_scan (see GCBO)
% eventdata  reserved - to be defined in a future version of MATLAB
% handles    structure with handles and user data (see GUIDATA)
h = handles.h;
obj1 = handles.probe;

arcrange = handles.arc.range; % get the specified rotary table's rotation angle

encoder0=get(h,'ENCODER',2); % get the initial position of the motor.
encoderoriginal=encoder0;

invoke(h,'jog',0,20);
currentangle=[]; % save all the real-time rotary table's rotation angle with respect to its starting point.
```

```
currentangle(1)=0; % define current angle as zero degree when rotary table at its starting point.
current=1;
fopen(obj1)
probedata=[];

% this while loop can control the rotary table to rotate with any specified angle with respect to its starting
point
while(1)
    encoder1=get(h,'ENCODER',2);
    data_ch_f= fscanf(obj1);
    while(length(data_ch_f)~=19);
      data_ch_f= fscanf(obj1);
    end
    data_ch=deblank(data_ch_f(1,1:5));
    probedata(current) = str2num(data_ch)/32768*10;
   currentangle(current,1)=(encoder1-encoderoriginal)*0.002247358942576249:
% calculate the rotary table's real-time rotation angle based on the motor's encoder value
    if(currentangle(current)>=arcrange)
      invoke(h,'DoStop',0)
% stop the motor real-time rotary table's rotation angle equals to or is bigger than the specified rotation
angle
      break
    end
    current=current+1;
end
handles.probe = probedata;
```

```
handles.table.angle = currentangle;
guidata(hObject,handles);
% axes1_CreateFcn(hObject, eventdata, handles);
update_axes1(hObject, eventdata, handles);



function [x1,y1]=connect_straight(x1,y1)
% connection    connect two points on a curve by straight line
% Inputs:
%    x1,y1:     vectors of a curve.
%    xj1,yj1:   first point on the curve to be connected.
%    xj2,yj2:   second point on the curve to be connected.

[xc,yc]=ginput(2);
i1=find_x_match(x1,xc(1));
i2=find_x_match(x1,xc(2));
xj1=x1(i1); xj2=x1(i2);
yj1=y1(i1); yj2=y1(i2);

slope=(yj2-yj1)/(xj2-xj1);
y_straight=yj1+slope.*x1(i1:i2);
dy=y_straight(1)-yj1;
y_straight=y_straight-dy;
ys1=y1(1:i1-1); ys3=y1(i2+1:end);
y1=[ys1' y_straight' ys3'];
```

```
y1_length=length(y1);
x1=linspace(x1(1),x1(end),length(y1));
x1=x1';
```

Appendix 2 Matlab Codes for SPP Data Stitching

This Matlab GUI programme below was developed to conduct the probe's data logging and data stitching.

```
function varargout = simple(varargin)
gui_Singleton = 1;
gui_State = struct('gui_Name',       mfilename, ...
                   'gui_Singleton',  gui_Singleton, ...
                   'gui_OpeningFcn', @simple_OpeningFcn, ...
                   'gui_OutputFcn',  @simple_OutputFcn, ...
                   'gui_LayoutFcn',  [] , ...
                   'gui_Callback',   []);
if nargin && ischar(varargin{1})
    gui_State.gui_Callback = str2func(varargin{1});
end
if nargout
    [varargout{1:nargout}] = gui_mainfcn(gui_State, varargin{:});
else
    gui_mainfcn(gui_State, varargin{:});
end
function simple_OpeningFcn(hObject, eventdata, handles, varargin)
handles.output = hObject;
guidata(hObject, handles);
function varargout = simple_OutputFcn(hObject, eventdata, handles)
varargout{1} = handles.output;


clear
```

```
format long g




%% Read Circle Data
function Circus_data_Callback(hObject, eventdata, handles)
files = dir('*.txt');
l = length(files);
Data=[];
Leng=[];

for i=1:l
    filename = strcat('a',num2str(i),'.txt');
    fid = fopen(filename);
    A = textscan(fid, '%f %f %*[^\n]');
    B=cell2mat(A);
    B(:,2)=Data_Smooth( B(:,2)',10,3 );
    Leng(i)=length(B)
    fclose(fid);
    Data = [Data;B];
end
msgbox(['complete! ' num2str(l) ' txt files.']);
setappdata(handles.Circus_data,'Data',Data);
setappdata(handles.Circus_data,'Leng',Leng);


%% Read Arc_data Data
```

```
function Arc_data_Callback(hObject, eventdata, handles)
[filename, pathname] = uigetfile('*.txt','Import Arc File•');
if pathname == 0
   return;
end
filepath = fullfile(pathname,filename);
fid = fopen(filepath, 'r');
Arc_data = textscan(fid,'%f %f %*[^\n]') ;
fclose(fid);
setappdata(handles.Arc_data,'Arc_data',Arc_data);

%% Read Circles Radius £¨n*1 matrix £©
function Circle_Radius_Data_Callback(hObject, eventdata, handles)
[filename, pathname] = uigetfile('*.txt','Circle_Radius_Data');
if pathname == 0
   return;
end
filepath = fullfile(pathname,filename);
fid = fopen(filepath, 'r');
Circle_Radius= textscan(fid,'%f %*[^\n]') ;
fclose(fid);
setappdata(handles.Circle_Radius_Data,'Circle_Radius',Circle_Radius);


%% Read Tilt_angle
function Tilt_angle_Callback(hObject, eventdata, handles)
```

```
Tilt_angle=str2num(get(handles.Tilt_angle,'string'));
setappdata(handles.Tilt_angle,'Tilt_angle',Tilt_angle);
function Tilt_angle_CreateFcn(hObject, eventdata, handles)
if ispc && isequal(get(hObject,'BackgroundColor'), get(0,'defaultUicontrolBackgroundColor'))
    set(hObject,'BackgroundColor','white');
end



%% Read Arc_off_axis_distance
function Arc_off_axis_distance_Callback(hObject, eventdata, handles)
Arc_off_axis_distance=str2num(get(handles.Arc_off_axis_distance,'string'));
setappdata(handles.Arc_off_axis_distance,'Arc_off_axis_distance',Arc_off_axis_distance);
function Arc_off_axis_distance_CreateFcn(hObject, eventdata, handles)
if ispc && isequal(get(hObject,'BackgroundColor'), get(0,'defaultUicontrolBackgroundColor'))
    set(hObject,'BackgroundColor','white');
end


%% Read Arc_Radius
function Arc_Radius_Callback(hObject, eventdata, handles)
Arc_Radius=str2num(get(handles.Arc_Radius,'string'));
setappdata(handles.Arc_Radius,'Arc_Radius',Arc_Radius);
function Arc_Radius_CreateFcn(hObject, eventdata, handles)
if ispc && isequal(get(hObject,'BackgroundColor'), get(0,'defaultUicontrolBackgroundColor'))
    set(hObject,'BackgroundColor','white');
end
```

```
%% --- Executes on button press in Stitching.
function Stitching_Callback(hObject, eventdata, handles)

Arc_data=cell2mat(getappdata(handles.Arc_data,'Arc_data'));
Arc_data(:,2)=Data_Smooth(Arc_data(:,2)',10,3 );
Circle_Radius=cell2mat(getappdata(handles.Circle_Radius_Data,'Circle_Radius'));
Circle_Number=length(Circle_Radius);
Tilt_angle=getappdata(handles.Tilt_angle,'Tilt_angle');
Arc_off_axis_distance=getappdata(handles.Arc_off_axis_distance,'Arc_off_axis_distance');
Arc_Radius=getappdata(handles.Arc_Radius,'Arc_Radius');
Leng=getappdata(handles.Circus_data,'Leng');
Data=getappdata(handles.Circus_data,'Data');
%% Generate Circle 3D Measurement Data
Leng

Rad=[];
for i=1:Circle_Number
    R=Circle_Radius(i)*ones(Leng(i),1);
    Rad=[Rad;R];
end
length(Rad);
for i=1:length(Rad)
    Circle_X(i)=Rad(i)*cos(Data(i,1)/180*pi);
    Circle_Y(i)=Rad(i)*sin(Data(i,1)/180*pi);
end
```

```
Circle_X=Circle_X'
Circle_Y=Circle_Y'


%%  Generate Arc 3D Measurement Data
solution=solve('x^2+y^2-Circle_Radius(1)^2','(y+Arc_off_axis_distance)^2+x^2-Arc_Radius^2') ;
theta=asin(eval(solution.x)/Arc_Radius)
theta(1,1)
Arc_X=[];
Arc_Y=[];
for i=1:length(Arc_data(:,1))
    Arc_Y(i)=-Arc_off_axis_distance-Arc_Radius*cos(Arc_data(i,1)/180*pi-theta(2));
    Arc_X(i)=Arc_Radius*sin(theta(2)-Arc_data(i,1)/180*pi);
end
Coordinate_Circle=[Circle_X,Circle_Y,Data(:,2)]
Coordinate_Arc=[Arc_X',Arc_Y',Arc_data(:,2)];
% ±ä»»£¿
%% Tilt Mirror
[error,a,b,c] =flatness_regression(Coordinate_Circle)
Coordinate_Circle(:,3)=error;
Tilt=-Tilt_angle/3600/180*pi-atan(c);
Coordinate_Arc=Coordinate_Arc*[1 0 0; 0 cos(Tilt) sin(Tilt);  0 -sin(Tilt) cos(Tilt) ];
%%([cos(Tilt) 0 -sin(Tilt); 0 1 0;  sin(Tilt) 0 cos(Tilt) ]*Coordinate_Arc')';



%% Solve intersection coordinate
X_c=[];
```

```
Y_c=[];
for i=1:Circle_Number
   solution=solve('x^2+y^2-Circle_Radius(i)^2','(y+Arc_off_axis_distance)^2+x^2-Arc_Radius^2') ;
   X_c=[X_c;eval(solution.x)]
   Y_c=[Y_c;eval(solution.y)]
end
X_c;
Y_c;
%% find intersection Z
for j=1:length(X_c)
      for i=1:length(Coordinate_Circle)
         deviation(i)=(X_c(j)-Coordinate_Circle(i,1))^2+(Y_c(j)-Coordinate_Circle(i,2))^2;
      end
      [value,number]=min(deviation);
      Z_inter_Circle(j)= Coordinate_Circle(number,3);

       for i=1:length(Coordinate_Arc)
         deviation1(i)=(X_c(j)-Coordinate_Arc(i,1))^2+(Y_c(j)-Coordinate_Arc(i,2))^2;
       end
      [value1,number1]=min(deviation1);
       Z_inter_Arc(j)=Coordinate_Arc(number1,3);


end
Z_inter_Circle;
Z_inter_Arc;
```

```
    Dev=Z_inter_Circle-Z_inter_Arc;


    for i=1:length(Z_inter_Arc)/2
       Piston(i)= (Dev(2*i-1)+Dev(2*i))/2;
    end
    Piston;
    j=1;
    for i=1:Circle_Number
      Coordinate_Circle(j:j+Leng(i)-1,3)=Coordinate_Circle(j:j+Leng(i)-1,3)-Piston(i);
      j=j+Leng(i);
    end
   [error,a,b,c] =flatness_regression(Coordinate_Circle);
   Coordinate_Circle_final(:,1)=Coordinate_Circle(:,1);
   Coordinate_Circle_final(:,2)=Coordinate_Circle(:,2);
   Coordinate_Circle_final(:,3)=error;
   Coordinate_Circle_final;
   pv=max(error)-min(error);
   rms=std(error);
%% Plot 3D surface
axes(handles.axis1);
[th3,r3]=meshgrid(0:pi/360:2*pi,00:2:120);
[xx,yy]=pol2cart(th3,r3);
zz=griddata(                Coordinate_Circle_final(:,1),                Coordinate_Circle_final(:,2),
Coordinate_Circle_final(:,3),xx,yy,'cubic');
 surf(xx,yy,zz);
 colorbar
```

```
% xlabel('X•Axis');
% ylabel('Y•Axis');
hold on;
%plot3(
Coordinate_Circle_final(:,1),Coordinate_Circle_final(:,2),Coordinate_Circle_final(:,3),'.','MarkerSize',2);
hold off;
view(0,90);
colorbar
axis square;
axis on;
shading interp;
axis tight;
    % plot 3D surface error map in an independent figure
    axes(handles.axis1);
    figure
    surf(xx,yy,zz);
    grid on
    axis([-120 120 -120 120])
    xlabel('X');
    ylabel('Y');
    zlabel('Probe Reading (mm)');
    shading interp;
    colorbar
set(handles.PV,'String',pv*1000);
set(handles.RMS,'String',rms*1000);
```

```
function PV_Callback(hObject, eventdata, handles)

if ispc && isequal(get(hObject,'BackgroundColor'), get(0,'defaultUicontrolBackgroundColor'))
    set(hObject,'BackgroundColor','white');
end




function RMS_Callback(hObject, eventdata, handles)
function RMS_CreateFcn(hObject, eventdata, handles)

if ispc && isequal(get(hObject,'BackgroundColor'), get(0,'defaultUicontrolBackgroundColor'))
    set(hObject,'BackgroundColor','white');
end

% --- Executes during object creation, after setting all properties.
function PV_1_CreateFcn(hObject, eventdata, handles)
% hObject    handle to PV_1 (see GCBO)
% eventdata  reserved - to be defined in a future version of MATLAB
% handles    empty - handles not created until after all CreateFcns called
```

Appendix 3 Matlab Codes for Data Filter

```
function [ y ] = Data_Smooth( x,n,m )

if 2*n+1<m+1
    error('11');
end

N=length(x);
t=(-n:n)';
T1=ones(2*n+1,1);
T2=repmat(t,1,m);
T=cumprod([T1 T2],2);
M=T*inv(T'*T)*T';

for i=1:n
    y(i)=M(i,:)*x(1:2*n+1)';
    y(N-n+i)=M(n+1+i,:)*x(N-2*n:N)';
end

X=[];
for i=1:2*n+1
     X=[X;x(i:N-2*n-1+i)];
end

y(n+1:N-n)=M(n+1,:)*X
```

```
y=y';
end
```

Appendix 4 Matlab Codes for Removing Circular Data Tilt

This Matlab programme below was developed in order to remove the tilt of all the concentric scans data collected by the chromatic probe.

```
function [ error,a,b,c] = flatness_regression(Coordinate_Circle)
X1=Coordinate_Circle(:,1);
X2=Coordinate_Circle(:,2);
Y=Coordinate_Circle(:,3);
X=[ones(length(X1),1), X1, X2];
solve=regress(Y,X);

for i=1:length(X1)
    error(1,i)=(solve(2,1)*X1(i,1)+solve(3,1)*X2(i,1)+solve(1,1)-
Y(i,1))/sqrt(solve(2,1)^2+solve(3,1)^2+1);
end

a=solve(1,1);
b=solve(2,1);
c=solve(3,1);
error=error';
```

Appendix 5 Matlab Codes for Chromatic Probe Data Logging

This Matlab programmes below was developed to conduct the chromatic probe's data logging when the rotary below remains static.

```
%connect probe
obj1 = instrfind('Type', 'serial', 'Port', 'COM7', 'Tag', '');
if isempty(obj1)
   obj1 = serial('COM7');
else
   fclose(obj1);
   obj1 = obj1(1)
end
set(obj1, 'BaudRate', 921600);
set(obj1, 'InputBufferSize', 4096);
set(obj1, 'OutputBufferSize', 4096);

current=1;
fopen(obj1)
data=[];
while(1)

      data_ch_f= fscanf(obj1);
      while(length(data_ch_f)~=19);
         data_ch_f= fscanf(obj1);
      end
%           fclose(obj1);
```

```
        data_ch=deblank(data_ch_f(1,1:5));
        data(current) = str2num(data_ch)/32768*1000;


         current=current+1;


end
% end
```

Appendix 6 Matlab Codes for Spherical Surface Data Stitching

This Matlab programme below was developed to conduct the data stitching for spherical testing surface.

```
function varargout = simple_optical(varargin)
gui_Singleton = 1;
gui_State = struct('gui_Name',       mfilename, ...
                   'gui_Singleton',  gui_Singleton, ...
                   'gui_OpeningFcn', @simple_optical_OpeningFcn, ...
                   'gui_OutputFcn',  @simple_optical_OutputFcn, ...
                   'gui_LayoutFcn',  [] , ...
                   'gui_Callback',   []);
if nargin && ischar(varargin{1})
    gui_State.gui_Callback = str2func(varargin{1});
end
if nargout
    [varargout{1:nargout}] = gui_mainfcn(gui_State, varargin{:});
else
    gui_mainfcn(gui_State, varargin{:});
end
function simple_optical_OpeningFcn(hObject, eventdata, handles, varargin)
handles.output = hObject;
guidata(hObject, handles);
function varargout = simple_optical_OutputFcn(hObject, eventdata, handles)
varargout{1} = handles.output;


clear
```

```
format long g

%% Read Circle Data
function Circus_data_Callback(hObject, eventdata, handles)
files = dir('*.txt');
l = length(files);
Data=[];
Leng=[];

for i=1:l
    filename = strcat('a',num2str(i),'.txt');
    fid = fopen(filename);
    A = textscan(fid, '%f %f %*[^\n]');
    B=cell2mat(A);
    B(:,2)=Data_Smooth( B(:,2)',30,3 );
    Leng(i)=length(B)
    fclose(fid);
    Data = [Data;B];
end
msgbox(['complete! ' num2str(l) ' txt files.']);
setappdata(handles.Circus_data,'Data',Data);
setappdata(handles.Circus_data,'Leng',Leng);

%% Read Arc_data Data
function Arc_data_Callback(hObject, eventdata, handles)
[filename, pathname] = uigetfile('*.txt','Import Arc File•');
```

```
if pathname == 0
   return;
end
filepath = fullfile(pathname,filename);
fid = fopen(filepath, 'r');
Arc_data = textscan(fid,'%f %f %*[^\n]') ;
fclose(fid);
setappdata(handles.Arc_data,'Arc_data',Arc_data);

%% Read Circles Radius £ï*1 matrix £©
function Circle_Radius_Data_Callback(hObject, eventdata, handles)
[filename, pathname] = uigetfile('*.txt','Circle_Radius_Data');
if pathname == 0
   return;
end
filepath = fullfile(pathname,filename);
fid = fopen(filepath, 'r');
Circle_Radius= textscan(fid,'%f %*[^\n]') ;
fclose(fid);
setappdata(handles.Circle_Radius_Data,'Circle_Radius',Circle_Radius);


%% Read Tilt_angle
function Tilt_angle_Callback(hObject, eventdata, handles)
Tilt_angle=str2num(get(handles.Tilt_angle,'string'));
setappdata(handles.Tilt_angle,'Tilt_angle',Tilt_angle);
```

```
function Tilt_angle_CreateFcn(hObject, eventdata, handles)
if ispc && isequal(get(hObject,'BackgroundColor'), get(0,'defaultUicontrolBackgroundColor'))
    set(hObject,'BackgroundColor','white');
end



%% Read Arc_off_axis_distance
function Arc_off_axis_distance_Callback(hObject, eventdata, handles)
Arc_off_axis_distance=str2num(get(handles.Arc_off_axis_distance,'string'));
setappdata(handles.Arc_off_axis_distance,'Arc_off_axis_distance',Arc_off_axis_distance);
function Arc_off_axis_distance_CreateFcn(hObject, eventdata, handles)
if ispc && isequal(get(hObject,'BackgroundColor'), get(0,'defaultUicontrolBackgroundColor'))
    set(hObject,'BackgroundColor','white');
end

%% Read Arc_Radius
function Arc_Radius_Callback(hObject, eventdata, handles)
Arc_Radius=str2num(get(handles.Arc_Radius,'string'));
setappdata(handles.Arc_Radius,'Arc_Radius',Arc_Radius);
function Arc_Radius_CreateFcn(hObject, eventdata, handles)
if ispc && isequal(get(hObject,'BackgroundColor'), get(0,'defaultUicontrolBackgroundColor'))
    set(hObject,'BackgroundColor','white');
end



%% --- Executes on button press in Stitching.
```

```
function Stitching_Callback(hObject, eventdata, handles)

Arc_data=cell2mat(getappdata(handles.Arc_data,'Arc_data'));
Arc_data(:,2)=Data_Smooth(Arc_data(:,2)',30,3);

Circle_Radius=cell2mat(getappdata(handles.Circle_Radius_Data,'Circle_Radius'));
Circle_Number=length(Circle_Radius);
Tilt_angle=getappdata(handles.Tilt_angle,'Tilt_angle');
Arc_off_axis_distance=getappdata(handles.Arc_off_axis_distance,'Arc_off_axis_distance');
Arc_Radius=getappdata(handles.Arc_Radius,'Arc_Radius');
Leng=getappdata(handles.Circus_data,'Leng');
Data=getappdata(handles.Circus_data,'Data');
%% Generate Circle 3D Measurement Data
Leng

Rad=[];
for i=1:Circle_Number
   R=Circle_Radius(i)*ones(Leng(i),1);
   Rad=[Rad;R];
end
length(Rad);
for i=1:length(Rad)
   Circle_X(i)=Rad(i)*cos(Data(i,1)/180*pi);
   Circle_Y(i)=Rad(i)*sin(Data(i,1)/180*pi);
end
Circle_X=Circle_X'
```

```
Circle_Y=Circle_Y'


%%  Generate Arc 3D Measurement Data
solution=solve('x^2+y^2-Circle_Radius(1)^2','(y+Arc_off_axis_distance)^2+x^2-Arc_Radius^2') ;
theta=asin(eval(solution.x)/Arc_Radius)
theta(1,1)
Arc_X=[];
Arc_Y=[];
for i=1:length(Arc_data(:,1))
    Arc_Y(i)=-Arc_off_axis_distance-Arc_Radius*cos(Arc_data(i,1)/180*pi-theta(2));
    Arc_X(i)=Arc_Radius*sin(theta(2)-Arc_data(i,1)/180*pi);
end
Coordinate_Circle=[Circle_X,Circle_Y,Data(:,2)]
Coordinate_Arc=[Arc_X',Arc_Y',Arc_data(:,2)];
% ±ä»»£¿
%% Tilt Mirror
[error,a,b,c] =flatness_regression(Coordinate_Circle)
Coordinate_Circle(:,3)=error;
Tilt=-Tilt_angle/3600/180*pi-atan(c);
Coordinate_Arc=Coordinate_Arc*[1 0 0; 0 cos(Tilt) sin(Tilt);  0 -sin(Tilt) cos(Tilt) ];
%%([cos(Tilt) 0 -sin(Tilt); 0 1 0;  sin(Tilt) 0 cos(Tilt) ]*Coordinate_Arc')';



%% Solve intersection coordinate
X_c=[];
Y_c=[];
```

```
for i=1:Circle_Number
   solution=solve('x^2+y^2-Circle_Radius(i)^2','(y+Arc_off_axis_distance)^2+x^2-Arc_Radius^2') ;
   X_c=[X_c;eval(solution.x)]
   Y_c=[Y_c;eval(solution.y)]
end
X_c;
Y_c;
%% find intersection Z
for j=1:length(X_c)
      for i=1:length(Coordinate_Circle)
         deviation(i)=(X_c(j)-Coordinate_Circle(i,1))^2+(Y_c(j)-Coordinate_Circle(i,2))^2;
      end
      [value,number]=min(deviation);
      Z_inter_Circle(j)= Coordinate_Circle(number,3);

       for i=1:length(Coordinate_Arc)
         deviation1(i)=(X_c(j)-Coordinate_Arc(i,1))^2+(Y_c(j)-Coordinate_Arc(i,2))^2;
       end
      [value1,number1]=min(deviation1);
       Z_inter_Arc(j)=Coordinate_Arc(number1,3);


end
Z_inter_Circle;
Z_inter_Arc;
     Dev=Z_inter_Circle-Z_inter_Arc;
```

```
for i=1:length(Z_inter_Arc)/2
   Piston(i)= (Dev(2*i-1)+Dev(2*i))/2;
end
Piston;
j=1;
for i=1:Circle_Number
  Coordinate_Circle(j:j+Leng(i)-1,3)=Coordinate_Circle(j:j+Leng(i)-1,3)-Piston(i);
  j=j+Leng(i);
end
[error,a,b,c] =flatness_regression(Coordinate_Circle);
Coordinate_Circle_final(:,1)=Coordinate_Circle(:,1);
Coordinate_Circle_final(:,2)=Coordinate_Circle(:,2);
Coordinate_Circle_final(:,3)=error;
Coordinate_Circle_final;

[s,radius]=sphereFit(Coordinate_Circle_final) ;
      for i=1:length(Coordinate_Circle)
          error(i,1)=sqrt((Coordinate_Circle_final(i,1)-s(1)).^2+(Coordinate_Circle_final(i,2)-s(2)).^2+
(Coordinate_Circle_final(i,3)-s(3)).^2)-radius;
      end
          Coordinate_Circle_final(:,1)=Coordinate_Circle(:,1);
Coordinate_Circle_final(:,2)=Coordinate_Circle(:,2);
Coordinate_Circle_final(:,3)=error;

pv=max(error)-min(error);
```

```
    rms=std(error);
%% Plot 3D surface
axes(handles.axis1);
[th3,r3]=meshgrid(0:pi/360/2:2*pi,0:0.5:160);
[xx,yy]=pol2cart(th3,r3);
zz=griddata( Coordinate_Circle_final(:,1), Coordinate_Circle_final(:,2),
Coordinate_Circle_final(:,3),xx,yy,'cubic');
 surf(xx,yy,-zz);%optical probe data is opposite to real data
 colorbar
xlabel('X•Axis');
ylabel('Y•Axis');
hold on;
%plot3(
Coordinate_Circle_final(:,1),Coordinate_Circle_final(:,2),Coordinate_Circle_final(:,3),'.','MarkerSize',2);
hold off;
view(0,90);
colorbar
axis square;
axis on;
shading interp;
axis tight;
    % plot 3D surface error map in a independent figure(peng)
    axes(handles.axis1);
    figure
    surf(xx,yy,-zz);%optical probe data is opposite to real data
    grid on
```

```
    axis([-160 160 -160 160])
    xlabel('X');
    ylabel('Y');
    zlabel('Probe Reading (mm)');
    shading interp;
set(handles.PV,'String',pv*1000);
set(handles.RMS,'String',rms*1000);


function PV_Callback(hObject, eventdata, handles)

if ispc && isequal(get(hObject,'BackgroundColor'), get(0,'defaultUicontrolBackgroundColor'))
   set(hObject,'BackgroundColor','white');
end



function RMS_Callback(hObject, eventdata, handles)

function RMS_CreateFcn(hObject, eventdata, handles)

if ispc && isequal(get(hObject,'BackgroundColor'), get(0,'defaultUicontrolBackgroundColor'))
   set(hObject,'BackgroundColor','white');
end
```

Publications

[1] Peng Zhang, Jie Li, Guoyu Yu, David D. Walker, "Development of swinging part profilometer for optics," Proc. SPIE 10151, Optics and Measurement International Conference 2016, 101510B (11 November 2016)

[2] Walker, David D., Yu, G., Bibby, M., Dunn, C., Li, H., Wu, H. Y., Zheng, X. and Zhang, P. (2016) Robotic automation in computer controlled polishing. Journal of the European Optical Society: Rapid Publications, 11. p. 16005. ISSN 1990-2573

References

[1] K. Schwab, *The fourth industrial revolution*. London: Portfolio Penguin, 2017.

[2] M. Dimmler, J. Marrero, S. Leveque, P. Barriga, B. Sedghi, and M. Mueller, "E-ELT M1 test facility," pp. 84441Y-84441Y-15.

[3] *E-ELT Construction Proposal*, 2011.

[4] P. Comley, P. Morantz, P. Shore, and X. Tonnellier, "Grinding metre scale mirror segments for the E-ELT ground based telescope," *CIRP Annals - Manufacturing Technology*, vol. 60, pp. 379-382, 2011.

[5] D. Walker, C. Atkins, I. Baker, R. Evans, S. Hamidi, P. Harris, *et al.*, "Technologies for producing segments for extremely large telescopes," pp. 812604-812609.

[6] D. Walker, G. Yu, A. Beaucamp, M. Bibby, H. Li, L. McCluskey, *et al.*, "More steps towards process automation for optical fabrication," pp. 103260S-103260S-8.

[7] G. Yu, D. D. Walker, and H. Li, "Research on fabrication of mirror segments for E-ELT," in *6th International Symposium on Advanced Optical Manufacturing and Testing Technologies (AOMATT 2012)*, 2012, p. 6.

[8] D. D. Walker, G. Yu, M. Bibby, H. Li, and C. R. Dunn, "Closing the metrology/process loop in CNC polishing," pp. 100090O-100090O-5.

[9] B. S. Hall, *Weapons and warfare in Renaissance Europe: gunpowder, technology, and tactics*. London;Baltimore, Md;: Johns Hopkins University Press, 1997.

[10] X. J. Jiang and D. J. Whitehouse, "Technological shifts in surface metrology," *CIRP Annals - Manufacturing Technology*, vol. 61, pp. 815-836, 2012.

[11] X. Jiang, P. J. Scott, D. J. Whitehouse, and L. Blunt, "Paradigm shifts in surface metrology. Part I. Historical philosophy," *Proceedings of the Royal Society a-Mathematical Physical and Engineering Sciences*, vol. 463, pp. 2049-2070, Sep 8 2007.

[12] X. Jiang, P. J. Scott, D. J. Whitehouse, and L. Blunt, "Paradigm shifts in surface metrology. Part II. The current shift," *Proceedings of the Royal Society a-Mathematical Physical and Engineering Sciences*, vol. 463, pp. 2071-2099, Sep 8 2007.

[13] D. J. Whitehouse and D. J. Whitehouse, *Handbook of surface and nanometrology*, 2nd ed. Boca Raton, FL: CRC Press, 2011.

[14] M. Johns, P. McCarthy, K. Raybould, A. Bouchez, A. Farahani, J. Filgueira, *et al.*, "Giant Magellan Telescope: overview," pp. 84441H-84441H-16.

[15] M. Johns, C. Hull, G. Muller, B. Irarrazaval, A. Bouchez, T. Chylek, *et al.*, "Design of the Giant Magellan Telescope," pp. 91451F-91451F-14.

[16] J. Nijenhuis, J. Heijmans, R. den Breeje, R. Hazelebach, J. de Vreugd, W. Crowcombe, *et al.*, "Designing the primary mirror support for the E-ELT," pp. 990616-990616-10.

[17] C. Gray, I. Baker, G. Davies, R. Evans, N. Field, T. Fox-Leonard, *et al.*, "Fast manufacturing of E-ELT mirror segments using CNC polishing," in *SPIE Optical Engineering + Applications*, 2013, p. 12.

[18] G. Yu, D. Walker, H. Li, X. Zheng, and A. Beaucamp, "Research on edge-control methods in CNC polishing," *Journal of the European Optical Society-Rapid Publications*, vol. 13, pp. 1-13, 2017.

[19] W. Wang, M. Xu, H. Li, and G. Yu, "Polishing large-aperture mirror using ultraprecise Bonnet and PSD result analysis," pp. 84160P-84160P-8.

[20] D. Walker, G. Yu, H. Li, W. Messelink, R. Evans, and A. Beaucamp, "Edges in CNC polishing: from mirror-segments towards semiconductors, paper 1: edges on processing the global surface," *Optics Express*, vol. 20, pp. 19787-19798, 2012/08/27 2012.

[21] G. Yu, D. Walker, and H. Li, "Implementing a grolishing process in Zeeko IRP machines," *Applied optics*, vol. 51, p. 6637, 2012.

[22] B. Bhushan, *Surface roughness analysis and measurement techniques* vol. 1, 2001.
[23] "BS EN ISO 4287:1998+A1:2009: Geometrical product specification (GPS). Surface texture: Profile method. Terms, definitions and surface texture parameters," ed: British Standards Institute, 2000.
[24] S. H. Bui and T. V. Vorburger, "Surface metrology algorithm testing system," *Precision Engineering,* vol. 31, pp. 218-225, 2007.
[25] *Exploring Surface Texture: A Fundamental Guide to the Measurement of Surface Finish*: Taylor Hobson, 2003.
[26] C. Mike and A. Joe, "A comparison of surface metrology techniques," *Journal of Physics: Conference Series,* vol. 13, p. 458, 2005.
[27] A. Weckenmann, T. Estler, G. Peggs, and D. McMurtry, "Probing Systems in Dimensional Metrology," *CIRP Annals - Manufacturing Technology,* vol. 53, pp. 657-684, 2004.
[28] T. J. Kamps, J. C. Walker, and A. G. Plint, "In situ stylus profilometer for a high frequency reciprocating tribometer," *Surface Topography: Metrology and Properties,* vol. 5, p. 34004, 2017.
[29] T. G. Mathia, P. Pawlus, and M. Wieczorowski, "Recent trends in surface metrology," *Wear,* vol. 271, pp. 494-508, 2011.
[30] K. J. Kim, C. S. Jung, and T. E. Hong, "A new method for the calibration of the vertical scale of a stylus profilometer using multiple delta-layer films," *Measurement Science and Technology,* vol. 18, pp. 2750-2754, 2007.
[31] T. V. Vorburger, H. G. Rhee, T. B. Renegar, J. F. Song, and A. Zheng, "Comparison of optical and stylus methods for measurement of surface texture," *International Journal of Advanced Manufacturing Technology,* vol. 33, pp. 110-118, 2007.
[32] T. V. Vorburger, H. G. Rhee, T. B. Renegar, J. F. Song, and A. Zheng, "Comparison of optical and stylus methods for measurement of surface texture," *The International Journal of Advanced Manufacturing Technology,* vol. 33, pp. 110-118, 2007.
[33] C.-X. J. Feng, A. L. Saal, J. G. Salsbury, A. R. Ness, and G. C. S. Lin, "Design and analysis of experiments in CMM measurement uncertainty study," *Precision Engineering,* vol. 31, pp. 94-101, 2007.
[34] R. J. Hocken and P. H. Pereira, *Coordinate Measuring Machines and Systems, Second Edition*, 2nd ed. Hoboken: Taylor and Francis, 2011.
[35] J. R. P. Angel and R. E. Parks, "Generation Of Off-Axis Aspherics," pp. 316-326.
[36] D. S. Anderson and J. H. Burge, "Swing-arm profilometry of aspherics," in *SPIE's 1995 International Symposium on Optical Science, Engineering, and Instrumentation*, 1995, p. 11.
[37] P. Su, C. J. Oh, R. E. Parks, and J. H. Burge, "Swing arm optical CMM for aspherics," pp. 74260J-74260J-8.
[38] M. T. Postek, P. Su, C. J. Oh, C. Zhao, J. H. Burge, V. A. Coleman, *et al.*, "Optical testing for meter size aspheric optics," vol. 8466, p. 84660S, 2012.
[39] A. Efstathiou, *Design considerations for a hybrid swing-arm profilometer to measure large aspheric optics*: University of London, University College London (United Kingdom), 2007.
[40] H. W. Jing, Z. H. Lin, L. F. Ma, S. B. Wu, and F. Wu, "Development and experimental validation of a versatile prototype Swing Arm Profilometer for measuring optical surfaces," *Journal of the European Optical Society-Rapid Publications,* vol. 6, 2011.
[41] M. Gao, H. Jing, T. Fan, L. Chen, and J. Li, "Calibrating the axes of the swing arm profilometer by the four-based laser trackers," pp. 96230M-96230M-8.
[42] Y. Wang, P. Su, R. E. Parks, C. J. Oh, and J. H. Burge, "Swing arm optical coordinate-measuring machine: high precision measuring ground aspheric surfaces using a laser triangulation probe," *Optical Engineering,* vol. 51, pp. 073603-073603, 2012.
[43] S. Chen, Y. Dai, X. Peng, and S. Li, "Error analysis and surface reconstruction for swing arm profilometry," *Measurement,* vol. 87, pp. 1-12, 2016/06/01/ 2016.
[44] "Optical surface metrology system non-contact surface texture measurement," vol. 73, ed: Penton Media, Inc., Penton Business Media, Inc. and their subsidiaries, 2008, p. 48.

[45] S. DeFisher and E. M. Fess, "Comparison of contact and non-contact asphere surface metrology devices," pp. 88840U-88840U-10.
[46] R. E. Renton, et al., W. H. Simmonds, and R. J. Smith, "Optical non-contact techniques for engineering surface metrology," ed. Luxembourg: OPOCE, 1995.
[47] X. Zou, X. Zhao, G. Li, Z. Li, and T. Sun, "Non-contact on-machine measurement using a chromatic confocal probe for an ultra-precision turning machine," *The International Journal of Advanced Manufacturing Technology,* vol. 90, pp. 2163-2172, 2017.
[48] A. A. Goloborodko, "Optical testing of reflective surfaces," pp. 90660Z-90660Z-7.
[49] "chromatic aberration," 3 ed: Oxford University Press, 2018.
[50] N. H, B. R.H, K. A, P. H, H. R, and S. H.A.M, "Ultra-high precision CMMs and their associated tactile or/and optical scanning probes," *International Journal of Metrology and Quality Engineering,* vol. 5, p. 204, 2014.
[51] H. Nouira, N. El-Hayek, X. Yuan, and N. Anwer, "Characterization of the main error sources of chromatic confocal probes for dimensional measurement," *Measurement Science and Technology,* vol. 25, p. 44011, 2014.
[52] D. Malacara, D. Malacara, D. Malacara, D. Malacara H, D. Malacara-Hernández, and D. M. Hernández, *Optical shop testing,* 3rd ed. Hoboken, N.J: Wiley-Interscience, 2007.
[53] J. H. Burge, "Applications of computer-generated holograms for interferometric measurement of large aspheric optics," pp. 258-269.
[54] C. Pruss, S. Reichelt, H. J. Tiziani, and W. Osten, "Computer-generated holograms in interferometric testing," 2004, p. 7.
[55] J. T. Rasanen, M. Savolainen, R. V. J. Silvennoinen, and K.-E. Peiponen, "Optical sensing of surface roughness and waviness by a computer-generated hologram," *Optical Engineering,* vol. 34, pp. 2574-2580, 1995.
[56] W. Wang and P.-j. Guo, "Optical testing of cylindrical surfaces with computer-generated holograms," pp. 89120T-89120T-7.
[57] X. Wei, Y. He, K. Xu, B. Gao, Q. Li, and L. Chai, "Computer-generated holograms for precision optical testing," pp. 96842C-96842C-8.
[58] C. Zhao and J. H. Burge, "Optical testing with computer generated holograms: comprehensive error analysis," pp. 88380H-88380H-12.
[59] Y.-Y. Cheng and J. C. Wyant, "Phase shifter calibration in phase-shifting interferometry," *Applied Optics,* vol. 24, pp. 3049-3052, 1985/09/15 1985.
[60] M. Bray, "Stitching interferometer for large plano optics using a standard interferometer," pp. 39-50.
[61] P. Murphy, J. Fleig, G. Forbes, D. Miladinovic, G. DeVries, and S. O'Donohue, "Subaperture stitching interferometry for testing mild aspheres," pp. 62930J-62930J-10.
[62] Z. Zhao, H. Zhao, F. Gu, H. Du, and K. Li, "Non-null testing for aspheric surfaces using elliptical sub-aperture stitching technique," *Opt Express,* vol. 22, pp. 5512-21, Mar 10 2014.
[63] M. Carbillet, A. Ferrari, C. Aime, H. Campbell, and A. Greenaway, "Wavefront sensing: from historical roots to the state-of-the-art," *European Astronomical Society Publications Series,* vol. 22, pp. 165-185, 2006.
[64] J. Schwiegerling and D. R. Neal, "Historical development of the Shack-Hartmann wavefront sensor," *Robert Shannon and Roland Shack: Legends in Applied Optics, edited by JE Harvey and RB Hooker—SPIE, Bellingham, WA,* pp. 132-139, 2005.
[65] S. Barbero, J. Rubinstein, and L. N. Thibos, "An improved Hartmann-Shack wavefront sensor for ocular aberrometry using wavefront slope and curvature measurements," *Journal of Vision,* vol. 5, pp. 48-48, 2010.
[66] J. R. Fienup, B. J. Thelen, R. G. Paxman, and D. A. Carrara, "Comparison of phase diversity and curvature wavefront sensing," in *Adaptive Optical System Technologies,* 1998, pp. 930-941.
[67] M. Rais, J.-M. Morel, C. Thiebaut, J.-M. Delvit, and G. Facciolo, "Improving wavefront sensing with a Shack-Hartmann device," *Appl. Opt. 55, 7836-7846 (2016). ,* vol. 55, p. 7836, 2016.

[68] J. R. Fienup, B. J. Thelen, R. G. Paxman, and D. A. Carrara, "Comparison of phase diversity and curvature wavefront sensing," pp. 930-940.
[69] A. H. Greenaway, H. I. Campbell, and S. Restaino, "Generalised Phase Diversity Wavefront Sensor," Berlin, Heidelberg, 2005, pp. 177-186.
[70] H. I. Campbell and A. H. Greenaway, "Wavefront Sensing: From Historical Roots to the State-of-the-Art," *EAS Publications Series*, vol. 22, pp. 165-185, 2006.
[71] L. Huang, M. Idir, C. Zuo, and A. Asundi, "Review of phase measuring deflectometry," *Optics and Lasers in Engineering*, vol. 107, pp. 247-257, 2018.
[72] S. Höfer, J. Burke, and M. Heizmann, "Infrared deflectometry for the inspection of diffusely specular surfaces," *Advanced Optical Technologies*, vol. 5, 2016.
[73] E. H. Frater and L. E. Coyle, "Deflectometry for measuring mount-induced mirror surface deformations," pp. 103730I-103730I-7.
[74] M. V. Gubarev, B. Ramsey, C. Atkins, and A. Eberhardt, "Development of a deflectometer for accurate surface figure metrology," pp. 96031T-96031T-7.
[75] G. P. Butel, G. A. Smith, and J. H. Burge, "Deflectometry using portable devices," *Optical Engineering*, vol. 54, pp. 025111-025111, 2015.
[76] L. Jiang, X. Zhang, F. Fang, X. Liu, and L. Zhu, "Wavefront aberration metrology based on transmitted fringe deflectometry," *Applied Optics*, vol. 56, p. 7396, 2017.
[77] M. C. Knauer, J. Kaminski, and G. Hausler, "Phase measuring deflectometry: a new approach to measure specular free-form surfaces," pp. 366-376.
[78] C. Peng, Y. He, and J. Wang, "Normal tracing deflectometry using a secondary light source," *J Synchrotron Radiat*, vol. 24, pp. 765-774, Jul 1 2017.
[79] I. Ridpath, "Ronchi test," ed, 2018.
[80] P. Su, R. E. Parks, L. Wang, R. P. Angel, and J. H. Burge, "Software configurable optical test system: a computerized reverse Hartmann test," *Applied Optics*, vol. 49, pp. 4404-4412, 2010/08/10 2010.
[81] P. Su, R. Parks, L. Wang, J. Burge, and R. Angel, "A new test for optical surfaces," *SPIE Newsroom*, 2011.
[82] B. Lam and C. Guo, "Complete characterization of ultrashort optical pulses with a phase-shifting wedged reversal shearing interferometer," *Light: Science & Applications*, vol. 7, p. 30, 2018/07/11 2018.
[83] D. D. Walker, G. Yu, M. Bibby, C. Dunn, H. Li, H. Y. Wu, *et al.*, "Robotic automation in computer controlled polishing," *Journal of the European Optical Society-Rapid Publications*, vol. 11, 2016.
[84] L. Xiong, X. Luo, H. X. Hu, Z. Y. Zhang, F. Zhang, L. G. Zheng, *et al.*, "Swing arm profilometer: high accuracy testing for large reaction-bonded silicon carbide optics with a capacitive probe," *Optical Engineering*, vol. 56, Aug 2017.
[85] L. Xiong, X. Luo, Z. Liu, X. Wang, H. Hu, F. Zhang, *et al.*, "Swing arm profilometer: analytical solutions of misalignment errors for testing axisymmetric optics," *Optical Engineering*, vol. 55, pp. 074108-074108, 2016.
[86] P. Zhang, J. Li, G. Yu, and D. D. Walker, "Development of swinging part profilometer for optics," pp. 101510B-101510B-8.
[87] E. Ramsden, *Hall-effect sensors: theory and applications*, 2nd ed. London;Amsterdam;: Newnes, 2006.
[88] D. J. Whitehouse, *Handbook of Surface and Nanometrology, Second Edition*: CRC Press, 2010.
[89] B. Swinyard, O. Auriacombe, T. Bradshaw, D. Brooks, J. Charlton, M. Crook, *et al.*, "The LOw Cost Upper atmosphere Sounder: the "Elegant Breadboard" programme."
[90] D. Aikens, J. E. DeGroote, and R. N. Youngworth, "Specification and control of mid-spatial frequency wavefront errors in optical systems," in *Optical Fabrication and Testing*, 2008, p. OTuA1.
[91] G. Yu, H. Li, and D. Walker, "Removal of mid spatial-frequency features in mirror segments," *Journal of the European Optical Society*, vol. 6, p. 17, 2011.

[92] D. Y.-H. Wang, R. E. E. Jr., and D. M. Aikens, *Implementation of ISO 10110 optics drawing standards for the National Ignition Facility* vol. 3782: SPIE, 1999.
[93] R. K. Kimmel, R. E. Parks, and O. S. A. S. Committee, *ISO 10110 optics and optical instruments : preparation of drawings for optical elements and systems : a user's guide*. Washington, DC: Optical Society of America, 2002.
[94] S. Babu and S. Babu, *Advances in chemical mechanical planarization (CMP)* vol. Number 86. Kidlington, England;Waltham, Massachusetts;Cambridge, England;: Woodhead Publishing, 2016.